



UPPSALA
UNIVERSITET

Examensarbete vid Institutionen för geovetenskaper
Degree Project at the Department of Earth Sciences
ISSN 1650-6553 Nr 335

Structural and Engineering Geological Investigation of Fracture Zones and Their Effect on Tunnel Construction

Struktur- och ingenjörsgelogisk undersökning
av förkastningszoner och deras påverkan
på tunnelbyggnation

Linda Alfvén

INSTITUTIONEN FÖR
GEOVETENSKAPER

DEPARTMENT OF EARTH SCIENCES

Examensarbete vid Institutionen för geovetenskaper
Degree Project at the Department of Earth Sciences
ISSN 1650-6553 Nr 335

Structural and Engineering Geological Investigation of Fracture Zones and Their Effect on Tunnel Construction

Struktur- och ingenjörsgelogisk undersökning
av förkastningszoner och deras påverkan
på tunnelbyggnation

Linda Alfvén

ISSN 1650-6553

Copyright © Linda Alfvén and the Department of Earth Sciences, Uppsala University
Published at Department of Earth Sciences, Uppsala University (www.geo.uu.se), Uppsala, 2015

Abstract

Structural and Engineering Geological Investigation of Fracture Zones and Their Effect on Tunnel Construction

Linda Alfvén

This thesis project was conducted in connection with the project, Stockholm's future sewer pipeline, which is a planned sewer pipe that will run through a tunnel from western to southern Stockholm. This tunnel will pass under Lake Mälaren between Eolshäll and Smedslätten, where there are two faults indicated on the geological map, that could affect the tunnelling and create risks during the construction. Geophysical- and water-loss measurements along with core drilling have been carried out in the area. The objectives of this thesis are to create a structural and engineering geological understanding of the passage beneath Lake Mälaren based on drill core mapping, field work, data from previous investigations and 2D-models of the tunnel excavation both within and outside the indicated fault zone. The core mapping supports the existence of one fault zone, which is indicated on the geological map supported by water-losses at several places along the drill core as well as core losses. Field work indicated the existence of a conjugate fracture sets.

The 2D-models present plastic behaviour of the rock in the fault zone as the worst case scenario during excavation with the highest deformation displacement. The excavation procedure and the tunnel form also play a significant role. Since this thesis highlights some significant risks and problems that can occur during tunnelling, its findings may be useful during the tunnel construction.

Keywords: Fault zone, drill core, tunnel construction, 2D models

Degree Project E1 in Earth Science, 1GV025, 30 credits

Supervisor: Steffi Burchardt

Department of Earth Sciences, Uppsala University, Villavägen 16, SE-752 36 Uppsala (www.geo.uu.se)

ISSN 1650-6553, Examensarbete vid Institutionen för geovetenskaper, No. 335, 2015

The whole document is available at www.diva-portal.org

Populärvetenskaplig sammanfattning

Struktur- och ingenjörsgelogisk undersökning av förkastningszoner och deras påverkan på tunnelbyggnation

Linda Alfvén

Denna uppsats är skriven med koppling till projektet, Stockholms framtida avloppsledning, vilket inkluderar en ny tunnel för transport av avloppsvatten från västra till södra Stockholm. Tunneln kommer att passera under Mälaren mellan Smedslätten och Eolshäll, där det är två förkastningar indikerade på geologiska kartor som kan orsaka stora risker för byggnationen av tunneln. Geofysiska mätningar, kärnboring och vattenförlustmätning har tidigare utförts i området. Målen för denna uppsats är att skapa en geologisk- och bergmekanisk förståelse för tunnelpassagen under Mälaren utifrån kärnkartering, fältarbete, data från tidigare undersökningar och 2D-modeller av tunneluttag i den indikerade zonen och utanför. Kärnkarteringen stödjer existensen av en förkastningszon som finns på den geologiska kartan. Flertalet vattenförluster är indikerade längs med hela kärnan tillsammans med en del förekomster av kärnförluster. Fältarbetet indikerar på förekomst av ett konjugerande sprickset. 2D-modeller över tunneln visade att olika egenskaper på berget samt hur uttaget av tunneln sker har betydelse för deformationernas storlek. Den här uppsatsen belyser några viktiga problem och risker som kan uppstå under tunnelbyggnationen, dessa upptäckter kan därför vara användbara och värdefulla under hela byggnationen.

Nyckelord: Förkastningszon, borrkärna, tunnelbyggnation, 2D-modeller

Examensarbete E1 i geovetenskap, 1GV025, 30 hp

Handledare: Steffi Burchardt

Institutionen för geovetenskaper, Uppsala universitet, Villavägen 16, 752 36 Uppsala (www.geo.uu.se)

ISSN 1650-6553, Examensarbete vid Institutionen för geovetenskaper, Nr 335, 2015

Hela publikationen finns tillgänglig på www.diva-portal.org

Table of contents

1. Introduction.....	1
2. Geological settings.....	3
2.1 Regional – Svecofennian orogen	3
2.2 Local geology	4
2.2.1 Bergslagen province	4
2.2.2 Geology of the Mälaren Passage, Eolshäll-Smedslätten	9
2.2.3 Stress field	10
3. Background information and methods.....	11
3.1 Structural and engineering geology	11
3.1.1 In-situ stress in Rock	11
3.1.2 Deformation = translation + rotation + strain.....	12
3.1.3 Strength	14
3.2 Geotechnical methods.....	15
3.2.1 Geophysical measurements	15
3.2.2 Drill core.....	16
3.2.3 Procedure.....	17
3.2.4 Water-loss measurements	17
3.3 Methods applied in this thesis	17
3.3.1 Drill core mapping.....	18
3.3.2 Sub-surface fracture analysis.....	19
3.3.3 Field work.....	19
3.3.4 2D modeling	19
4. Results	23
4.1 Geophysical measurements	23
4.2 Water-loss measurements	26
4.3 Drill core mapping.....	27
4.4 Sub-surface fracture analysis.....	30
4.5 Field work.....	34
4.6 2D modeling	36
4.6.1 Tunnel without support.....	36
4.6.2 Tunnel with pre-installed support.....	38

Table of contents (continued)

4.6.3	Tunnel excavation in two steps	39
4.6.4	Round tunnel with internal pressure.....	43
4.6.5	Summary	46
5.	Discussion.....	47
5.1	Fracture analysis	47
5.2	2D-modelling.....	49
6.	Conclusions.....	50
7.	Acknowledgments	51
8.	References.....	52
Appendix 1	54
Appendix 2	55
1.	Models with pre-installed support	55
2.	Models with excavation in two steps.....	56
3.	Round models with elastic properties and pre-installed bolt in stage 1	59
4.	Round models with plastic properties and pre-installed bolt in stage 1	64
5.	Round model with elastic properties and bolts installed in stage 3.....	69
6.	Round model with plastic material and bolts installed in stage 3	74

1. Introduction

Stockholm is one of Europe's fastest growing cities with a population that is constantly increasing by approximately 20 000 people every year. That means more usage of water and human waste that needs to be taken care of. To be able to respond to this need Stockholm Vatten started the project Stockholm future sewer pipe (SFAL) that includes rebuilding and renewing of the existing drainage system in Bromma and Henriksdal. Bromma sewage treatment will be closed and the cleaning processes will be concentrated to Henriksdal purifier which will be enlarged to address the need of a higher water capacity. As a result a new sewer tunnel will be built from Bromma to Henriksdal to transport the waste water from the western Stockholm to Henriksdal purifier (Figure 1).



Figure 1. Tunnel line from Bromma (A) to Henriksdal (H) (Stockholm vatten, 2015).

The new sewer tunnel will be about 15 km long and will vary in depth below ground level between 30-90 m. The closure of the Bromma purifier opens up the possibility of building new homes in an attractive area. Furthermore the new tunnel and the movement of all the cleaning processes to Henriksdal will end the existing heavy transports with sewer sludge through the residential areas of Sickla. As a result of renewing the cleaning system in Henriksdal the emission levels of phosphorus and nitrogen to the Baltic Sea will decrease.

Construction of the tunnel is planned to start in the beginning of 2016 and will take two years. This thesis will focus on the area in the passage between Smedslätten and Eolshäll where the tunnel will pass beneath Lake Mälaren (Figure 2).



Figure 2. Map over the research area with the tunnel line (Stockholm Vatten, 2015).

The pre-investigations started in 2013 which is when different geological- and geophysical measurements were carried out. Geological maps from SGU (Persson et al, 2001) show two fracture zones meeting in the passage. They are both interpreted as normal faults, whilst one strikes NE-SW and the other strikes NW-SE. However, the current knowledge of the zones is only interpretations and they are not further described or characterized.

Fault dimension and characteristics is crucial information that can be applied in both engineering and geological purposes. Concerning the project, the main interest has been whether the characteristics of the fault zones possess any risks for the future tunnel stability. The aim of this project is therefore to (1) interpret the geophysical and geological data, (2) characterize the fracture zones and (3) illustrate how they will affect the tunnel construction.

2. Geological settings

2.1 Regional – Svecofennian orogen

The research area is located within the Bergslagen province, which was formed during the Svecofennian orogen. The Svecofennian domain is the central part of the Fennoscandian shield, bordered by the Archean basement in the northeast, the Sveconorwegian domain in the southwest and the Caledonides in the west (Figure 3) (Gaal & Gorbatshev, 1987). The Fennoscandian shield gets successively younger from the northeast towards the south and southwest. (Gorbatshev & Bogdanova, 1993).

Three major orogenic events increased crustal formation of the Fennoscandian shield, which was then reworked by two later orogenic events. The first orogeny occurred 2.9-2.6 Ga and was called the Lopian orogeny, it was followed by the major Svecofennian orogeny 2.0-1.7 Ga and finally the Gothian orogeny 1.75-1.5 Ga. Reworking of the Fennoscandian crust occurred 1.2-0.9 Ga by the Sveconorwegian orogeny and the Caledonian orogeny (0.5-0.4 Ga). The Svecofennian domain stretches over a large area of the Fennoscandian shield and covers the main part of the bedrock in Sweden, reaching all the way to western Finland and to a small part of Russia (Figure 3). It was formed between 2.0-1.7 Ga with most of the crustal formation occurring between 1.9-1.87 Ga. Crystalline rocks build up most of the crust, of both supracrustal and plutonic origin.



Figure 3. Geological overview map of the Fennoscandian shield with Bergslagen region indicated on the red square (Modified from Högdahl & Sjöström, 2001).

Subdivision of the formation of Svecofennian crust can be made into two periods based on composition, deformation and migmatization of the rocks (Baltybaev et al, 2006). The first period, which is the early crustal formation in the northern area of the Svecofennian domain during 1.9-1.87 Ga, is composed mainly of igneous calc-alkaline granitoids ranging from gabbros to diorites to the dominating granites. This period corresponds to the major formation of the Proterozoic crust and characterizes the peak of the Svecofennian orogeny which includes ductile deformation, metamorphism and emplacement of large plutonic complexes (Baltybaev et al., 2006; Gaál & Gorbatshev, 1987), and the crustal deformation in a brittle manner started to occur around 1.8-1.7 Ga (Saintot et al, 2011). The late crustal formation period mainly occurred in the south of the Svecofennian domain and consists mainly of the intrusion of sedimentary-type granites and migmatites. Most of the Svecofennian rocks have been affected by subsequent deformation and metamorphism during 1.9-1.85 Ga (Andersson et al, 2006).

The processes for the evolution of the Svecofennian orogeny have been debated and several tectonic models have been presented. An early tectonic model was proposed by Gaál and Gorbatshev (1987) in which they defined a subduction zone dipping WNW resulting in arc accretion to the Archean border. Later this early model was, refined by several other scholars such as for example Gorbatshev & Bogdanova (1993) and Nironen (1997), which developed a more detailed evolution of the Svecofennian orogeny, although the concept and order of events are similar.

2.2 Local geology

2.2.1 Bergslagen province

Bergslagen is located in the central part of the Svecofennian domain in the southeast of Sweden. The province hosts a large curving ore belt approximately 200 km long, extending from NNE to E, which consists of volcano-sedimentary and plutonic rock units. Bergslagen has been an important mining district where the mining dates back as far as one thousand years and the area hosts several thousand mineral deposits (Oen, 1987).

The geology in Bergslagen is complex and has been affected by metamorphic events, ductile deformation and igneous activity in different tectonic cycles. The tectonic evolution of Bergslagen has been interpreted as an accretionary continental margin in front of a NE-dipping subduction zone with back-arc extension and igneous activity (Beunk & Page, 2001; Hermansson et al, 2008; Korja & Heikkinen, 1995; Oen, 1987). Hermansson et al. (2008) present a possible model for the tectonic evolution of Bergslagen between 1.91–1.84 Ga (Figure 4), which has been adapted from models by Lathinen et al (2005). The hypothesis for this model is a continent-microcontinent collision. Beneath the microcontinent and the continent there was a SW-dipping subduction zone. Due to the retreat of the subduction zone a new generation of back-arc extension and volcanism occurred. The extension caused the microcontinent to collide with a continent in the NE, which caused the subduction to stop and major

compression occurred. At the same time a new, followed by the NE-dipping, subduction zone located SW of the accreted microcontinent was initiated, followed by hinge retreat in the new subduction zone that caused compression to change into back-arc extension and volcanism primarily moving in a new SW direction.

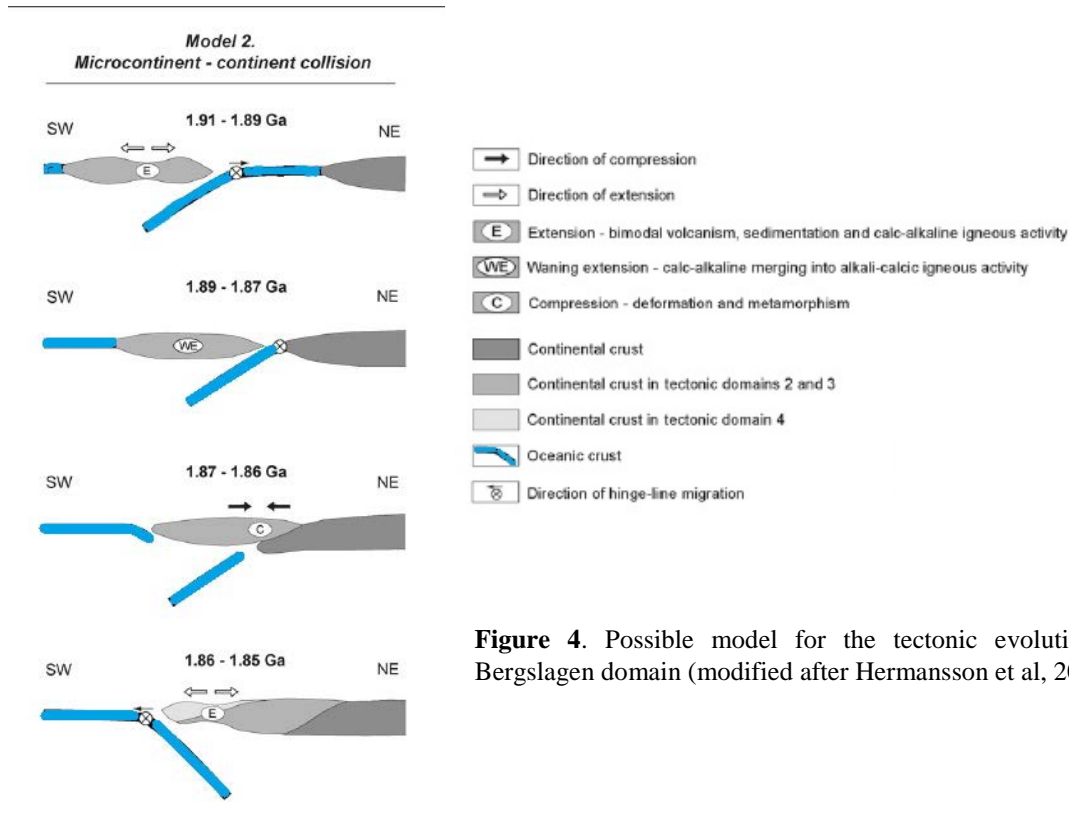


Figure 4. Possible model for the tectonic evolution of Bergslagen domain (modified after Hermansson et al, 2008).

Bergslagen is comprised of felsic to intermediate metavolcanic rocks together with metasedimentary rocks and calc-alkaline intrusive rocks (Figure 5) (Korja & Heikkinen, 1995; Oen, 1987). The meta-volcanosedimentary rocks in west of Bergslagen are referred to as the supracrustal sequence with a thickness of about 7-12 km. It mostly consists of felsic pyroclastic rocks with some basic intrusions and stratigraphically younger sequences of volcanogenic sediments (Oen, 1987). The meta-volcanics consist both of rhyolites and basalts, while the meta-sediments consist mainly of greywackes with some argillitic material together with limestone and dolomites. The intrusive plutonic rocks that intersect the supracrustal rocks indicate compositional variation from gabbro, diorite, tonalite to granodiorite and granite (Larsson & Larsson 2007). The granitoids comprise I-type, S-type and A-type granites. They are classified by their relationship to the Svecofennian orogeny. The I-type granites were formed above the subduction zone and are characterized as synorogenic (1.9-1.86 Ga). The S-type granites are derived from partial melting of the metasediments

and characterizes a late orogenic stage (1.84-1.8 Ga) and the A-type rapakivi batholiths formed after the orogeny in an extensional setting (1.65-1.54 Ga) (Korja & Heikkinen, 1995).

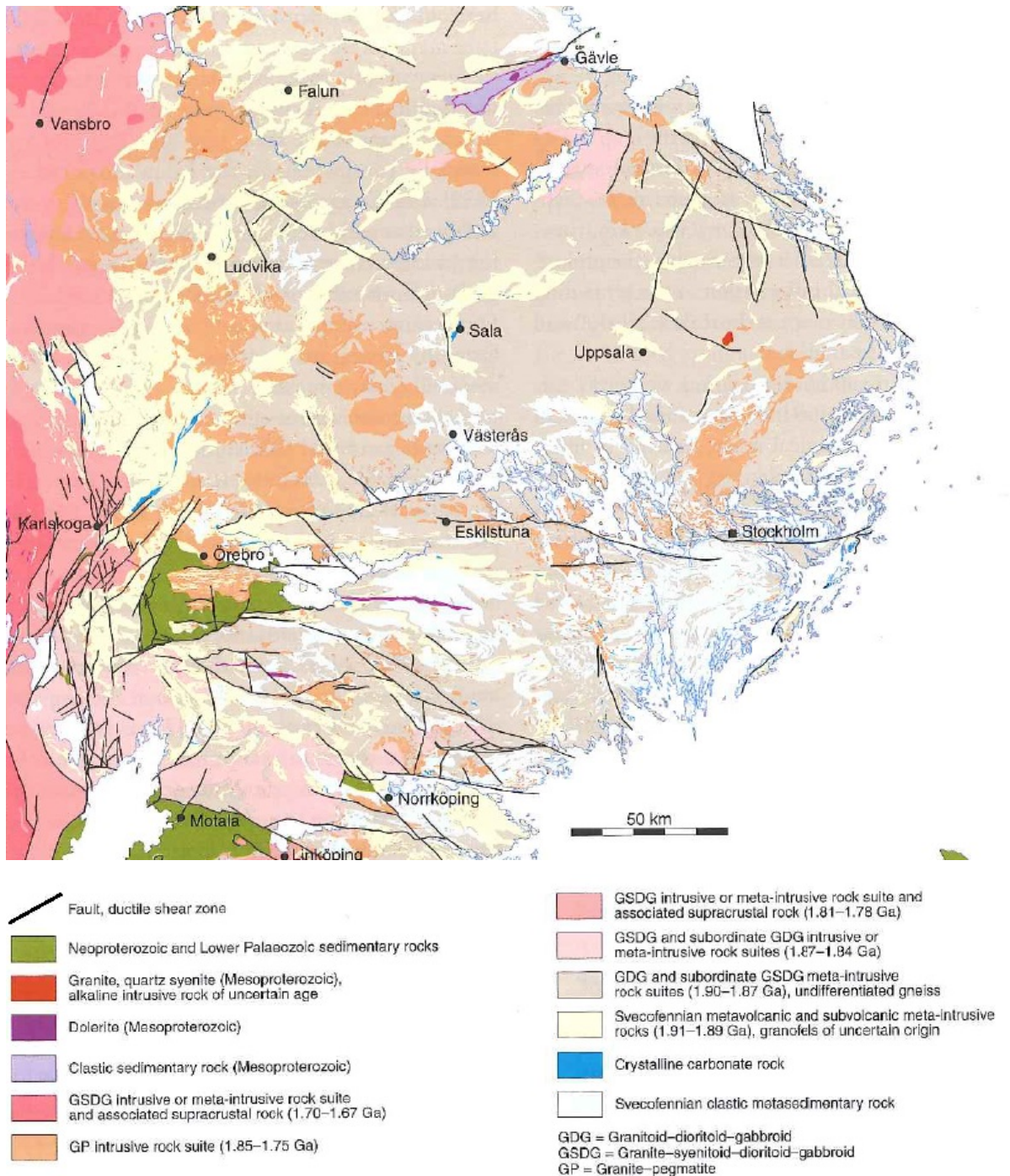


Figure 5. Geological map from Bergslagen province (Copyright by Stephens et al, 2009, SGU).

The metamorphic grade in the area is dominated by lower to upper amphibolite facies (Figure 6). A small area of greenschist-facies rocks is found in the west, and some areas have been highly metamorphosed up to granulite-facies. Subgreenschist-facies and non-metamorphic areas are also present and dominate to the west. The main deformation fabric and depositional structures are

overprinted in the areas of peak metamorphism (granulite-facies); where migmatites, gneisses and pegmatites are common (Stephens et al, 2009).

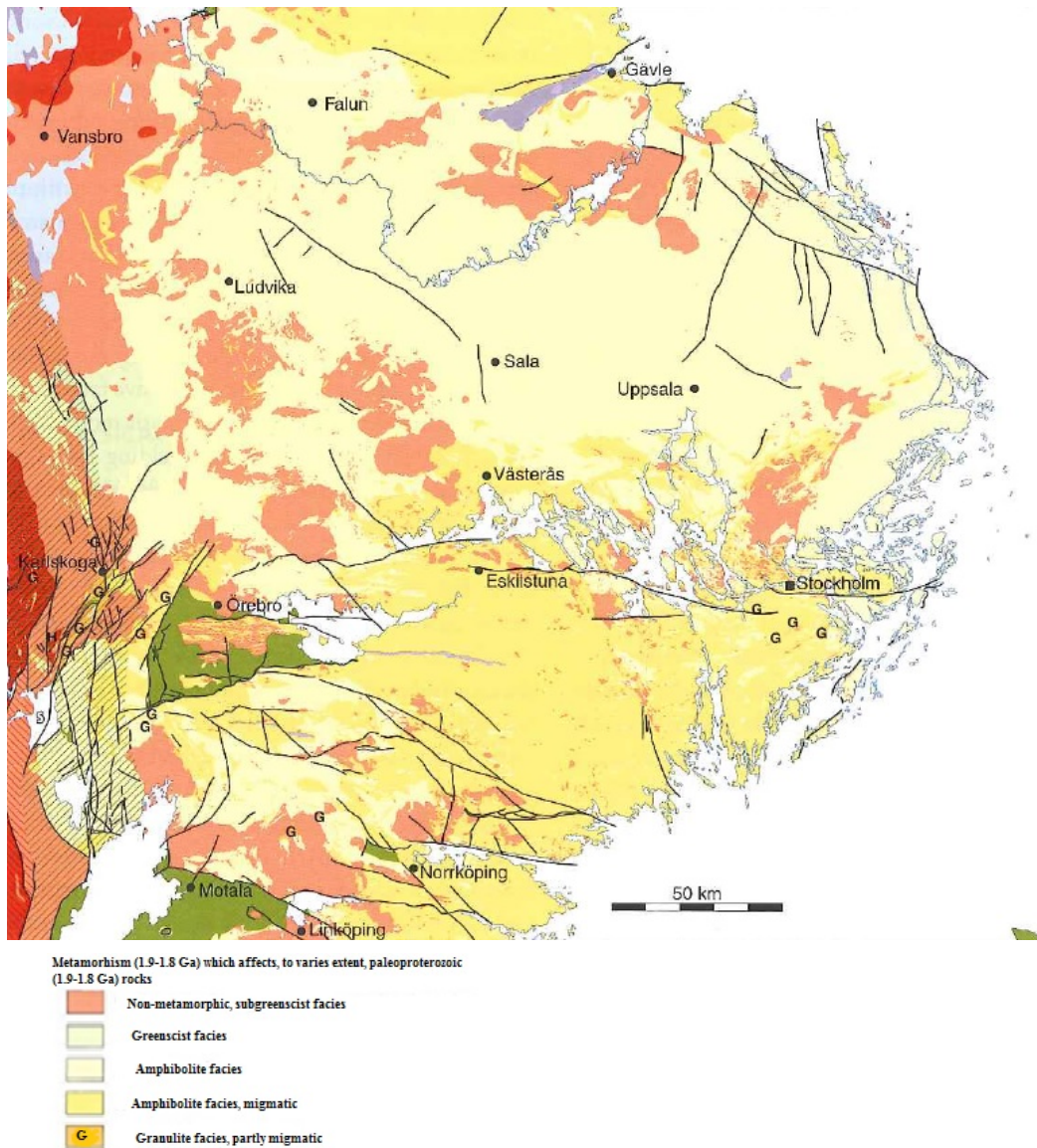


Figure 6. Map of metamorphic grade in Bergslagen province (Copyright by Stephens et al, 2009, SGU).

Figure 7 shows Bergslagen with its structural trends and domains together with magnetic anomalies. In this map Bergslagen has been divided into four different parts depending on the different tectonic foliation and metamorphic grade, (1) the northern, (2) the central, (3) the southern and (4) the western areas. The northern area (1) shows a network of steeply dipping, highly ductile strain belts that strike WNW-ESE which was formed under amphibolite-facies conditions. Later during low-grade metamorphism, brittle deformation took place along these zones. In the central area (2), which is the main part of Bergslagen, major folding with constructional ductile strain dominates and two major fold phases have been identified (Stephens et al, 2009). The folds of the older one (F_1) are tight, isoclinal

folds that are overturned to the west with axial planes dipping east. The stress orientation for the F_1 folding is east-west. Refolding of the earlier F_1 folds resulted in the upright F_2 -folds deformation (Persson & Sjöström 2003; Stålhös 1976; Stephens et al, 1996). The compression direction of the younger, second deformation phase, F_2 , was in north-south direction. Intensity variation of the folding was suggested by Stålhös (1991) and explained by competence differences between the intrusions, massive volcanic rocks and layered supracrustal rocks. An east-plunging stretching lineation has been recognized as well as a steeply dipping foliation (S_1) sub-parallel to the bedding (S_0) and parallel to the axial surface of F_1 -folds with an east-west strike (Persson & Sjöström 2003; Stålhös 1991; Allen et al 1996). In the southern domain (3) amphibolite-facies metamorphosed structural belts with WNW-ESE strike, resembling the north domain, dominate together with a few smaller zones with lower metamorphic grade but with the same orientation. The western part of the domain is affected by folding resembling the structures in the central area (2). In the western part (4) a complex interference of both pre-Sveconorwegian and Sveconorwegian structures occurs. It is dominated by greenschist metamorphic conditions with a ductile high-strain zone that strikes N-S. The Svecofennian higher-grade metamorphic rocks and the un-deformed rocks are located between the Sveconorwegian affected rocks (Stephens et al. 1996; 2009). The high magnetic anomalies are thought to be generated by magnetite, buried amphibolite and gabbroids.

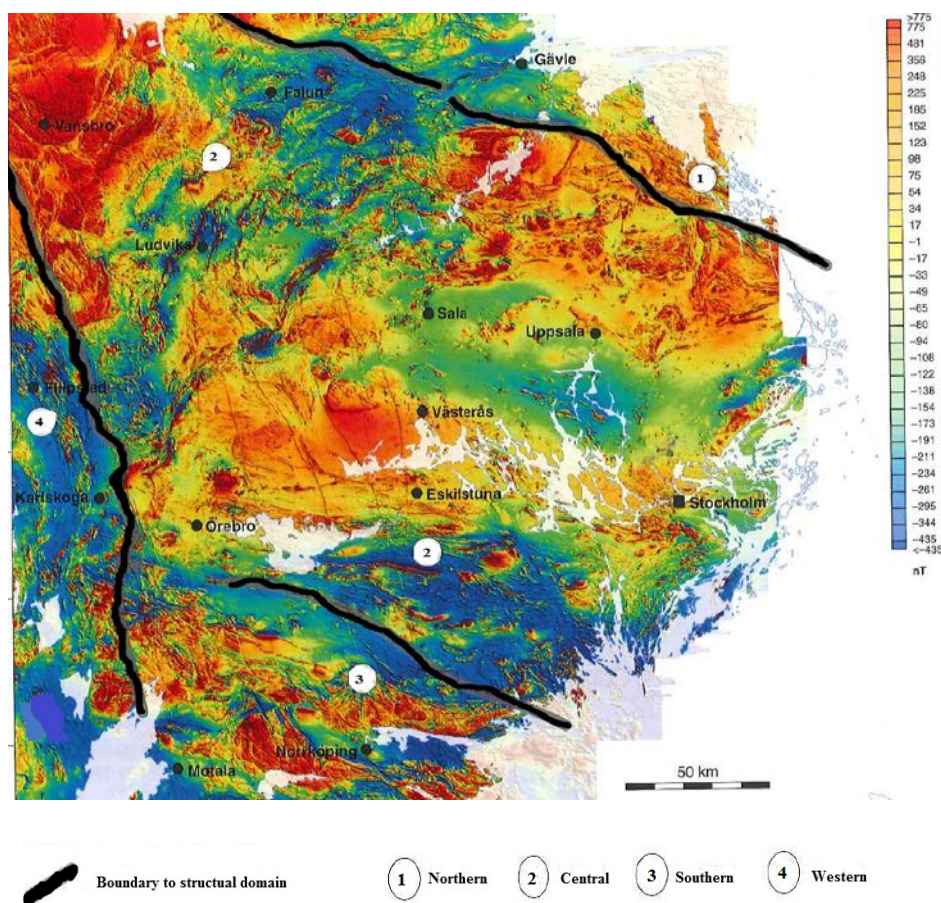


Figure 7. Magnetic anomaly map with the four different structural domains (Stephens et al. 2009). Red indicates the highest anomaly and blue the lowest.

2.2.2 Geology of the Mälaren Passage, Eolshäll-Smedslätten

The study area for this thesis lies on the Southwest coast of Stockholm in the Mälaren Passage between Smedslätten and Eolshäll (Figure 8). The rocks in the area are dominated by garnet-bearing metagreywackes and mica schists as well as granites and granodiorites. Two types of granites are found in the area, the first is grey to reddish colored, even-grained and uniform (also known as the “Stockholmsgranit”) with excessive pegmatite- and aplite dykes and the second is greyred-red, uneven-grained and uniform. The supracrustal rocks and the deep plutonic rocks have been metamorphosed into gneiss to different degrees. The metamorphic conditions are interpreted to have reached a temperature of 700°C and a pressure of 4 kbar which corresponds to approximately 15 km depth in the crust (Stålhös 1969).

Younger granites, pegmatite and aplite dykes are also a common feature throughout the area. These are mostly present north of Stockholm and occur as narrow strings in the bedrock with a prominent ENE- WNW direction. Later intrusions of basaltic magma created metabasite dykes with a dominant E-W direction. They range from decimeters up to meters in width, and are deformed and often amphibolite altered. Swarms of narrow mafic dykes striking NW-NNW are found, as well as several other generations of younger dykes (Persson et al 2001).

The shear zone network in the area comprises three systems with different directions, NW-SE, NE-SW and E-W. The prominent shear zones form clay filled valleys together with longitudinal lakes. Two fracture zones are interpreted to occur in the study area based on the map from SGU (Figure 8), one with an NE-SW orientation and the other with a NW-SE orientation.

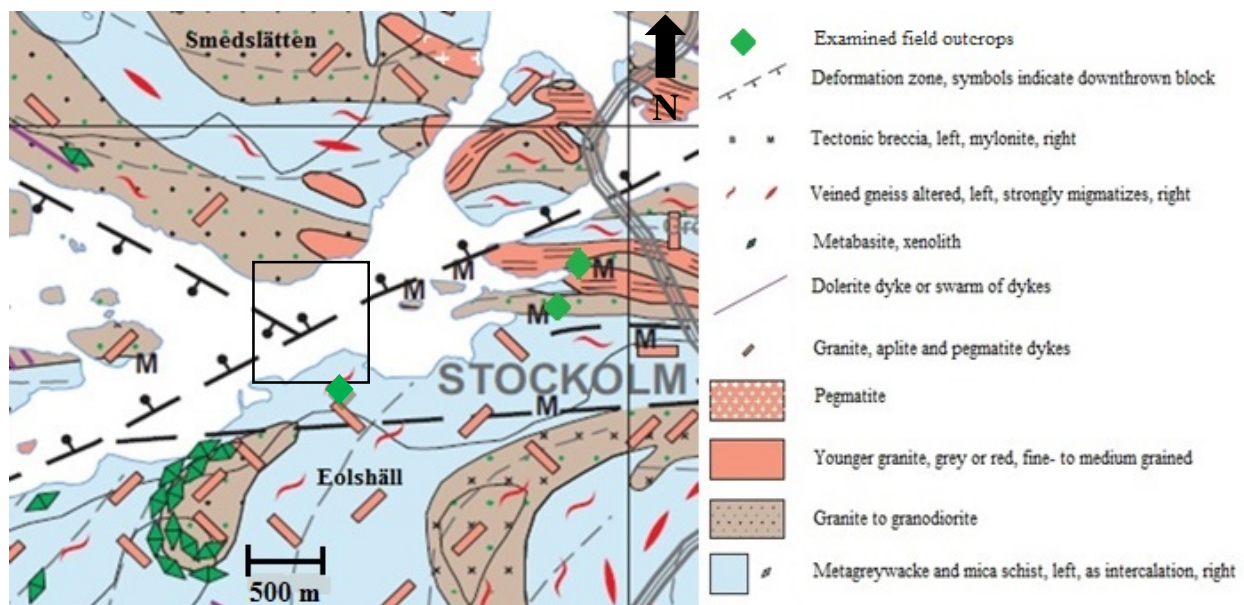


Figure 8. Bedrock map, the black square indicates the Mälaren passage area and green diamonds the location of the additional examined outcrops. (Persson et al, 2001).

2.2.3 Stress field

Several in-situ stress measurements together with focal mechanism of earthquakes have identified the global stress field, including Sweden and Scandinavia. The sources for the present day stress field in the Northern Europe are ridge-push force from the mid-Atlantic ridge, the postglacial uplift following the latest glaciation and the continent-continent collision between Africa and Europe (Stephensson 1988 Bungum et al 1991). The measurements have identified a dominating NW-SE compressive horizontal stress orientation in Scandinavia (Figure 9).

The vertical stress (σ_v) that corresponds to the weight of the overburden rocks is the smallest stress observed, consequently both the maximum horizontal stress (σ_H) and the minimum horizontal stresses (σ_h) are higher. In the uppermost crust where the rocks are less isotropic and homogenous, small scale stress variations occurs from the dominating NW-SE maximum compressional horizontal stress. The gravitational and tectonic stress field is affected by the existence of faults and irregularities of fracture patterns (Stepansson 1988 & 1991).

A detailed study of the stress field in Bergslagen has been carried out for the research and investigation of the Forsmark waste disposal. Even though Forsmark lies around 100 km away from Stockholm the information of the stress regime can still be useful. The results from their measurements indicated that a thrust fault regime dominated. This corresponds to the maximum horizontal compressive stress and the minimum horizontal compressive stress being larger than the vertical compressive stress ($\sigma_H < \sigma_h < \sigma_v$). The dominating orientation of σ_H is NW-SE which correspond to the regional NW-SE direction.

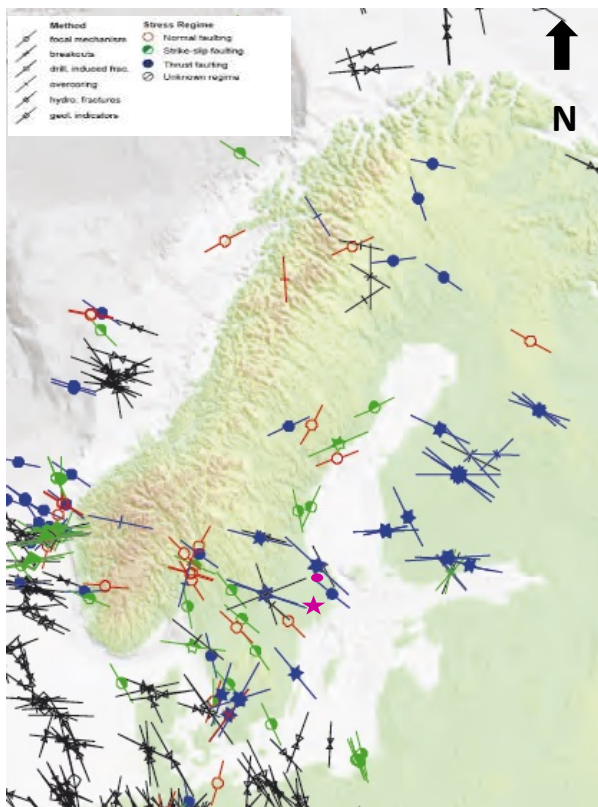


Figure 9. Stress map of Sweden. The purple star marks the research area and the purple dot is the location of Forsmark (Modified after Stephenson, 1998).

The magnitude of the different stresses varies with depth. SKB has defined an orientation of the stress field to 145° (SKB, 2007). Microcrack studies on granites performed in southern Sweden has revealed information about the recent stress direction in basement rocks. Several measurements were made from Uppsala and Västervik and the stress orientation discovered was approximately 140° (Krumbholz et al, 2014).

3. Background information and methods

This chapter outlines background information together with the different methods used for the pre-investigations in the research area from 2013 and the additional methods made for this thesis.

3.1 Structural and engineering geology

The procedure of excavating a rock tunnel below the surface is complex and different pre-investigations need to be considered. The most important one is to examine the surface and sub-surface geology. Depending on the type of geology present in that specific area the excavation could be more or less complicated. Some main factors that play a significant role when building a tunnel are the in-situ stress, rock quality and presence of joints and water. In addition, the effect of time should not be underestimated. Today construction works are required to have a lifetime of at least 100 years. This demands that weathering, natural and/or man-made, is taken into consideration for during this long period of time (Bell 2010).

3.1.1 In-situ stress in Rock

Undisturbed rock mass at depth is subjected to certain in-situ stress conditions as a result of the overburden load and tectonic conditions. The overburden load is the weight from material above any given level that causes a vertical compression (vertical stress, σ_v) of the unconfined specimen. The other parameter is the tectonic stresses that the rock has been subjected to, either from present day tectonic activity or residuals from past tectonic activity (Bell, 2010). The tectonic stresses are strongly directional and mostly horizontal (horizontal stress, σ_h). Stress is defined as a force (F) acting on a surface or a point (area, A) and the relationship is defined as

$$\sigma = \frac{F}{A} \text{ (Pa)} \quad (1)$$

The surface can for example be an internal feature such as a fault or joint. When this force is acting on the surface it can be inclined to the surface which can be resolved into two components, one perpendicular to the plane called normal stress (σ_n) and another that acts tangential to the surface which is called shear stress (σ_s). When defining the stress at a point within a rock mass it is necessary to enclose that point into a small volume that is surrounding it. The stress at that certain point can then be represented by a cube with three stress components on each of the sides, one normal (direct) stress (σ)

and two shear stresses (τ) (Figure 10A). There are now nine stress components, however the pairs of shear stresses (τ_{xy}, τ_{yx}), (τ_{zy}, τ_{yz}) and (τ_{xz}, τ_{zx}) are referred as conjugate shear stresses, hence they have the same value. There are now six independent components of stress at a point ($\tau_{xy}, \tau_{yz}, \tau_{xz}, \sigma_x, \sigma_y, \sigma_z$). These values will vary dependent on the axial orientation as they are referred to, however it is always possible to find a coordinate axes in which all of the shear stress components will vanish. These axes are called the principal axes of stress and the forces that are acting on the surface plane of that volume element are called principal stresses. These stresses are positive (compressional) and normal, and are denoted the symbols σ_1, σ_2 and σ_3 , where σ_1 is the major principal compressive stress, σ_2 the intermediate principal compressive stress and σ_3 the minor principal compressive stress (Figure 10B) (Hoek & Brown, 1980). Any stress field, whether natural or man-made can be described with principal stresses.

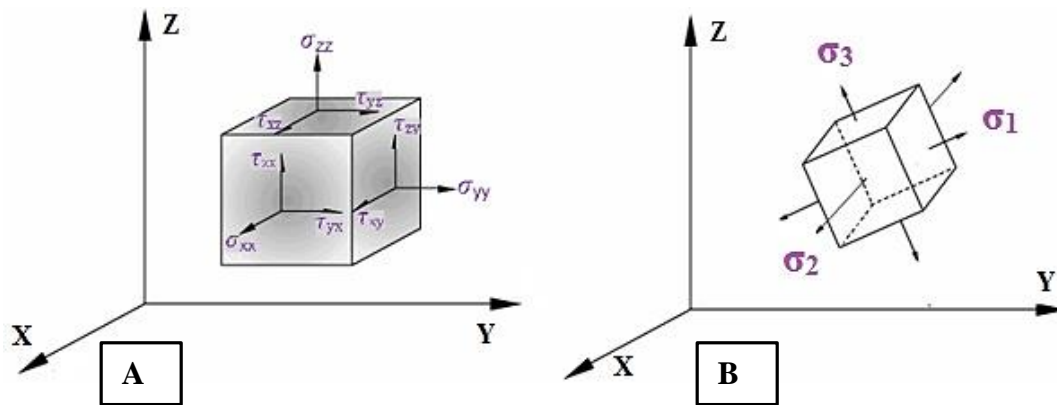


Figure 10A and B. Stress components. Figure 10A is all the stress components at a point. Figure 10B is the principal compressive stresses (modified after Hoek & Brown, 1980).

The magnitude and orientation of the current tectonic stress field affect the response on the ground during excavation. In the vicinity of the opening the current stress field will be disrupted and new stresses are induced around the tunnel face. The direction and magnitude of the stresses in the ground varies at different locations and the knowledge of these is crucial when designing a tunnel. The instability of the rock enhance large consequences on the behavior of the excavation (Hoek & Brown, 1980; Bell, 2010).

3.1.2 Deformation = translation + rotation + strain

Deformation of a rock mass is defined by how a material changes or responds to certain forces that are applied to it. How the rock mass will respond depends on the type of stress, the stress rate that is applied and the environmental conditions such as temperature and depth. Strain is a word widely used within geology when talking about deformation. The definition of strain is change in shape, size or volume of a material. Strain and stress are concepts that overlap and are linked to each other when describing

deformation processes. Stress is the force causing deformation and strain is how the material is being deformed. Based on these two parameters there are three different stages or types of deformation, elastic, ductile (plastic) and brittle (S.K Ghosh 1993). Figure 11 shows the relationship between stress and strain and what type of deformation that is generated.

Elastic deformation of a rock mass occurs from small differentiated stresses that are less than the yield strength of the rock. Within this range the shape change is small in response to the stress and the deformation occurs successively, such as bending or stretching. If the stress applied to the rock begins to decrease the material will return to its initial state.

Ductile (plastic) deformation is defined as permanent deformation without fracturing. Ductile deformation can occur for a long time if conditions are stable (e.g creep deformation). Folding is a result of ductile deformation. It forms when compressional stresses are acting on the rock over a long time and the strain rate is low. The structures can vary from grain scale up to several km in length and width. There are different kinds of folds with the simplest ones being monocline, antiform and syncform. Monocline folds forms when the horizontal stratum is bent upwards with the resulting fold limbs being horizontal. When the horizontal stratum has been folded upwards and the resulting two limbs are dipping away from the hinge it is called an anticline fold. Syncline folds are the opposite of anticline, where the strata instead have been folded downwards and the two limbs of the fold are dipping inwards.

Brittle deformation is when the rock is being deformed to the extent that it breaks. The process begins with fracturing of the rock along its weaker parts, resulting in fault displacement along the fracture. The size of the fracture planes and displacement varies from micro- to macro scale. Faults can be divided into several types depending on the direction of displacement. The main types are dip-slip and strike-slip faults. Dip-slip is when the offset occurs in the dip direction of the fault and strike slip is when the offset is horizontal and parallel to the strike of the fault. Normal faults occur in extensional stress settings and reverse faults in compressional stress settings. Strike slip faults are a result of shear stresses.

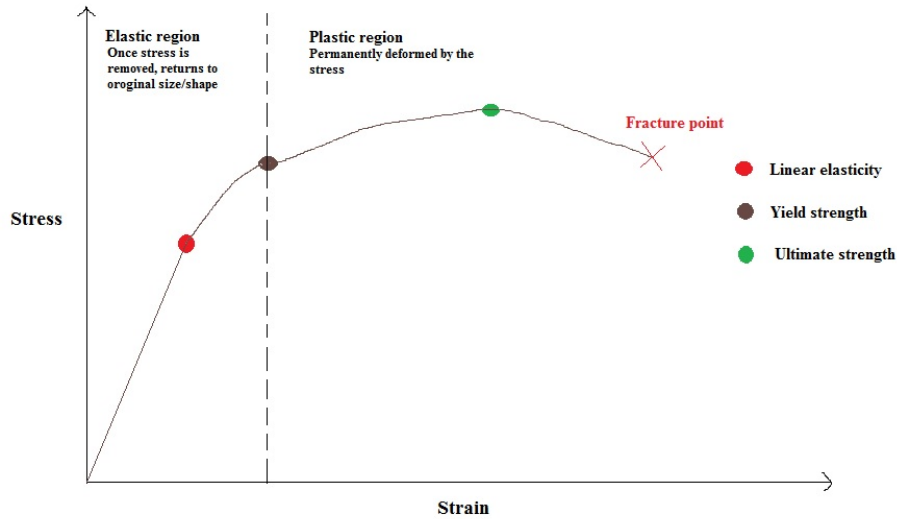


Figure 11. Stress and strain relationship and the resulting elastic and plastic deformations before the rock fractures. The red dot represents the end of the linear elastic relationship. The brown dot represents the yield strength, where the deformation transitions to a plastic behavior. The green dot represents the ultimate strength of the material and the cross represents the fracture point.

3.1.3 Strength

The strength of a rock is a measure of its ability to resist failure under stress. Rocks close to cavities are often to a certain degree intersected with fractures and are weaker. After the excavation, if the rock cannot resist the newly formed principal stress state the rock will fail. There are different types of strengths such as tensile-, compressive- and shear strength which are directly connected to the type of stress applied to the rock.

The majority of hard rocks behave elastically if the stress level is below their yield strength. Calculating axial strain (ϵ) of a deformed rock is the ratio between the decreased length (dl) of the deformed material and the original length (l) (Equation 2). Strain and stress rates in elastic material often show a linear relationship (Figure 11) from where the Young's Modulus (E), which is a measure of stiffness of an elastic material, can be calculated. The relationship is defined by equation 3:

$$\epsilon = \frac{dl}{l} \quad (2)$$

$$E = \frac{\sigma}{\epsilon} \quad (3)$$

3.2 Geotechnical methods

This chapter outlines the earlier investigation methods that have been made in the project and was available for this thesis.

3.2.1 Geophysical measurements

Geophysical measurements were carried out on Lake Mälaren by Ramböll Denmark in June 2013. Seismic measurements were carried out in the Mälaren passage between Eolshäll and Smedslätten, along Bromma's southwest beach line and around Stora Essingen. Resistivity measurements were performed in four lines in the Mälaren passage. The purpose of the geophysical measurements was to localize and estimate the depth to the bedrock and also to localize the boundary between the different layers.

The reflection seismics was performed using a single channel low frequent marine reflection seismic method. The equipment comprises a Georesources Geospark 200 sparker as a source and a hydrophone streamer with five elements as receiver. Both the sparker and streamer were dragged 15 m behind the boat with an offset of 6 m. The method for reflection seismics is based on sound waves. By generating sound waves that propagates into the Earth's crust they will eventually reflect back differently depending on the bedrocks composition. The time it takes for the wave to travel from the sender, hence reflect on the material and travel back to the receiver, is logged. Due to different densities of rock, soil and ocean sediments the reflected wave time appear differently and the boundary between the sediment layers and the bedrocks subsurface can therefore be detected.

Resistivity measurement is a method where the ground is mapped based on materials electric resistance. This is done by transmitting direct current through electrodes to the ground. Four electrodes are used for one measuring point, two for transmitting direct current and two for measuring the potential. For this project Ramböll Denmark used a cable that was 441 m long with 64 electrodes with spacing of 7 meters between them. During the measurements a current of 0,7 Ampere was sent though the electrodes with current pulses varying from 0,6-1,2 seconds. The instrument from which the data was logged is a Terrameter LS from ABEM Instruments AB. Resistivity logging was also performed in several points in the water in Lake Mälaren with a resistivity probe that gives high vertical resolution and the possibility to log several points in a short time (Wisén, 2013).

In 1968, AB Prospector did refraction seismic over the passage. Comparison with the other seismic methods revealed that the refraction seismic gives more information about the bedrocks quality and is a good method to interpret areas with poor rock quality, i.e potential weakness zones. The method is similar to the reflection seismic. An elastic wave is sent towards the ground and geophones on the surface detect the velocities of the P-wave. The P-wave is compressional and it can travel through any type of media (solid, gas, fluid). The velocity of the wave depends on different parameters, such as density, pore-fluids, pressure and saturation. Non- or less cohesive, weathered rocks corresponds to lower velocities. The main focus has therefore been on the low-velocity zones in the Passage.

3.2.2 Drill core

In order to find crucial information about the sub-surface geology, core drilling was carried out from October 2014. Core drilling for construction work is performed to determine the quality of the rock and to establish if any large weakness zones are present in the area. If the zones are present and drilled through important information such as orientation, extent and their location in relation to the tunnel can be determined. This is of great value, both in order to determine the required reinforcement needed and construction methods.

The drill core information for this Master thesis is provided from a borehole located on the south shore of Mälaren, between Eolshäll and Smedslätten (Figure 12). The drill core length was intended to be approximately 400 m, but because of delays and drilling problems, the available length for the thesis was 271 m. All the different parameters of the borehole are presented in Table 1. During drilling procedure the orientation of the borehole changed. With the increasing length of the borehole the elevation slowly decreased. Figure 12 shows a profile of the borehole and how the dip decreases with length.

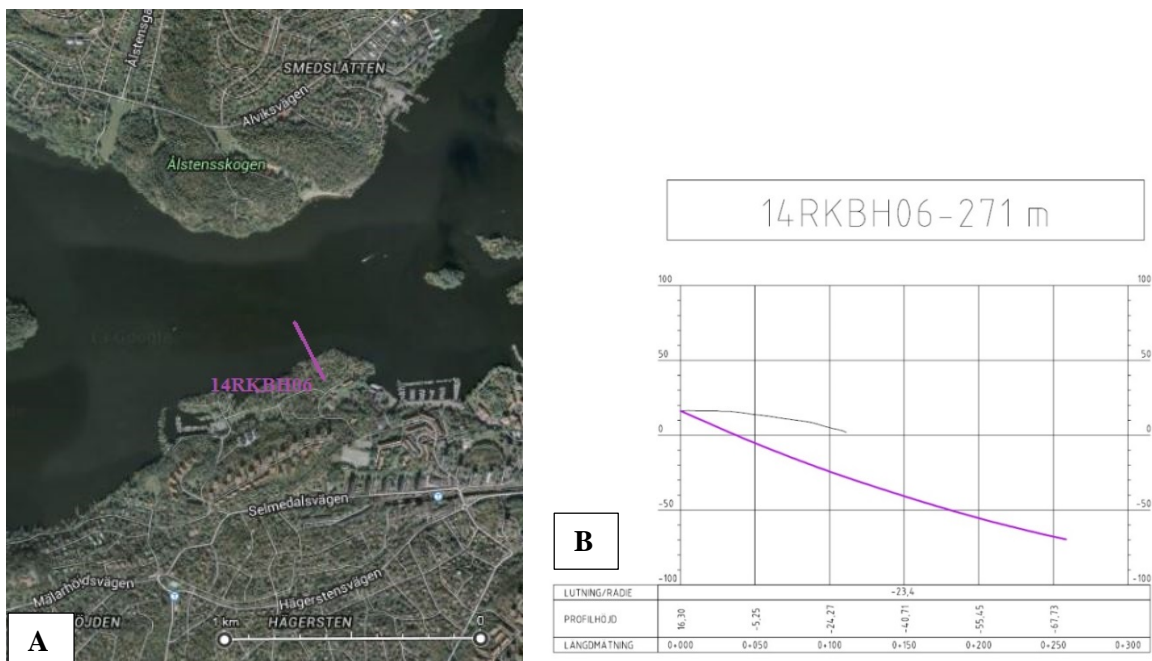


Figure 12. Picture A is an aerial map with the borehole location (image:google maps, 2015). Picture B is the borehole profile and the line on top is the ground area (AutoCad, 2015).

Table 1. Borehole parameters.

Borehole	Length (m)	Strike (°)	Dip (°)	Bore hole diameter (mm)	Core diameter (mm)
14RKBH06	271	332.5	23.4	76	50

3.2.3 Procedure

The procedure of core drilling begins with a drill bit being mounted on a core tube. The bore machine puts a pressure on the tube which makes it rotate together with the core bit and starts to eat its way through the rock. Within this tube there is a stationary inner tube that collects the drill core. Depending on the quality of the rock different tubes are used, for this borehole a triple tube was used to minimize small rock fragments, poor parts and clay disappear.

The core was oriented with a Reflex Act II Rd. This product measures the orientation of the drill core continuously while drilling, and with the advanced digital technology it provides consistent and accurate orientation data. The infrared technology and time stamping decreases the risk for human error. The Act II Rd is mounted between the drill core head and the inner tube. When the inner tube is full (commonly after 3 m) and taken up on the ground, the core head is detached and a digital device is connected to the Act II Rd. Turning the tube into the right orientation is made by hand and the digital device indicates on a screen when it is in right position. The short side of the inner tube the last core piece is marked with a pencil in the lower edge of the tube (closest to the ground) and after that a mark on the long side of the same piece is made to be sure not to lose the information. This method is good when drilling in hard, fine and massive rock, however when the rock quality is poorer and the core bit is not fixed in the tube or the drilling procedure is disrupted and hard to get an orientation.

3.2.4 Water-loss measurements

Water-loss measurements were carried out in the borehole. This was done in 3 m sections with two different pressure values made in the three steps, 2 bar – 4 bar – 2 bar. Each section and pressure range was measured for five minutes. The results show how many liters of water that has disappeared out of the hole through fractures and weakness zones in each section at the different pressures.

3.3 Methods applied in this thesis

This chapter outlines the methods that have been applied in this thesis. Four main softwares have been used to acquire crucial information from the background data. These are DIPS 6.0, AutoCad, Roclab and Phase2 8.0 (RS2). Dips is a structural geology software which was used to obtain orientation of the measured fractures and to evaluate the main fracture groups. The second software, AutoCad was used to create the borehole profiles and the third software, RocLab, was used to determine and calculate the rock parameters needed for the modeling. Phase was used for the reinforcement 2D-modelling of the tunnel. It is a numerical modeling program that calculates stress and strain of the rock and visualizes how the tunnel will affect those parameters.

3.3.1 Drill core mapping

Drill core mapping was carried out on the 271 m long core. Lithological characterization and fracture minerals were mapped. First, the entire core had to be oriented by rearranging the different core bits between all fractures. The pencil line, from the marked orientations made during the drilling, is then extended through the entire core. Since the core has many fractures and the drilling procedure was problematic, there were many areas without orientation marks that decreased the possibility for orientation. After that, several different sections with varied length were marked through the borehole based on rock type and fracture intensity. All the mapping parameters and loggings were done for each section. For the lithological determination grain size, color and rock type were determined in each of the sections together with the main fracture minerals.

For the mechanical part of the mapping different rock mass classifications were determined, such as RQD, Q and RMR. The Q system was introduced by Barton et al (1974) and is based on several case histories of underground excavation. The numerical value of the Q-index varies on a logarithmic scale from 0,001 to 1,000 and is based on six parameters which are calculated according to this equation (During 2006):

$$Q = \frac{RQD}{J_n} * \frac{J_r}{J_a} * \frac{J_w}{SFR} \quad (4)$$

The first parameter is the Rock Quality Designation (RQD). It is defined as the percentage of intact core pieces longer than 10 cm for the total length of the core. It is calculated according to equation 5 and the values given are in a percentage and ranges from 0-100%.

$$RQD = \frac{\text{total length of core pieces } > 10 \text{ cm}}{\text{Total length of core}} * 100 \quad (5)$$

The second parameter is J_n which is the joint set number. The quote RQD/J_n is a rough measurement of block or particle size of the rock. J_r is the joint roughness number and J_a is the joint alteration number. This quote, J_r/J_a , corresponds to the frictional characteristics and the roughness of the joint walls or the filling material; generally speaking it is the inter-block shear strength. J_w is the joint water reduction factor and SFR is the stress reduction factor. The quote J_w/SFR corresponds to the active stress in the rock. For drill cores this is hard to establish since you only see a small part of the whole bedrock. Therefore these two parameters are often set to 1. Table 2 shows the different index values and rock classes for Q.

The second system is the Rock Mass Rating system (RMR). This system is also based on six parameters. The first parameter is the uniaxial compressive strength of the rock, hence how hard the rock is. The second parameter is the Rock Quality Designation (RQD). The third one is spacing of discontinuities, the distance between each fracture, and the fourth the condition of the discontinuities (e.g. rough or planar). The fifth is the groundwater conditions and lastly the orientation of the discontinuities. Table 2

shows the different rock classes and the total value for the rock based on the six parameters for RMR (During, 2006).

Table 2. Q- and RMR values and rock classes (Modified after Barton et al 1976:During 2006).

Rock class and values for Q and RMR								
Q								
>400	400-100	100-40	40-10	10-4	4-1	1-0.1	0.1-0.01	0.01-0.001
Exceptional good	Extremely good	Very good	Good	Acceptable	Poor	Very poor	Extremely poor	Exceptional poor
RMR								
100-81	80-61	60-41	40-21	20-0				
Very good	Good	Fair	Poor	Very poor				

3.3.2 Sub-surface fracture analysis

In order to characterize the subsurface fracture network and gather some fracture data from the zone fractures were measured and analyzed. In the worst parts of the drill core orientation could not be made and hence fractures could not be measured. The method used is simple but good and it gives a presentable value and an idea of the main direction of the fractures and network- or groups of fractures. A core piece is oriented on a table in the same direction as the borehole was drilled, strike 332.5° and dip 23.4°, and when in right position the fracture surface is measured with a compass to get the strike and dip. The results were plotted in the stereographic projection plot program Dips 6.0. A total of 125 fractures were measured. The analyses were made both with all the fractures together and also divided into two intervals, 0-135 m and 180-270 m. Measurements from the zone is sparse due to lack of orientation.

3.3.3 Field work

In order to get more information about the research area, additional field work was carried out. The outcrop area was picked after a careful study of the geological map (Figure 8). The area hosts the same rock types as the drill core and lies close to the fracture zone. The main purpose was to gather more information about the area and also to look for kinematic indicators and the existence of mylonite.

3.3.4 2D modeling

Rocks respond differently to excavation depending on the rock quality since the strength will differ. To visualize stability problem in different rock qualities different 2D-models have been made based on two sections from the core and with different material properties. All the analysis has been determined and compared based on displacement. The computed data for every model is presented in Appendix 1.

3.3.4.1 RocLab

RocLab is a software used to assess rock strength parameters. Both the generalized Hoek-Brown criterion and the Mohr-Coulomb fit can be established. Visualization in form of strength as a function of major and minor principal stress of the input parameters is given which enables the user to visualize how the variation in a rock parameter would change the strength. The models were made based on parameters from the Hoek-Brown classification. This classification is based on four different parameters that need to be established. The first one is the unconfined compressive strength of intact rock (σ_{ci}). The second parameter is the geological strength index (GSI), which is based on the blockiness of the rock and the surface fracture properties. The intact rock parameter (m_i) is the third one and is a specific value for each rock that affects the slope of the failure curve. Lastly the fourth parameter is the disturbance factor (D), which expresses the excavation damage of the rock mass close to the tunnel. When these values are put into RocLab the generalized Hoek-Brown strength parameters of the rock mass can be determined. There are three parameters given, m_b , s and a . The first parameter, m_b , is a reduced value for the rock mass constant m_i for the intact rock. Parameters s and a are constants which are depended on the characteristics of the rock mass.

3.3.4.2 Phase2

Phase2 is a 2D elasto-plastic finite element stress analysis program for underground or surface excavation in rock and soil. Different stress parameters, rock properties, reinforcement methods and much more can be modelled in Phase2. All the parameter properties are defined in different stages in the model setup that is calculated and then the results are displayed. In this stage it is possible to visualize the displacement, stress vectors, yielded elements, failure contour and much more.

3.3.4.3 Model Setup

By analyzing the information from the core mapping different representable values for the rock parameters to be used in RocLab were established (Figure 13). One set of parameters were made for good quality rock and one set were made for poor quality rock (the zone). The quality differences are represented by changing the two parameters, unconfined compressive strength of intact rock (σ_{ci}) and geological strength index (GSI). GSI is the parameter that is changing the most. This is because of the larger fracture intensity of the poor quality rock and the more altered fracture surface.

Parameters for Good Rock Parameters for Poor Rock

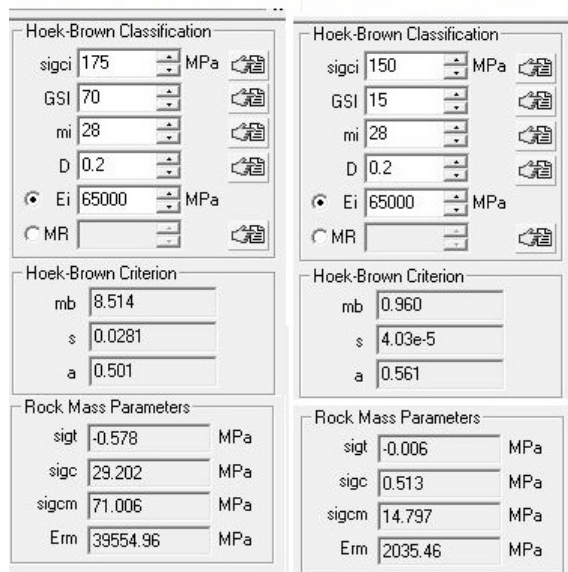


Figure 13. Parameters for good and poor rock quality used in the models. The Hoek-Brown classification is the input parameters while the Hoek-Brown criterion and Rock Mass Parameters are the calculated values.

In Phase2 a horseshoe tunnel was constructed with length of 7 m, height of 8 m and roof of 2 m with a total area of 71 m². An outer grid was set as three times the tunnel size followed by meshing of the area. The finite elements are smaller close to the tunnel to increase the model resolution there. From RocLab the Generalized Hoek-Brown values (mb, a and s) and the Young’s modulus (Erm in RocLab) were copied into Phase2 to set the different material properties. Both plastic and elastic properties were set for good respectively poor quality rock. Table 3 shows the assigned materials number and parameters for the different models when further discussed. The same stress field was used in all models with σ_1 being the largest, vertical stress of 10 MPa and the horizontal stresses σ_3 and σ_2 were given a value of 5 MPa.

Table 3. The four material parameters calculated with in the different models based on their properties.

	Rock Quality	Properties
Material 1	Good	Elastic
Material 2	Poor	Elastic
Material 3	Good	Plastic
Material 4	Poor	Plastic

3.3.4.4 Description of the different models

Four different types of models were made to mainly illustrate how the fracture zone (the poor rock quality) will affect the construction of the tunnel compared to the areas outside of the zone. They also illustrate how, and if, the excavation method and the time when reinforcement is installed, affect the deformation and displacement of the rocks. The models are explained further below. In the reinforced models the same bolt- and concrete properties have been used (data presented in Appendix 1).

3.3.4.5 Tunnel without support

The first and simplest model is the tunnel being excavated without support to see how the deformation propagates and how it differs between the different materials. In stage one in this model, the material properties were set and the excavation occurred in stage two.

3.3.4.6 Tunnel with preinstalled bolt pattern

These models are a continuation from the previous models, but here a bolt pattern has been installed in the first stage then the excavation of the tunnel was made in stage two. The model was made to demonstrate the effect of installing the support close to the tunnel face.

3.3.4.7 Tunnel excavation in two steps

Another way of excavating the tunnel, to see if the displacement change, is by excavating it in two steps. Therefore this model was made in four stages and the tunnel was excavated at the roof first and then the floor and it was pre-reinforced. At stage one bolts and liner were added to the top half of the tunnel. Excavation of the tunnel top was set for stage two. In stage three bolts and liner were added to the bottom half of the tunnel. Finally in stage four the bottom of the tunnel was excavated.

3.3.4.8 Round tunnel with internal pressure

The fourth model is a round tunnel. This tunnel geometry does not correspond to the geometry of the constructed tunnel. This, however, allowed modelling of the rock response to excavation to see if the rock would deform before the reinforcement was installed. The procedure of this model is to add a uniform distributed internal load in stage one. The direction and magnitude of the load is equal and opposite to the in-situ stresses applied in the model to generate a balance between the pressure in the tunnel and the stresses in the rock. After that the magnitude of the load is gradually being reduced from factor 1 (magnitude same as stress) to 0 (no load applied) in stage 1-10. To determine when to install the bolts in this model an additional one was made with bolts added in stage one and then generated to stage 0. The stage where the bolts started to yield was determined to be the best stage for installation of support.

4. Results

4.1 Geophysical measurements

The area where reflection seismic and resistivity measurements were carried out is presented in figure 14. Blue lines show the reflection seismic measurements and the four purple lines represent the resistivity measurements. The reflection seismic gave an indication of the layer boundaries. The seismic and resistivity measurements were interpreted together to estimate the depth to the bedrock.

The result is presented in figure 15. A white area where no data occurs toward the east which is

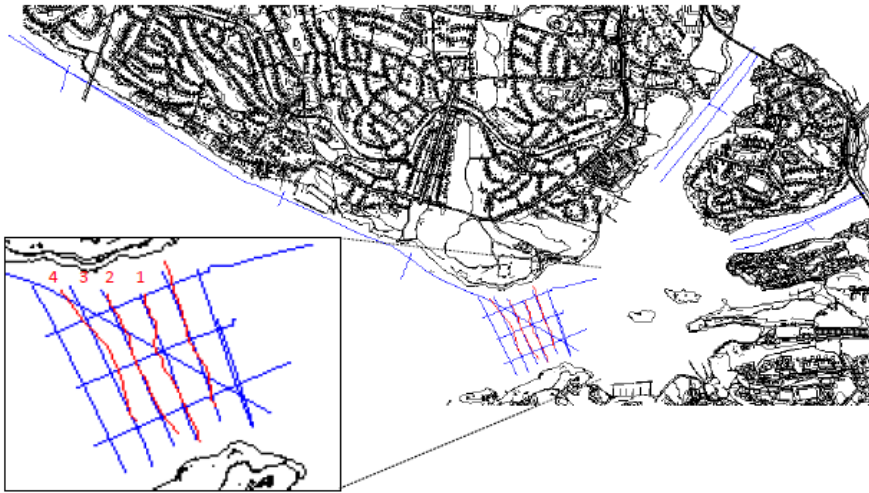


Figure 14. The area where reflection- and resistivity seismic was carried out. Blue lines represent the reflection measurements and purple lines the resistivity measurements (Wisén, 2013)

interpreted as technical problems or gas filled organic sediments (Wisén 2013).

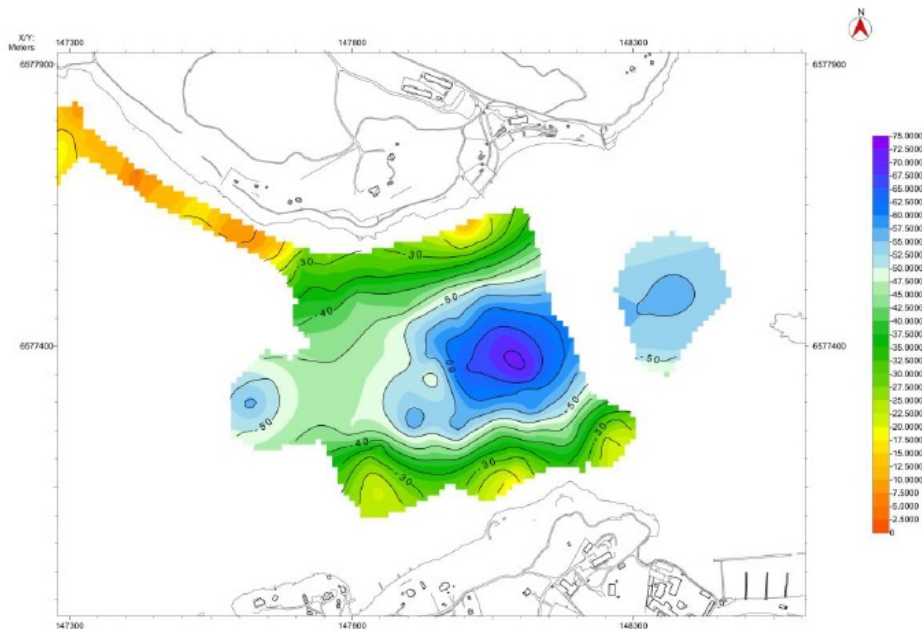


Figure 15. Elevation map of the area with the interpreted bedrock depth from both seismic- and resistivity measurements

The results of the resistivity measurements are profiles from the four lines (Figure 16-19). These have later been modified together with the geotechnical drilling measurements (see below) to get a better interpretation of the bedrock. The resistivity profiles are oriented from north to south (Smedslätten to Eolshäll) with line 3 closest to the borehole (Figure 18). The small white lines in the resistivity profiles represent the geotechnical JB-drillings and the numbers above them are the distance from the respective line. The resistivity of the water in Mälaren was also logged and the average value was 68 Ohm. Profiles 2-4 enhance some areas with a decrease or drop in resistivity. These decreases indicate that there should be something with a lower conductivity in these areas. This could possibly be because of a poorer rock quality which likely increases the water flow in the areas.

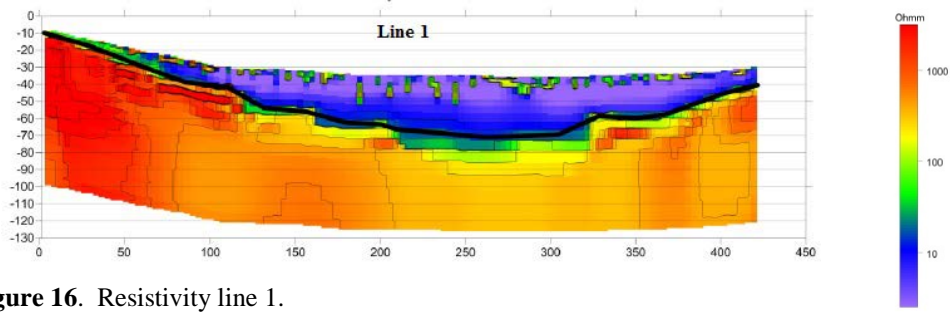


Figure 16. Resistivity line 1.

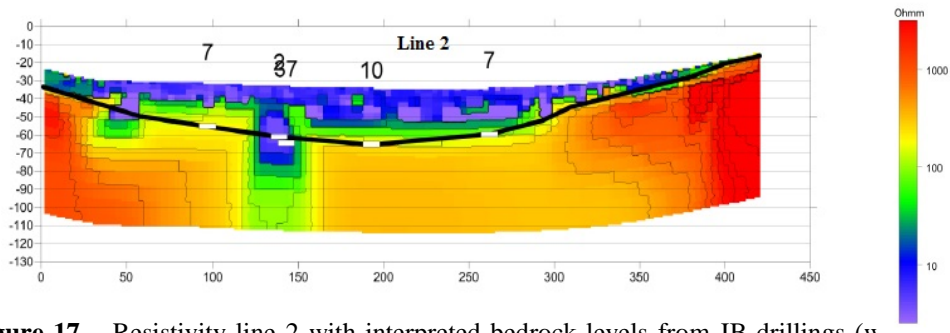


Figure 17. Resistivity line 2 with interpreted bedrock levels from JB-drillings (white box). The numbers are the JB-drilling distance from the line in meters.

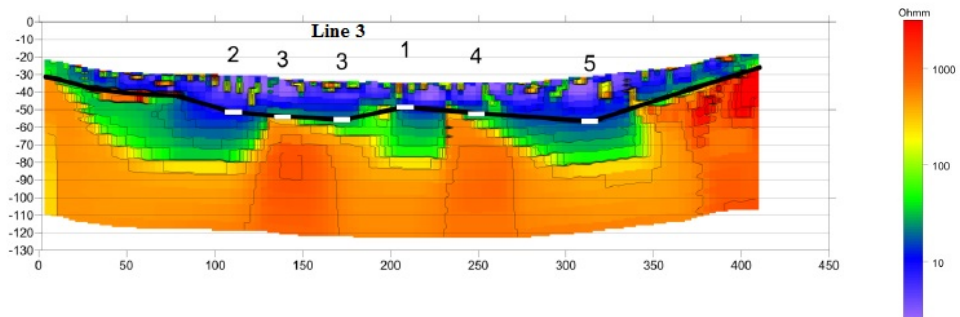


Figure 198. Resistivity line 3 with interpreted bedrock levels from JB-drillings (white box). The numbers are the JB-drilling distance from the line in meters.

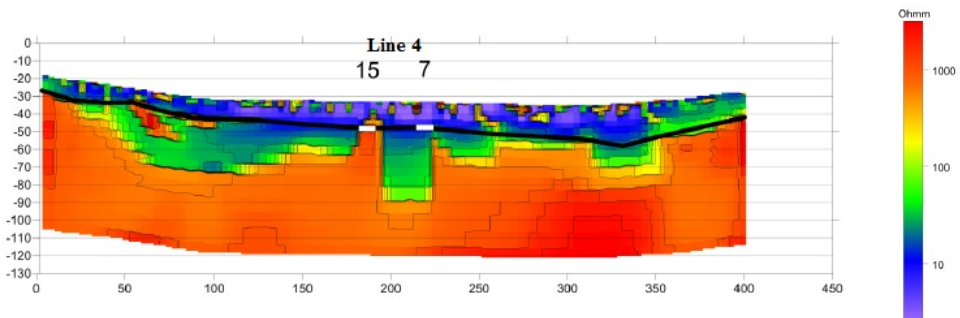


Figure 189. Resistivity line 4 with interpreted bedrock levels from JB-drillings (white box). The numbers are the JB-drilling distance from the line in meters.

Figure 20 shows the resistivity lines and the borehole in a plan view. The light blue lines are the four resistivity lines (1-4 from E-W) and the purple lines are the areas with a decrease in resistivity noted from the profiles. The blue line is the borehole and it is notably that the borehole does not reach the anomalies from the resistivity measurements.

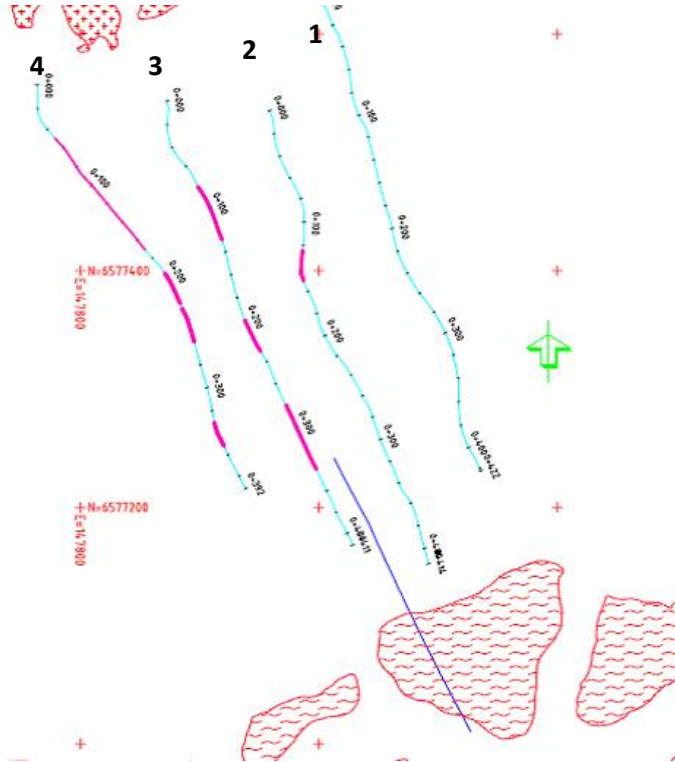


Figure 20. Borehole and resistivity measurements.

4.2 Water-loss measurements

The results presented in table 4 are the borehole sections where water-losses were present. In the other sections no water-loss was detected. Water-losses were detected almost along the entire borehole but with different intensities and distances. The most frequent losses appear after borehole length 200 m with only a few sections in the first 100 m. There are four sections or three main areas with the most prominent water-losses with the highest almost up to 9.0 liter/min. The first area is a six meter long section in the interval 139.0-145.0 m, the second in the interval 226.0-229.0 and the third at 166.0-169.0 m (Table 4).

Table 4. Results of water-loss measurements in the borehole in liters/min.

Bore hole length (m)	Water-loss l/min			Total water-loss l/min
	2 bar	4 bar	2 bar	
31.0-34.0	-	0.10	-	0.10
49.0-52.0	1.10	2.0	1.0	4.10
52.0-55.0	0.60	1.40	0.30	2.30
124.0-127.0	0.30	0.90	0.50	1.70
127.0-130.0	0.70	1.40	0.65	2.75
139.0-142.0	1.80	3.90	1.70	7.40
142.0-145.0	2.20	4.10	2.10	8.40
163.0-166.0	0.40	1.10	0.40	1.90
166.0-169.0	1.80	2.60	1.60	6.00
178.0-181.0	0.40	1.60	0.50	2.50
199.0-202.0	0.30	0.60	0.40	1.30
220.0-223.0	1.00	2.10	1.00	4.10
223.0-226.0	1.10	2.00	0.90	4.00
226.0-229.0	2.20	4.60	1.90	8.70
238.0-241.0	0.90	1.25	1.00	3.15
241.0-244.0	0.60	0.85	0.60	2.05
244.0-247.0	1.10	1.40	1.00	3.50
265.0-268.0	0.30	0.60	0.40	1.30
268.0-271.0	0.40	0.90	0.60	1.90

4.3 Drill core mapping

The drill core is dominated by dark-grey meta-greywacke locally found with garnets. The color, grain-size, quartz and feldspar content vary through the core. The most common fracture minerals are calcite, pyrite and chlorite. There are a few smaller areas with more fractured rock along the entire core and a larger zone with intensely fractured rock between 130-185 m with many areas of crushed rock and core losses (Figure 21).



Figure 21. Meta-greywacke in the drill core length interval 157.0-164.45m.

A graph of Q and RMR-values are presented in figure 22. The x-axis represents the different systems values and classes and the y-axis represents the boreholes length in meters. The main part of the core has a value between 1 and 10 in the Q-system, and thus meaning poor to acceptable rock quality. Between 130-185 m the rock quality is extremely poor, which indicates an area of a larger fracture zone. The same trend can also be seen for the RMR-system. This is also supported by the water-loss measurements which had the three highest values within this interval.

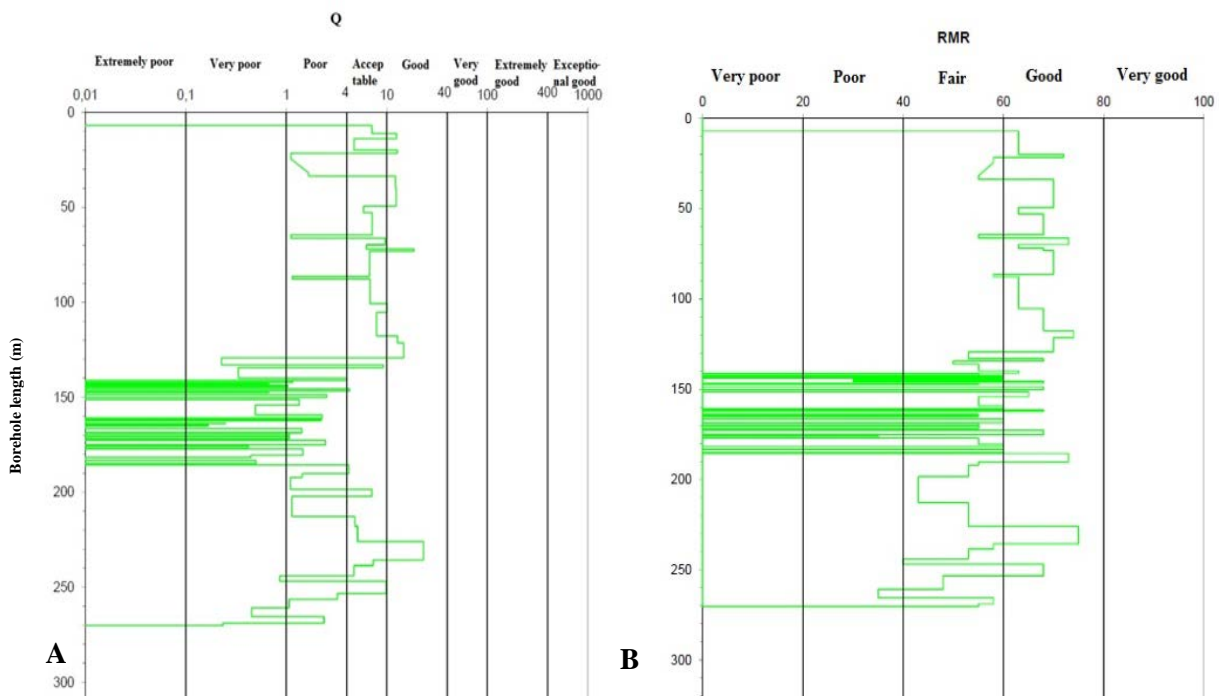


Figure 22A. Graph of Q-values logged on the drill core **B.** Graph of RMR values logged on the drill core.

A fracture zone approximately 55 m thick in the core interval 130-185 m was found. Figure 23 shows the extent and location of the zone on the drill core. The dominating rock type is meta-greywacke

with interspersed rock of granitic texture rich in feldspar and quartz. The grain size varies from fine- to coarse grained. The rock is rich in dark mica, with parts of very brittle character where the core pieces break easily. The open fracture intensity varies through the zone but is overall very high with close spacing. Healed calcite fractures appear in a wide range of the fracture zone but they are more intense and thick the last 20 m. For the first 30 m the prominent fracture mineral is graphite. Calcite and chlorite is also present as well as some clay. A clay altered core piece is present at 177 m length.

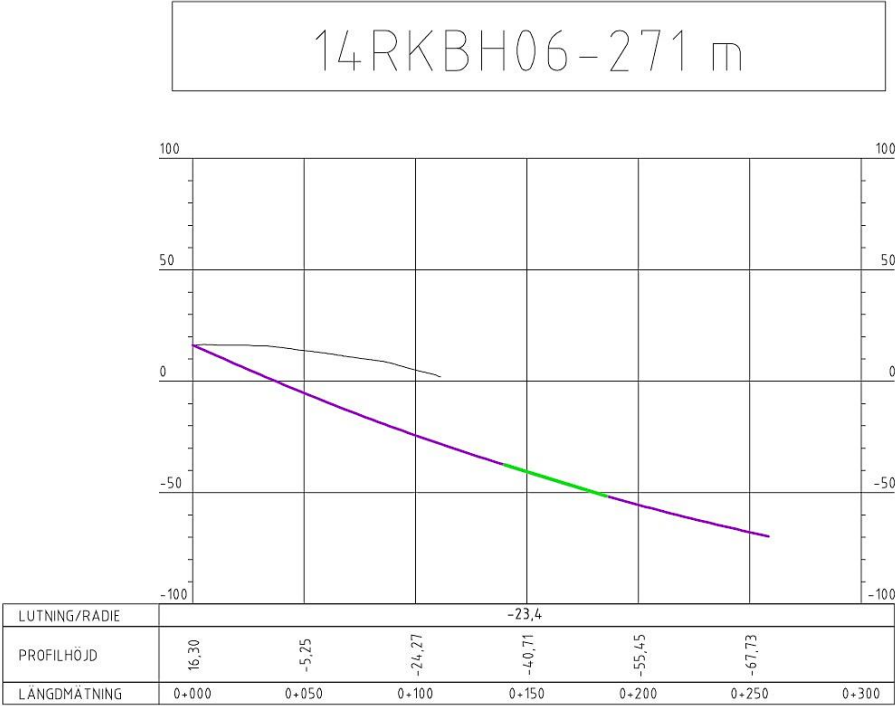


Figure 23. Profile of the drill core with the detected zone marked in green.

18 core losses occur along the fracture zone in the core length interval 140-185 m, with the longest one being 1.5 m followed by two of 1.4 m (Figure 24). The total length of all the core losses is 13.25 m, and in the interval of the zone that corresponds to 24 % of the entire length. Between the core losses the rock is very fractured and brittle.

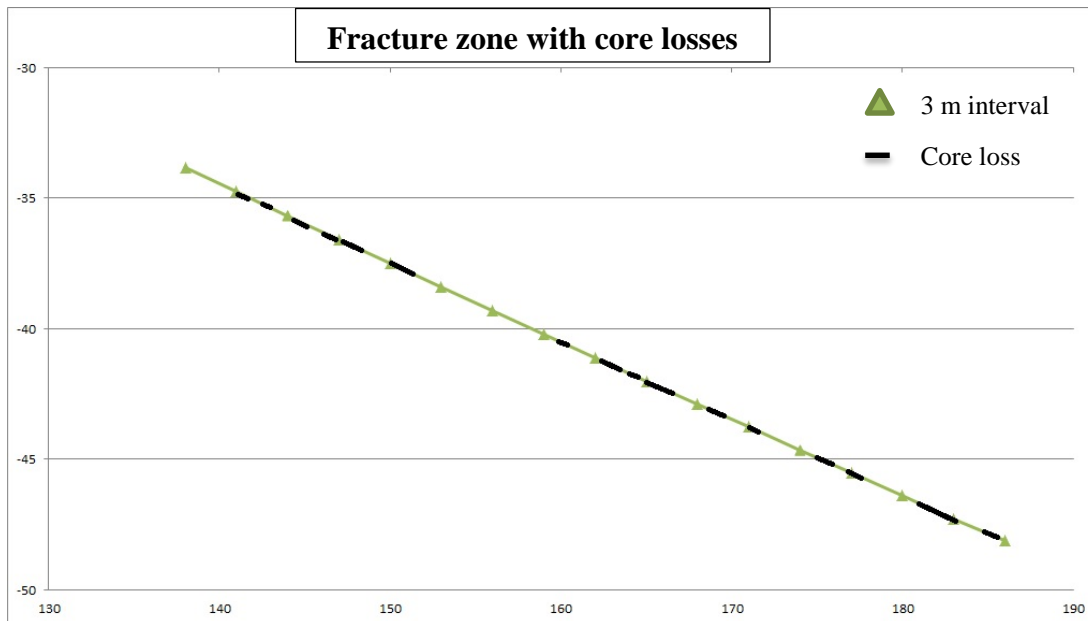
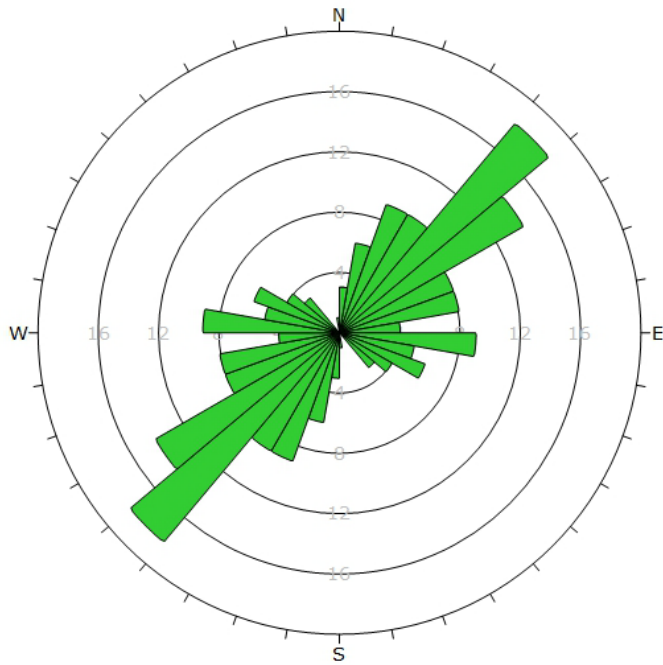


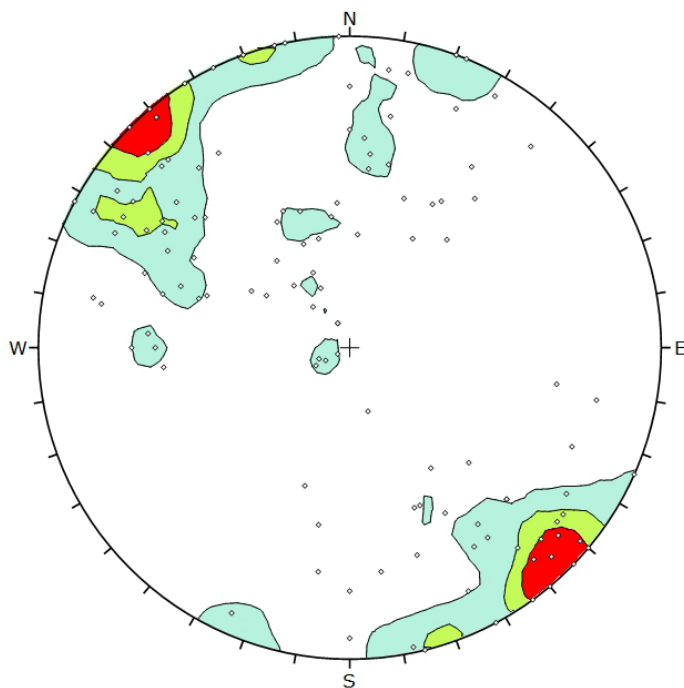
Figure 24. Profile of the zone with all the core losses marked as black lines.

4.4 Sub-surface fracture analysis

The results of the subsurface fracture measurement include rose and pole plots where the latter shows the poles to planes. The rose plots describe the strike of the fractures and the pole plots also indicate the dip of the fractures. Figure 25 shows the measurements from the entire core (0-271 m). The rose plot has two major fracture sets striking NE-SW and SE-NW. In figure 26 the measurements in front of the zone is presented (0-130 m). They correspond well to the plots from the entire core. The last plot (Figure 27) shows all the measurements after the fracture zone (185-271 m). In this range there is one additional set determined, striking NNE-SSW. There were also sub-horizontal planes, which cut the drill core in length e.g. in its own direction. These fractures were not as frequent as the others but they are worth noticing since they had a sub-vertical dip.



Plot Mode	Rosette
Plot Data	Apparent Strike
Face Normal Plunge	0.0
Face Normal Plunge	90.0
Bin Size	10°
Outer Circle	20 planes per arc
Planes Plotted	107
Minimum Angle To Plot	45.0°
Maximum Angle To Plot	90.0°



Symbol	Feature
◊	Pole Vectors
Color	
	Density Concentrations
	0.00 - 2.25
	2.25 - 4.50
	4.50 - 6.75
	6.75 <
Maximum Density	10.42%
Contour Data	Pole Vectors
Contour Distribution	Fisher
Counting Circle Size	1.0%
Plot Mode	
Plot Mode	Pole Vectors
Vector Count	125 (125 Entries)
Hemisphere	Lower
Projection	Equal Angle

Figure 25. Rose and pole plot from fractures in core length interval 0-271 m.

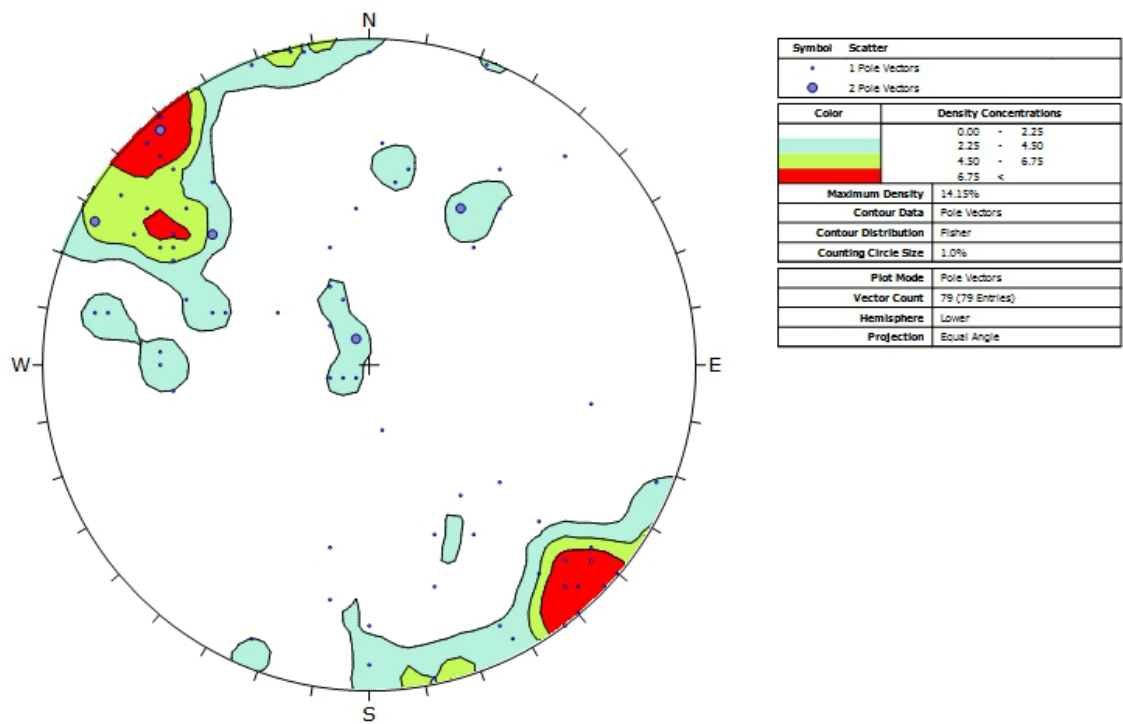
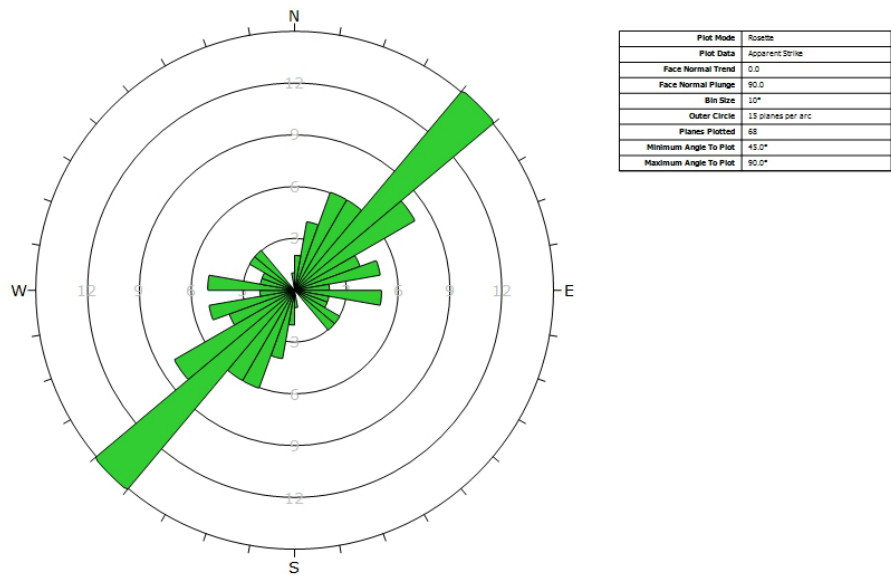
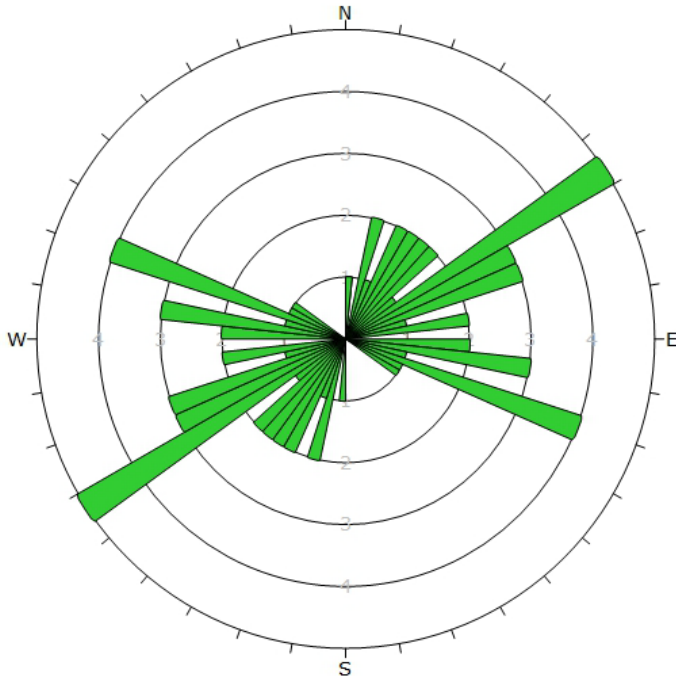
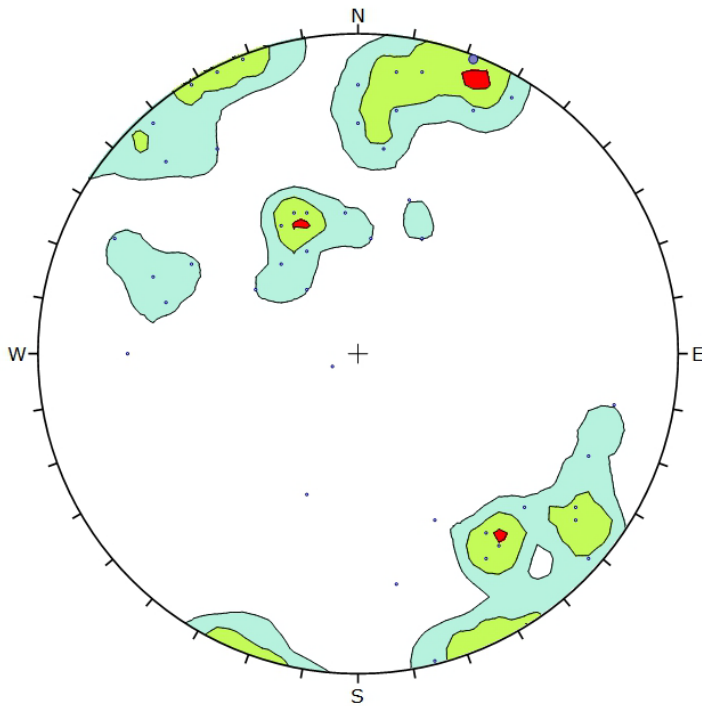


Figure 26. Rose and pole plot of fractures in core length interval 0-130 m.



Plot Mode	Rosette
Plot Data	Apparent Strike
Face Normal Trend	0.0
Face Normal Plunge	90.0
Bin Size	5°
Outer Circle	5 planes per arc
Planes Plotted	39
Minimum Angle To Plot	45.0°
Maximum Angle To Plot	90.0°



Symbol	Scatter
•	1 Pole Vectors
•	2 Pole Vectors
Color	Density Concentrations
	0.00 - 2.25
	2.25 - 4.50
	4.50 - 6.75
	6.75 <
Maximum Density	7.26%
Contour Data	Pole Vectors
Contour Distribution	Fisher
Counting Circle Size	1.0%
Plot Mode	Pole Vectors
Vector Count	46 (46 Entries)
Hemisphere	Lower
Projection	Equal Angle

Figure 27. Rose and pole plot from fractures in core length interval 185-271 m.

4.5 Field work

The examined outcrops consist of meta-greywacke and meta-granitoids (Figure 8). Occasional occurrence of mylonite were found which followed the foliation direction mainly E-W. No prominent shear sense indicator was found. Although in the granodioritic suite a quartz- and feldspathic vein with a bending foliation with a sinistral sense of shear was found (Figure 28). Conjugate fracture sets were found on an outcrops horizontal surface (Figure 29). Fractures on the examined outcrops and its surroundings were measured and added into DIPS and presented as a rose plot (Figure 30).



Figure 28. Granodioritic suite showing a deformed quartz and feldspatoitic vein bending with a sinistral sense of shear. The black lines indicates the bending and the orange arrows the sense of shear.



Figure 29. Conjugate fracture set on a horizontal wall. The compass is 17 cm long.

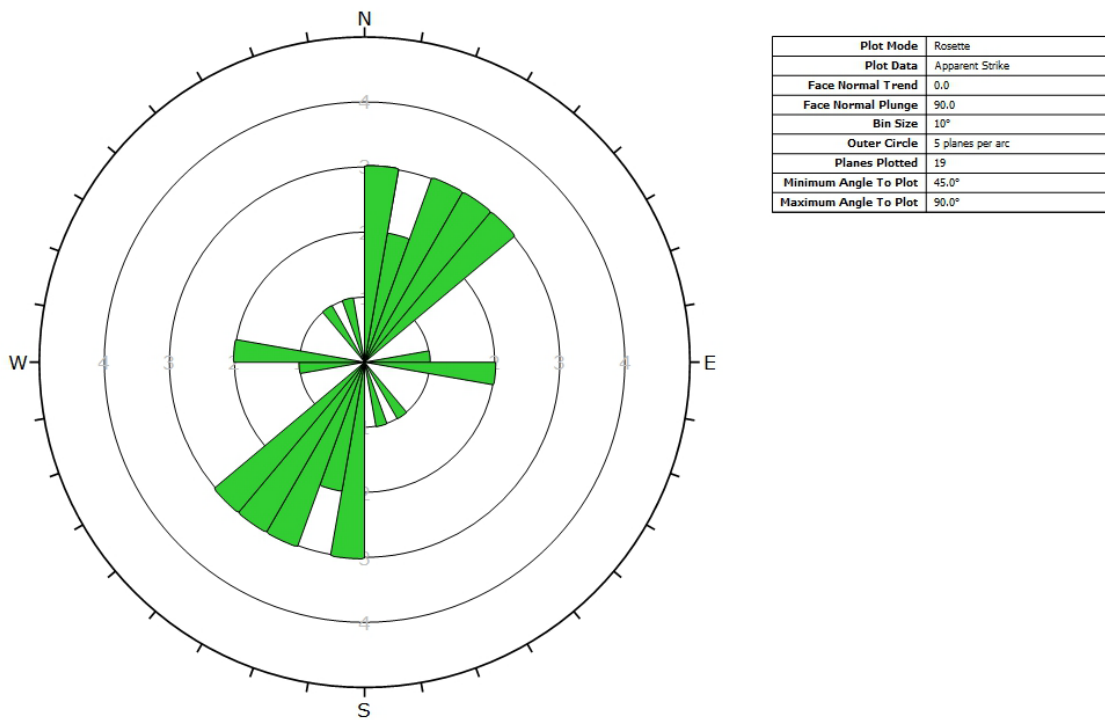


Figure 30. Rose plot from field measurements.

4.6 2D modeling

Several models have been completed in order to see the displacement differences between them, but only a few of them will be presented in the results. All the others are found in Appendix 2. All the models made without support are presented. For the other three model types only the once with the poor quality rock material will be presented.

4.6.1 Tunnel without support

The first four models (Figure 31-34) show the displacement of the rocks without any support. The tunnel contour is the black horseshoe area while the deformed tunnel contour is the outer border of the white tunnel area. The displacement vectors are indicated by red arrows (Figure 31) and the deformation are present as displacement in meters. The first model with the good quality rock and elastic properties (material 1) has a displacement of 0.002 m (Figure 31). The second model with the poor quality rock and elastic material (material 2) has a maximum displacement of 0.04 m (Figure 32). The third model with good quality rock and plastic material (material 3) has a maximum displacement of 0.002 m (Figure 33). The last model with the poor quality rock and the plastic properties (material 4) has a maximum displacement of 0.06 m (Figure 34).

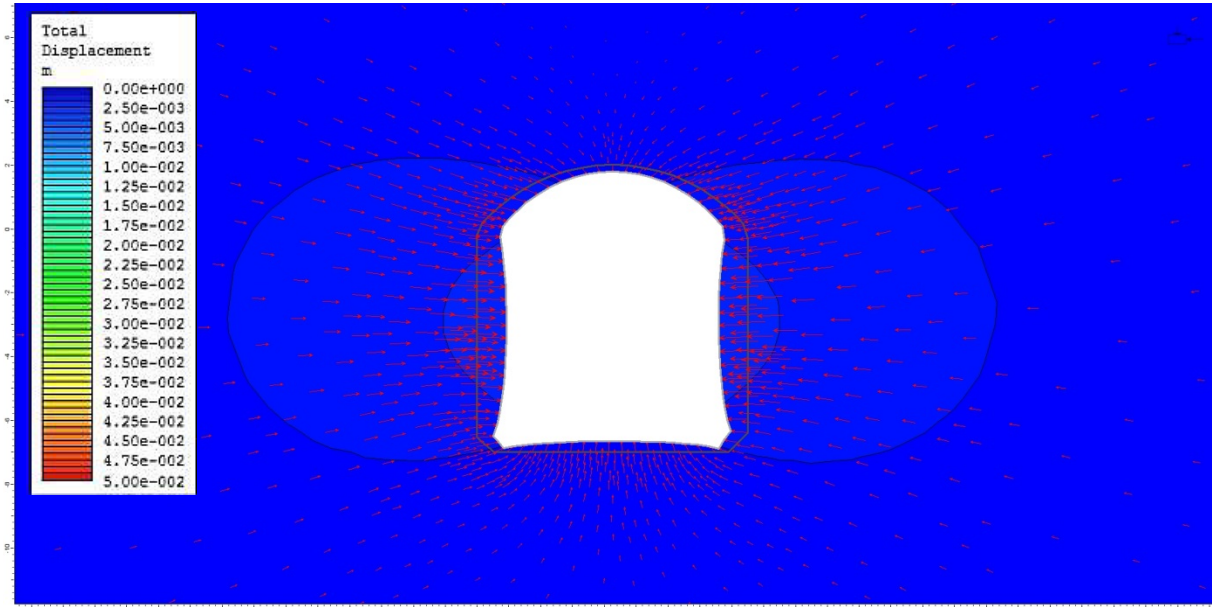


Figure 31. Stage 2 with red displacement vectors for the good quality rock and elastic properties (material 1).

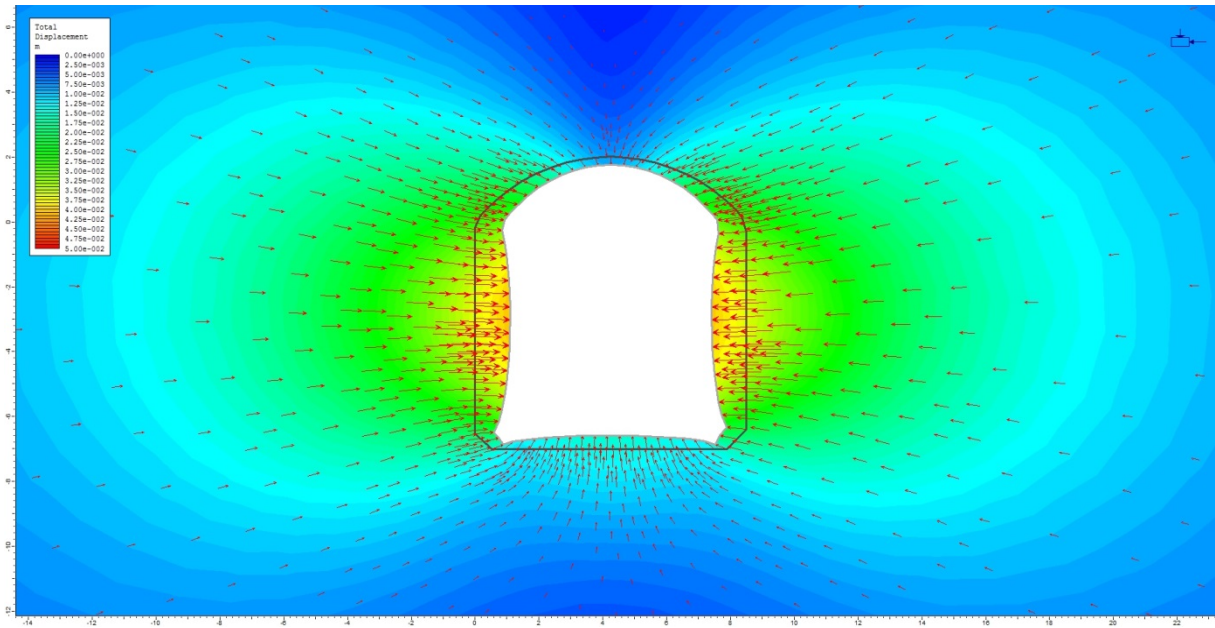


Figure 32. Stage 2 with red displacement vectors for the poor rock and elastic properties (material 2).

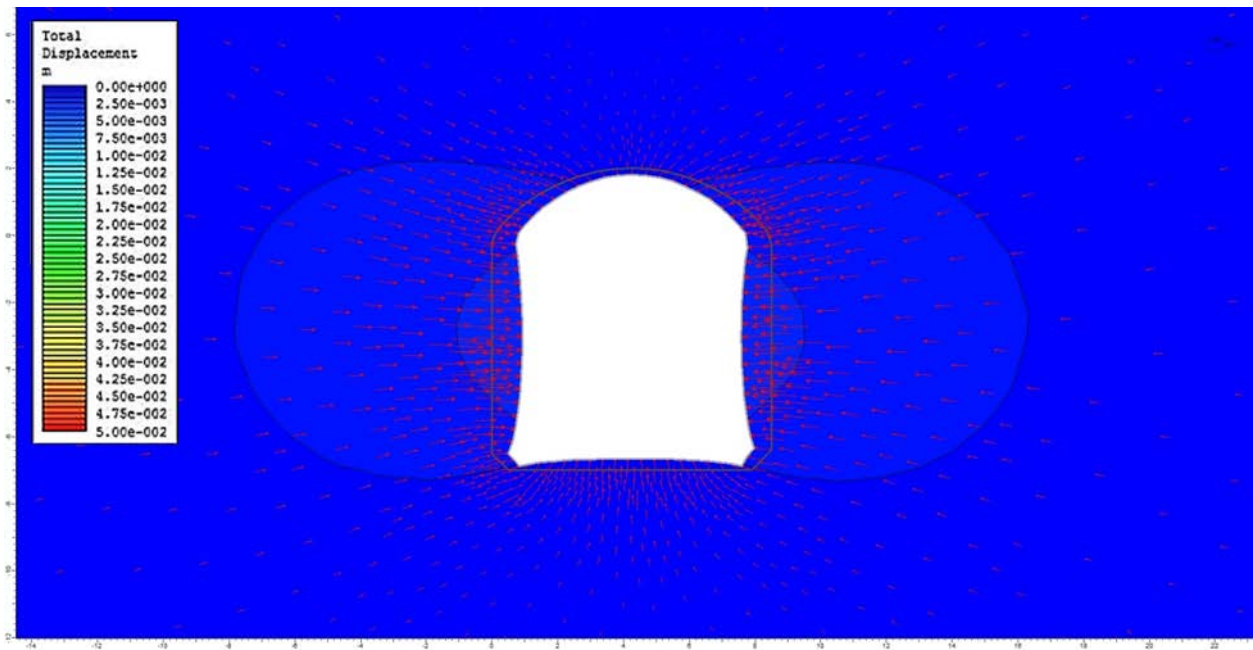


Figure 33. Stage two with red displacement vectors for the good rock and plastic properties (material 3).

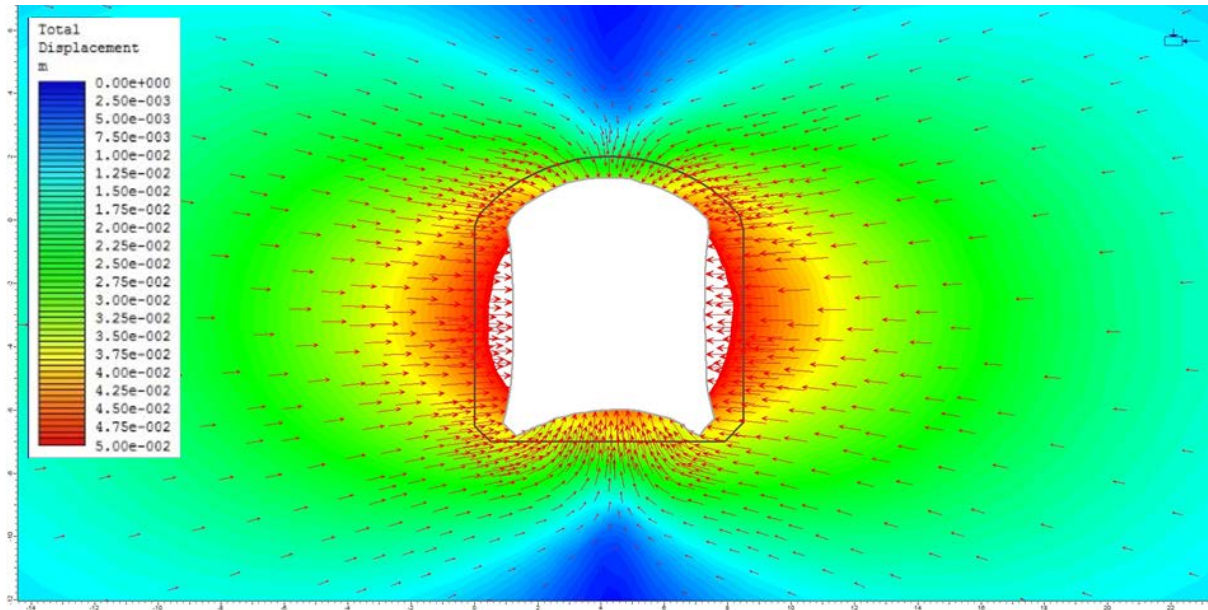


Figure 34. Stage two with red displacement vectors for the poor rock and plastic properties (material 4).

4.6.2 Tunnel with pre-installed support

These two models have pre-installed bolt and concrete before excavation (stage 1). The displacement, yielded bolt, yielded concrete and deformation contour is visible. The elastic model has a maximum displacement of 0.015 m (Figure 35). The bolts in the elastic model experience tension close to the tunnel walls where the highest displacement occurs. In the plastic model the maximum displacement is 0.04 m (Figure 36). The majority of all the bolts are ripped apart due to tension. The roof is not affected as much as the side walls where the yielding in the bolts extends its length.

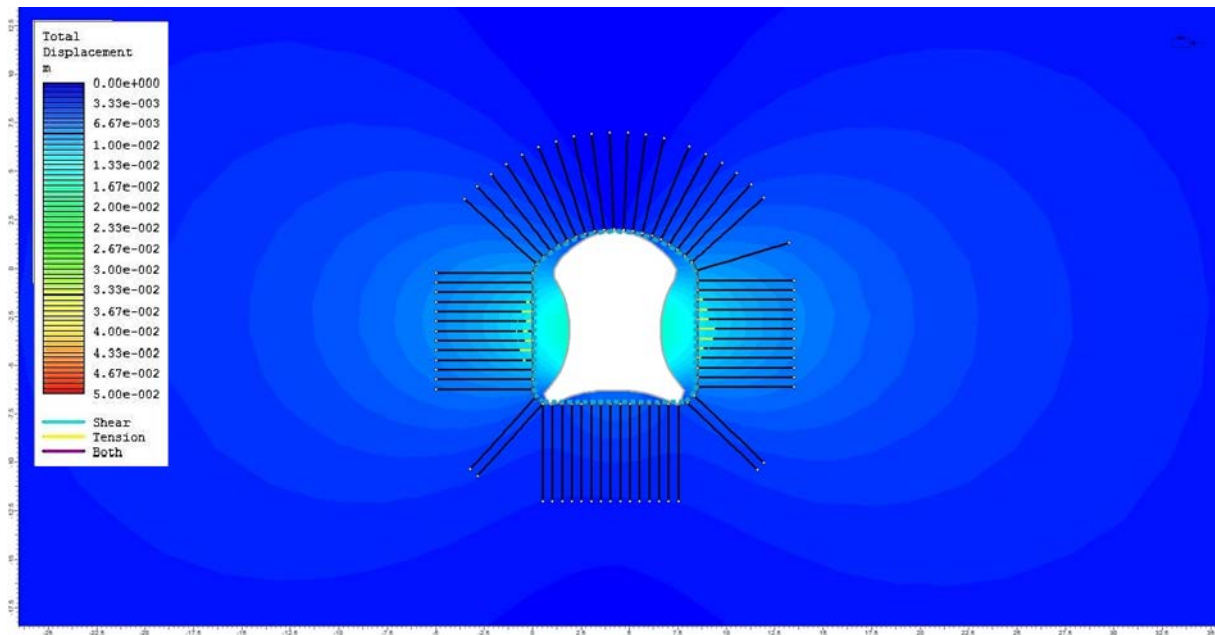


Figure 35. Stage two with pre-installed bolts and concrete for material 2 with yielded bolts (yellow area).

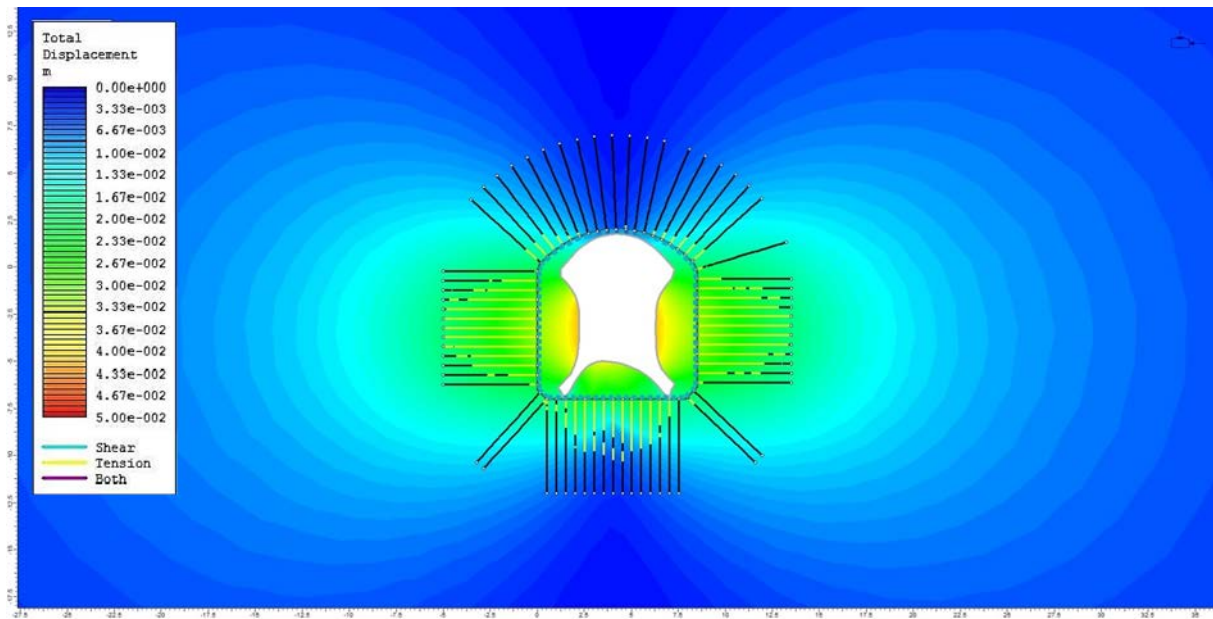


Figure 36. Stage two with pre-installed bolts and concrete for material 4 with yielded bolts (yellow area).

4.6.3 Tunnel excavation in two steps

These models (Figure 37-43) are excavated in two steps to see if the overall displacement will decrease and if the bolts yielding decrease. Both the models have the same stage one where bolts and concrete are added to the top of the tunnel before excavation. All models show the displacement contour of the tunnel, displacement in meter and the yielded bolt and shot-concrete. In stage two for the elastic model (Figure 38) the maximum displacement is 0.025 m and located in the tunnel walls but the largest displacement area is in the tunnel floor. In stage three the additional bolt and shot-concrete are added so the displacement stays the same (Figure 39). In the final stage the displacement has increased to 0.035 m in the tunnel wall but decreased in the tunnel floor (Figure 40).

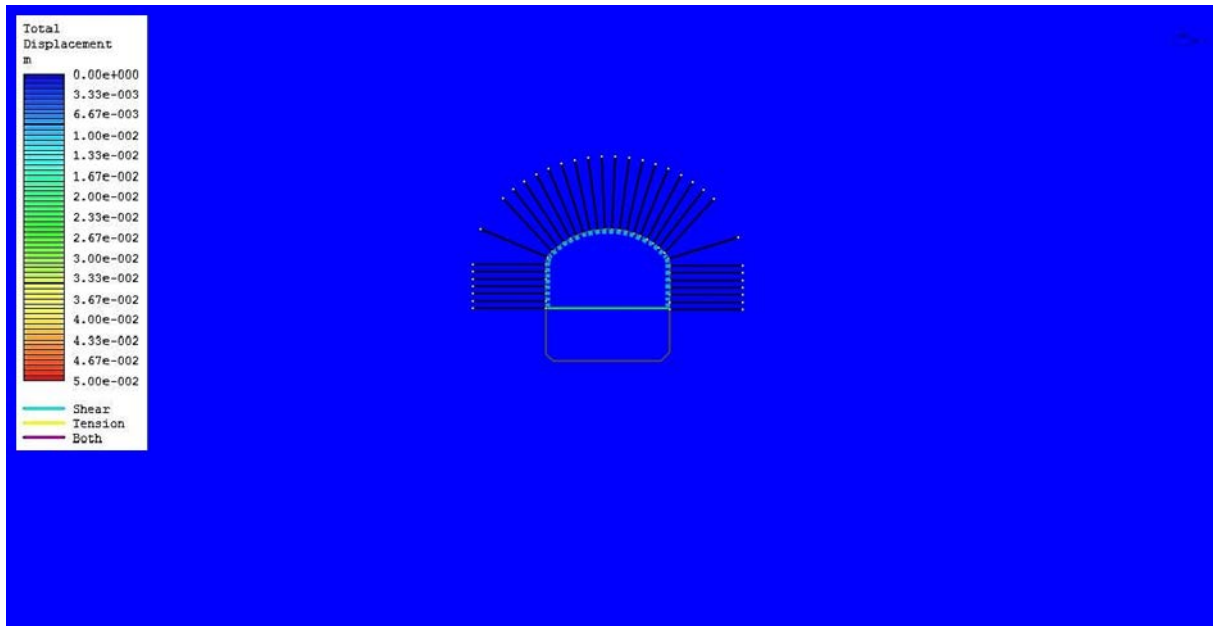


Figure 37. Stage one for all models with excavation in two steps. Pre-installed bolts and liner of the top half of the tunnel.

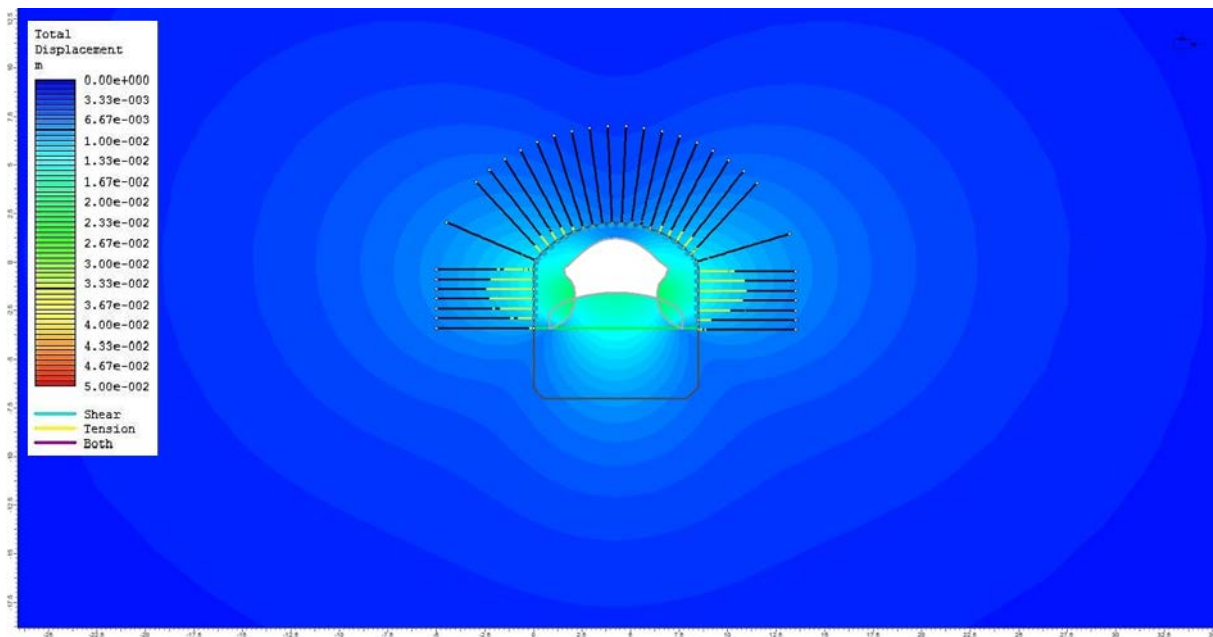


Figure 38. Stage two for material 2, excavation of the top half of the tunnel with yielded bolts (yellow area).

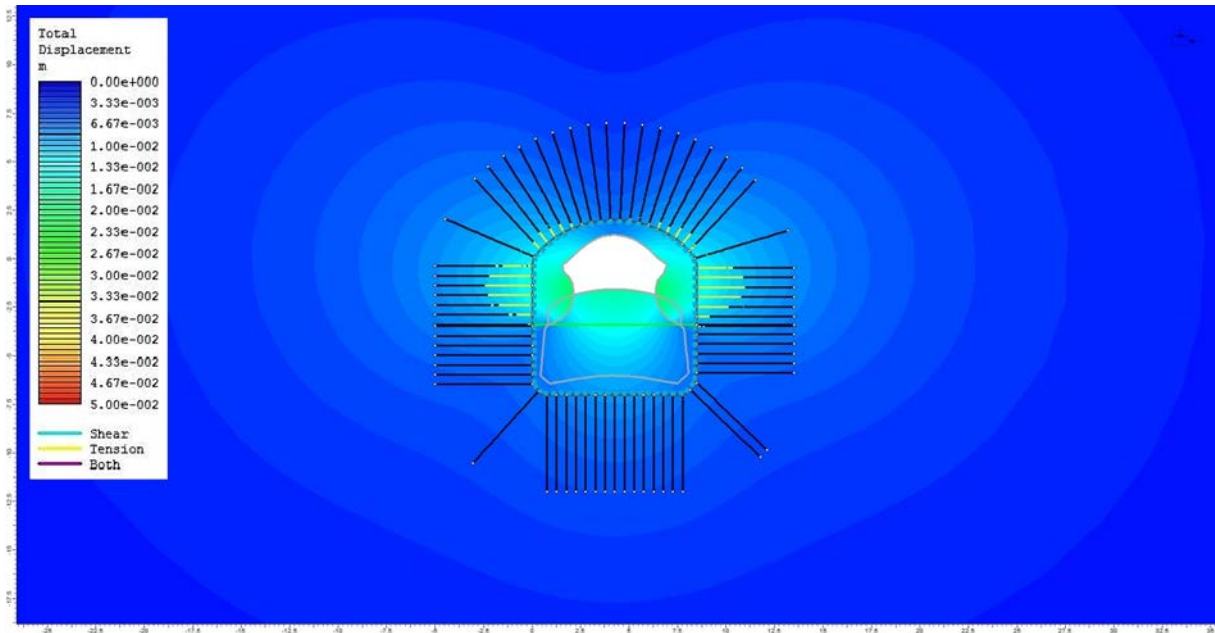


Figure 39. Stage three for material 2. Pre-installation of bolts and shot-concrete in the bottom of the tunnel, with yielded bolts (yellow area).

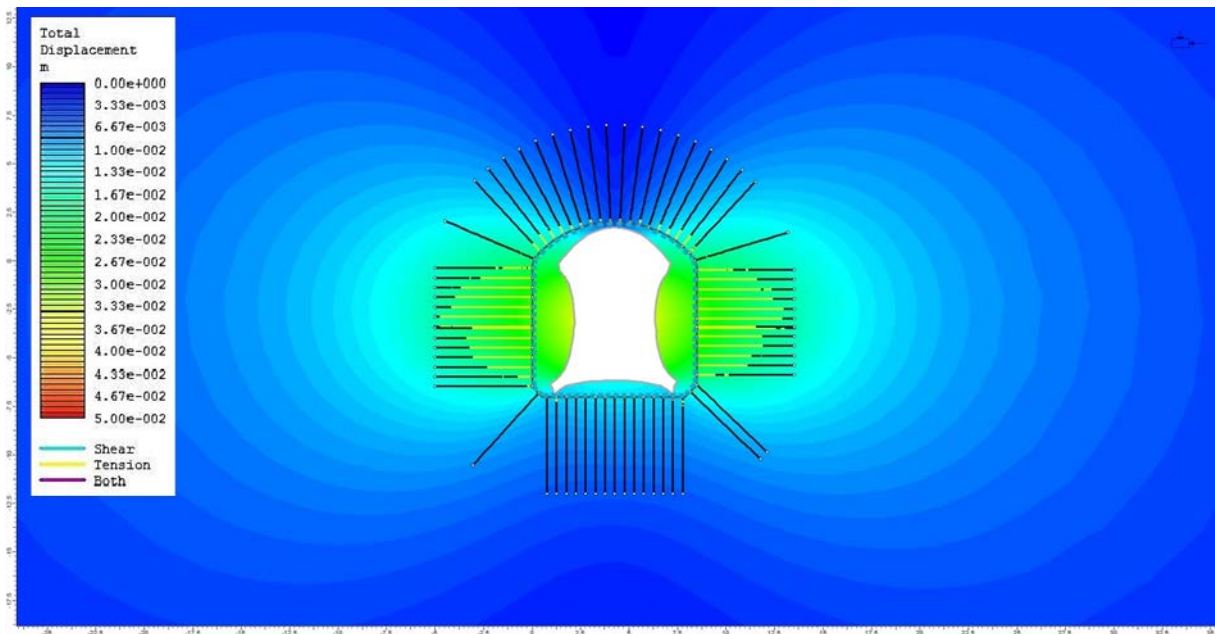


Figure 40. Stage four, excavation of the bottom part of the tunnel, for material 2 with yielded bolts (yellow area).

In the plastic model in stage two the maximum displacement occurs in the tunnel floor with a displacement of 0.03 m (Figure 43). The bolts are yielding in the roof and walls. In the tunnel walls the displacement is 0.035 m. In stage three the displacement is unchanged (Figure 44). In the final fourth stage when the tunnel floor is excavated, the maximum displacement has moved to the tunnel walls and is now 0.045 m (Figure 45).

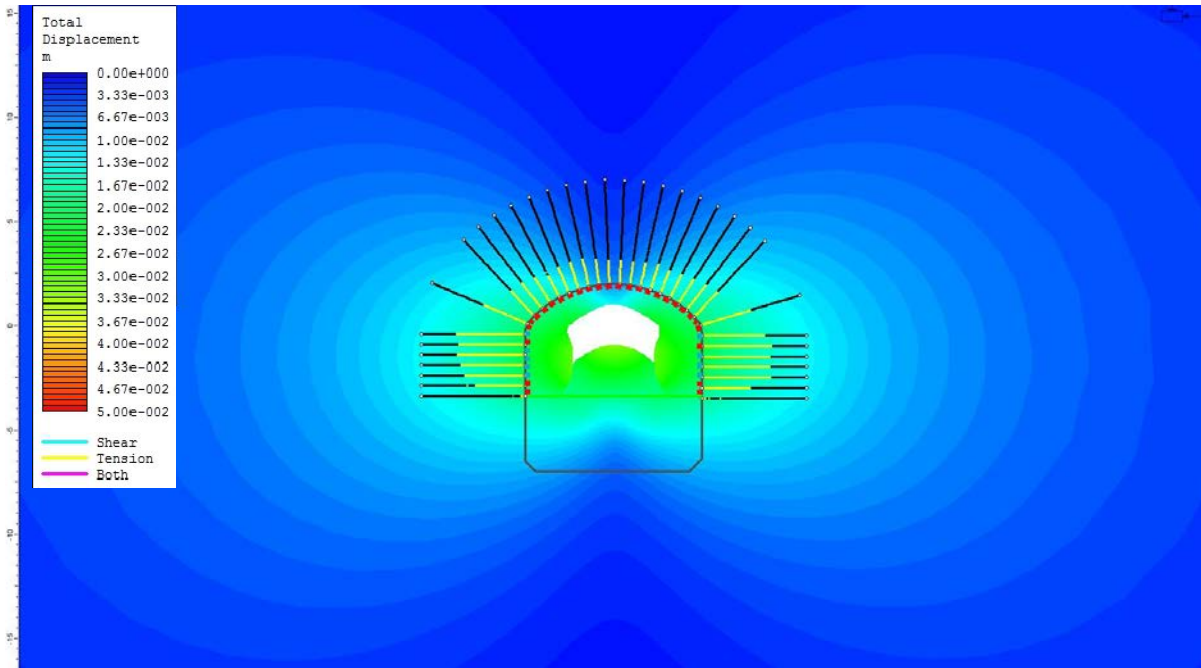


Figure 41. Stage two for material 4, excavation of the top tunnel with yielded elements. Yielding bolts (yellow area) yielding concrete (red area).

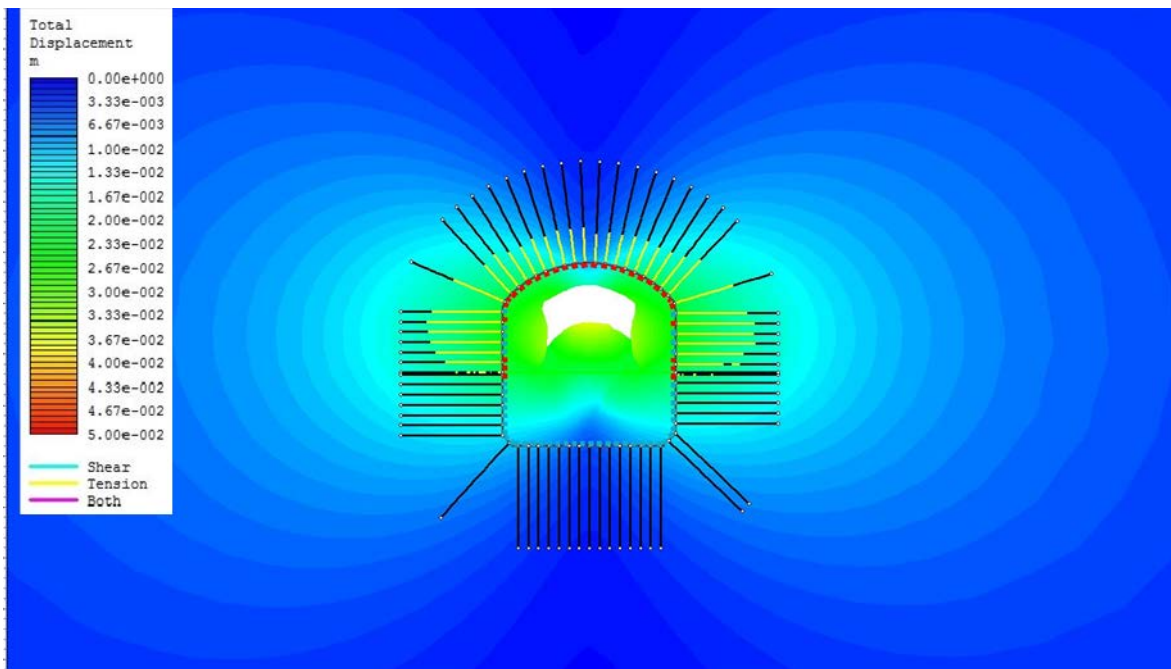


Figure 42. Stage three for material 4, pre installation of bolts and liner on the bottom half of the tunnel. Yielding bolts (yellow area) yielding concrete (red area).

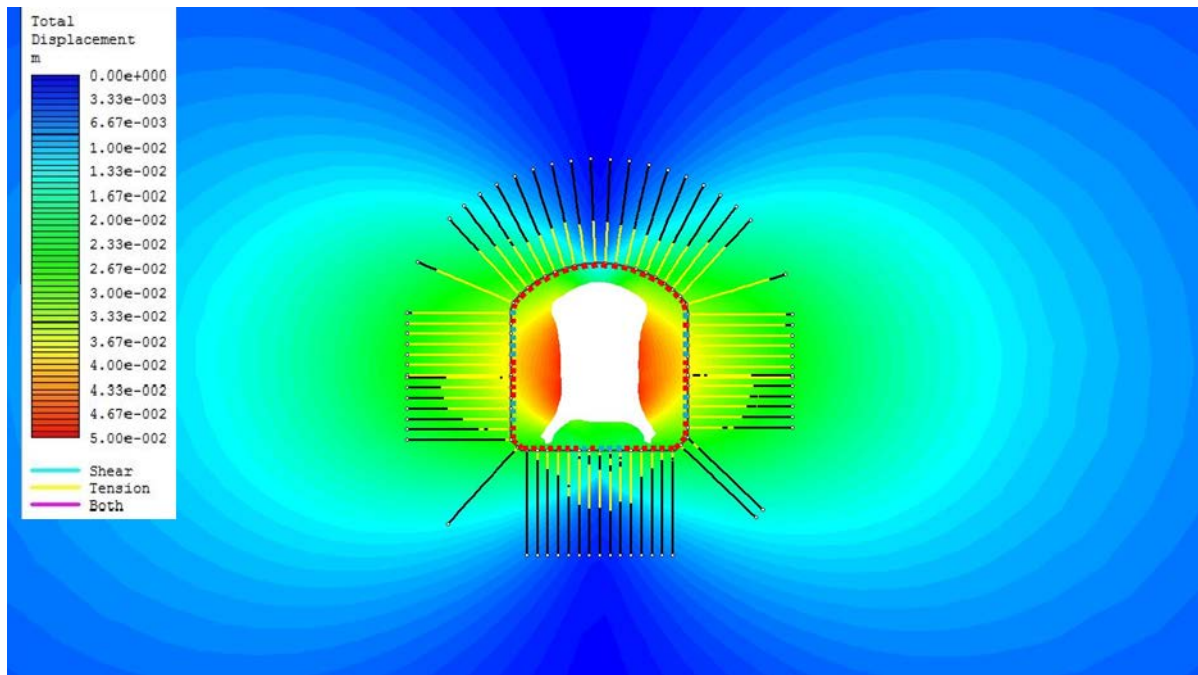


Figure 43. Stage four for material 4, Excavation of tunnel floor. Yielding bolts (yellow area) yielding concrete (red area).

4.6.4 Round tunnel with internal pressure

Two round models was made with the elastic- and plastic poor quality rock and with rock bolts and shot-concrete installed in stage one (Appendix 2). The result showed that the optimal stage to install bolt and concrete for best support was in stage three. In this stage the maximum internal load was 4 MPa and the bolts started to yield i.e support needs to be added; therefore the reinforcement was set in this stage for the models presented below. The results are from stage three (installed support) and stage ten (no load applied). The models show displacement contour of the tunnel, displacement in meters and the yielded bolt and concrete are.

The tunnel is being excavated in the initial stage which is when the load inside the tunnel is added. This stage does not show any displacement which was the intension. The arrows and numbers inside the tunnel are the direction and magnitude of the added load (Figure 44). When looking at stage three in the elastic model where the bolt and concrete is added the maximum displacement is 0.017 m and the magnitude of the load is maximum 4 MPa (Figure 45). In stage ten the maximum displacement is 0.027 m and the load is 0. In the tunnel wall the bolts are experience yielding about one third of the bolt length (Figure 46).

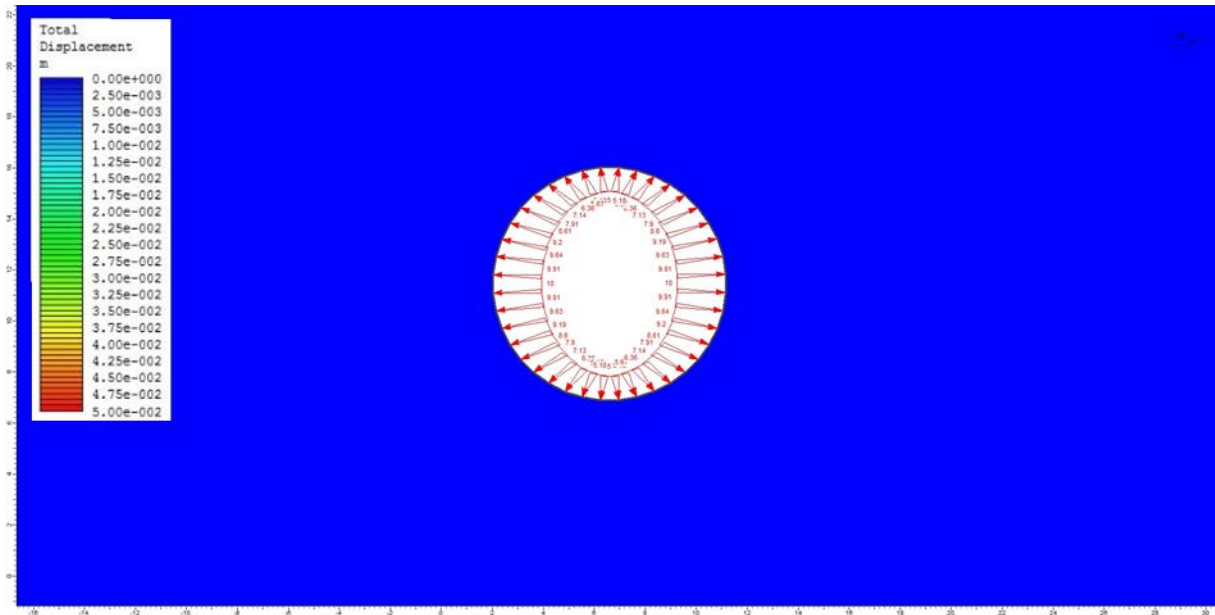


Figure 44. Initial stage for all the round models. The direction and magnitude of the load is the same as the in-situ stress.

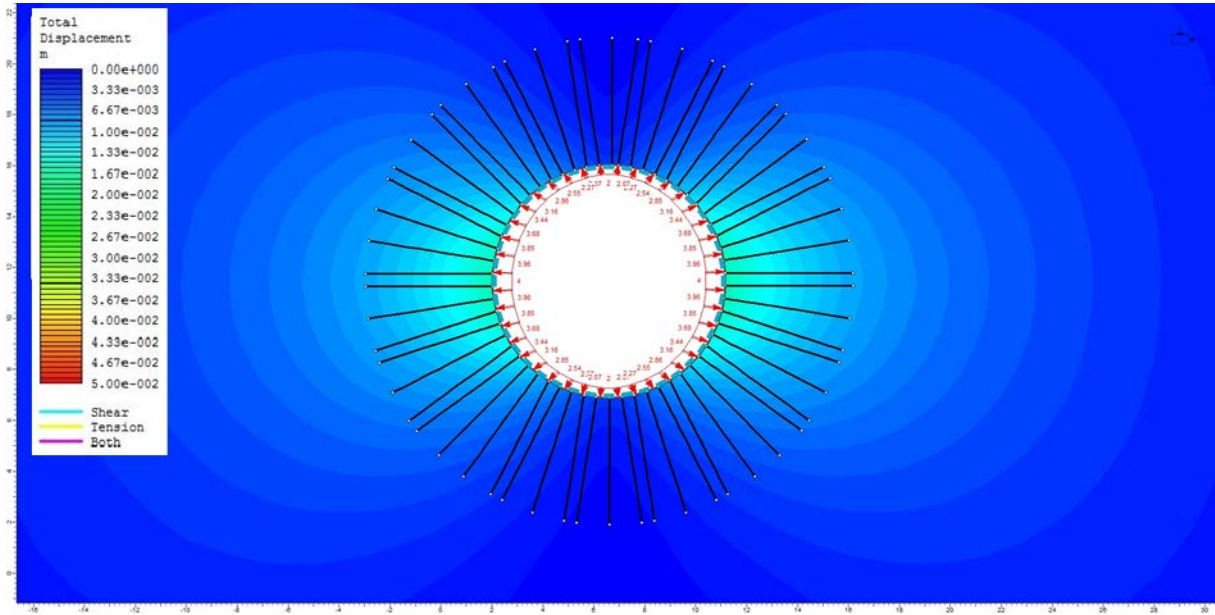


Figure 45. Stage three for material 2 when bolts and concrete are added. The maximum load is 4 MPa.

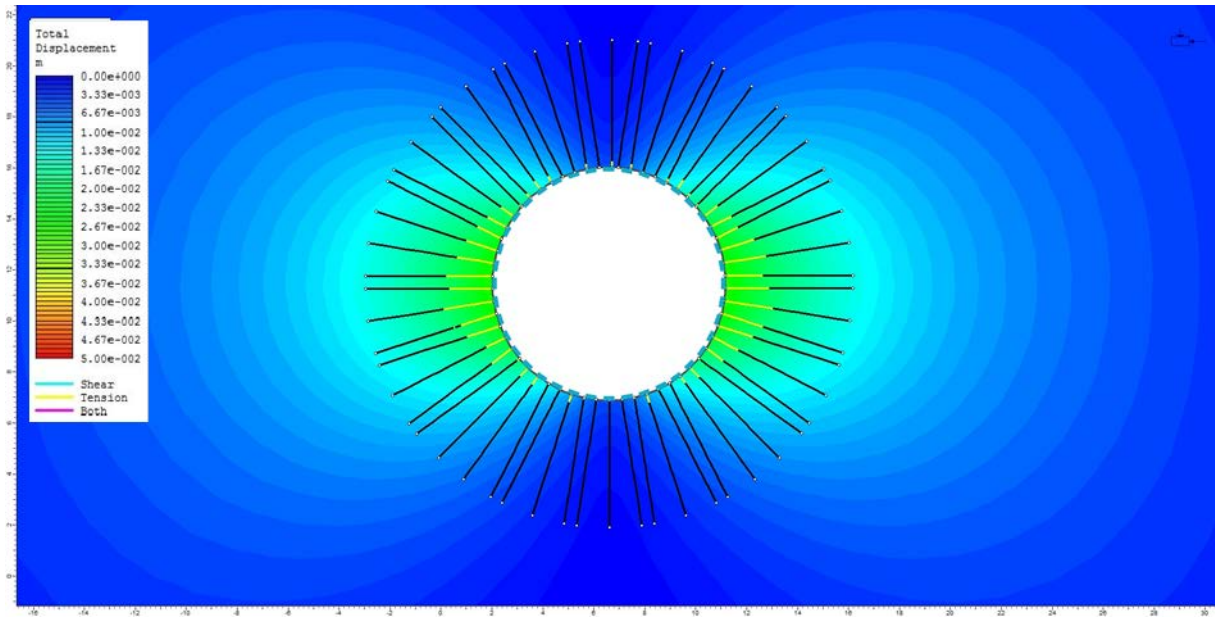


Figure 46. Stage ten for material 2, no load is applied and yielded bolts are indicated (yellow areas).

Stage three in the plastic model shows a maximum displacement of 0.018 m with the same load (Figure 47). In stage ten the maximum displacement is 0.027 m. The displacement is again concentrated in the wall sides of the tunnel (Figure 48).

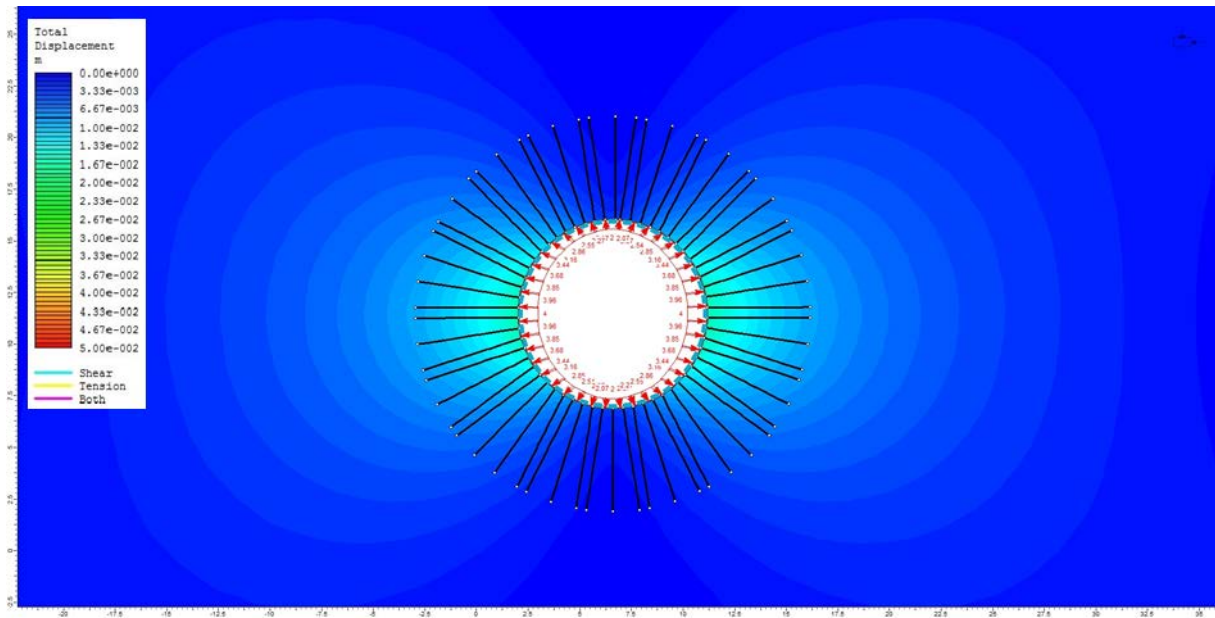


Figure 47. Stage three for material 4 with bolts and liner. Maximum load is 4 MPa.

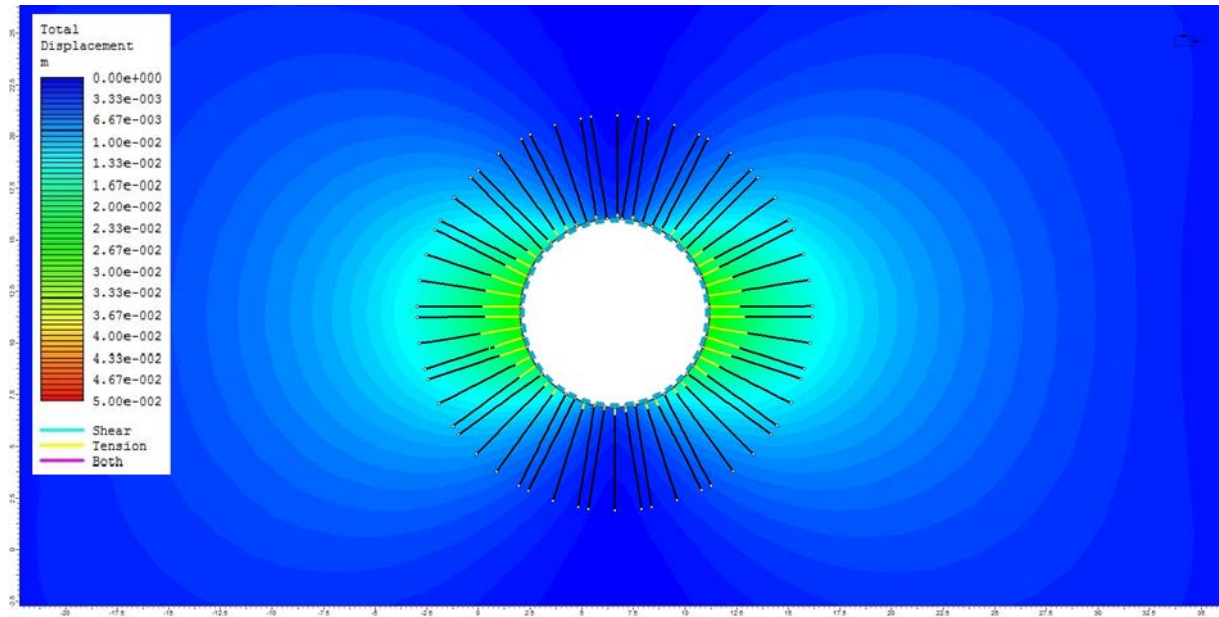


Figure 48. Stage ten for material 4, no load applied and yielded bolts (yellow area).

4.6.5 Summary

From all the models presented in the result a summary table of their maximum displacement was made, shown in Table 5.

Table 5. Summary of maximum displacement for each model.

Model	Maximum displacement (m)			
	Elastic-good	Elastic-poor	Plastic-good	Plastic-poor
Tunnel without support	<i>0.002</i>	<i>0.04</i>	<i>0.002</i>	<i>0.06</i>
Tunnel with preinstalled support	<i>0.002</i>	<i>0.035</i>	<i>0.002</i>	<i>0.041</i>
Tunnel excavation in two steps	<i>0.002</i>	<i>0.035</i>	<i>0.02</i>	<i>0.045</i>
Round tunnel with internal pressure (stage 3)	-	<i>0.017</i>	-	<i>0.018</i>
Round tunnel with internal pressure (stage 10)	-	<i>0.027</i>	-	<i>0.027</i>

5. Discussion

5.1 Fracture analysis

The core logging and the high water-losses identified one fracture zones crossing the area between Eolshäll and Smedslätten. The general orientation of the zones is NE-SW and WNW-ESE. From the drill core mapping three dominating fracture orientations were found (Figure 25). The first has a NE-SW orientation with a dominating sub-vertical dip. The second fracture orientation is E-W with a dominating sub-vertical dip. The third set has an NW-SE orientation with a steep to sub-vertical dip. Further down, after 185 m core length a possible conjugate set can be identified with NE-SW and WNW-ESE orientation (Figure 27).

Fractures found in field showed four different orientations with the dominating NE-SW direction. A conjugate fracture set with a different orientation than the set identified in the drill core was found, which indicates that these are different fractures. A vertical N-S orientated fracture set was found, however it is not as common in the drill core, which could be explained by the orientation of the borehole that strike almost N-S (332.5°). The direction of the borehole also limits the presence of fractures orientated in the same direction, as the fracture set found in field (Figure 29). The presence of this fracture set has to be considered during tunneling although it does not appear in the drill core. A conjugate fracture set with similar orientation as in the drill core, NE-SW and WNW-ESE was found (Figure 27 and 30). The WNW-ESE and NE-SW orientation of the conjugate set coincide with the orientation of the two fracture zones interpret on the geological map by SGU (Figure 8).

The fracture orientations in field and in the drill core that showed the same orientations are interpreted to be the same sets. The fractures have similar dip (steep to sub-vertical) which further supports the interpretation of the sets being the same. Conjugate fracture sets are usually found in settings where faulting has occurred. Moderate dipping fractures ($<60^\circ$) are associated with dip-slip faulting while steep to sub-vertical dipping fractures are associated with strike-slip movement (Burg, 2014). The conjugate fracture set found in the drill core has a steep dip, which can be linked to a strike-slip movement of the fracture set. Ideally conjugate brittle shear fractures has an dihedral angle of $\sim 60^\circ$ (Figure 48),(Singhal & Gupta, 2010;Ismat, 2015). The dihedral angle between the conjugate set in figure 27 is approximately 50° , which is very similar to the ideal angle and supports the interpretation of the fractures being sheared.

The present maximum compressive stress (σ_1) has an orientation of NW-SE (SKB, 2007; Krumbholz et al, 2014). Considering the NE-SW oriented fractures and the orientation of the present day stress field, it is unlikely that these fractures are subjected to opening since they are oriented perpendicular to present day compression direction. The WNW-ESE oriented fractures have a less inclined angle to the maximum compressive direction and it could be subjected to further opening of the fractures. The observed kinematic indicator in field corresponds to a ductile deformation (Saintos, 2011).

The drill core mapping shows a rock quality from the Q-values between poor and acceptable for the core (Figure 22). The fracture zone oriented NE-SW is clearly indicated on the graphs with poor rock quality and low Q- and RMR- values. The fractures with WNW-ESE orientation occurs more frequently further down in the passage e.g. longer drill core length compared to the beginning of the drill core. The drill core mapping revealed poorer rock quality and higher fracture intensity in the end of the core (Figure 22) which could be interpret as the appearance of the fracture zone deeper down and further out in the passage and perhaps with worse quality. If the two zones intersect with each other further down the rock quality could also be interpreted to be worse in that area. The core losses are confusing, since the drill casing used during the drilling was a triple tube, which is thought to pick up all small rock pieces and even clay, the reason for this is not known. An interpretation of what these cavities initially could have been made of is brittle rock that easily breaks apart and when that rock is drilled through it gets affected by high water pressure from the bore machine and could be grind down to very small fragments and transported away by water. Fault gouge is rock fragments that have been cemented together with clay and a very weak fault gouge could have been the initial rock.

The extent of the zone together with the core-losses and the uncertainty of what type of rock or material that was originally in these cavities will be a significant problem for the construction. The quality of the material will be very poor and the excavation process has to be carefully performed and adapted for these areas, especially since the Lake Mälaren is above the tunnel with a high water pressure. The resistivity anomalies does not reach the drill core location and no linkage between there results and the drill core could be made. Although the resistivity anomalies can indicate other areas with low rock quality and fracture areas in the passage.

5.2 2D-modelling

The different excavation methods gave different displacement results in the models. All the models that represent the rock of poor quality have a higher displacement and the stability effect of the zone will be much less than the surrounding rock. When pre-installing bolts and shot-concrete before tunnel excavation the deformation displacement decreases in both the elastic and plastic poor quality rock (Figure 35-36). The different materials respond differently on the models. The plastic models are a continuation of the elastic model. From the Hoek-brown criteria the plastic model is calculated to exceed its strength and failure will therefore occur around the opening. When the stress reaches the material strength around the excavating opening the rock closest to the opening will fail. The load will then have to redistribute itself around the excavated area and further away from the tunnel face until the load is lower than it was causing failure. This leads to an increase of deformation away from the tunnel face and the volume of the deformed rock is depending on the extent of the failure propagation. This is what happens in the worst models when the plastic failure exceeds the bolts (Figure 36). The round model illustrated the deformation propagation and support stability in the tunnel if the rock is subjected to some deformation before installing reinforcement. The rock mass before excavation is affected by in-situ stresses. If these are given time to redistribute, they will be smaller and re-oriented. If the reinforcement is installed after that the bolts, in this case will not be affected by such high stresses and the load could also be less and the bolt will hold better. Even though the round tunnel has a different geometry compared to the other models, the connection between the decrease in deformation and less yielding of bolts if the rock deforms before installing support, can be made. In the plastic two-step excavation model the zone of deformation is located both in the tunnel walls and the tunnel roof (Fig 40-42) compared to the plastic one-step excavation model where the deformation only occurs in the tunnel walls (Fig 34-35). In the two-step model when excavating the top half of the tunnel the load will, as mentioned before, redistribute around the opened area and when excavating the bottom half of the tunnel the stresses and load will be oriented differently compared to the initial stage which causes this deformation differences. The deformation in the roof in the first step could be the cause of a smaller excavation area and the failure will be concentrated on the top. This deformation needs to be considered when choosing excavation method. Overall, the reinforcements that were tested in the models will not be enough to support the tunnel, especially in the zone, and will not work properly since the bolts are yielding. Furthermore, the NE-SW and the WNW-ESE oriented fractures have an unfavorable orientation for the tunnel excavation, where these two planes in correlation with sub-horizontal planes can be expected to cause wedging in the tunnel roof (Hoek & Brown, 1980). Based on the models and the geology of the area, with varying rock quality and the occurrence of two large fault zones would be expected to make tunnel excavation in the passage very challenging.

6. Conclusions

The Stockholm future sewer pipeline project includes a new tunnel that will run from western- to southern Stockholm where a new purifier will be built. The tunnel will be 1.5 km long and it will pass Lake Mälaren between Smedslätten and Eolshäll. The previous geophysical and geological data showed possible risks regarding the tunnel construction e.g. two faults intersecting in the passage. The purpose for this thesis was to interpret the geological and geophysical data, characterize the fracture zones and illustrate how they will affect the tunneling.

The following conclusions can be drawn from the study:

- The acquired geological data supports the existence of two sub-vertical faults in the passage, indicated on the geological map from SGU (Person et al, 2001).
- Three dominating fracture orientations were found. The dominated one has an NE-SW orientation. The second one is oriented E-W and the third has a WNW-ESE orientation and all with a sub-vertical dip.
- In the last part of the drill core a conjugate fracture set was identified with NE-SW and W NW-ESE orientation. Their dihedral angle and sub-vertical dip indicates a shearing relationship.
- The present maximum compressive stress is oriented NW-SE, which could cause an opening of fractures oriented WNW-ESE.
- The 2D-models showed that the fault zones experience the largest displacement, with the plastic material being worst, and none of the models could stabilize the rock in these zones.
- The fracture sets identified could cause block fall and wedges during tunneling.
- The excavation method has to be carefully chosen to prevent deformation in the roof.
- The tunneling will be challenging in the passage and the excavation process needs to be carefully performed with extra caution in the area where the fault zones are present.

For future work the whole drill core needs to be mapped so that the geophysical measurements can be linked together with the core logging and the occurrence of the other zones extent can be establish. The reinforcement in the models has to be modified with something stronger for the zones to prevent failure. A 3D-analysis is to prefer to be able to see the rock failure propagation in the front of the tunnel after excavation of each section.

7. Acknowledgments

I would like to express my gratitude to all the people who has helped me complete this thesis. Without your support and guidance this thesis would not be possible to finish. First I would like to thank my supervisors Steffi Burchardt, Uppsala University and Christer Andersson, Ramböll. I would also like to thank Ramböll who provided me with all the geological and geophysical data and the modelling program, which made it possible for this thesis to exist. At last I would like to thank my colleagues at Ramböll for their support.

8. References

- Allen, R.L, Lundström, I, Ripa, M, Simenov, A, Christofferson, H 1996, 'Facies analysis of a 1.9 Ga Continental margin, back-arc, felsic caldera province with diverse Zn-Pb-Ag-(Cu-Au) sulfide and Fe oxide deposits, Bergslagen region, Sweden', *Economic Geology*, vol. 91, pp. 979–1008.
- Andersson, U. B, Eklund, O, Fröjdö, S, Konopelko, D 2006, '1.8 Ga magmatism in the Fennoscandian Shield; lateral variations in subcontinental mantle enrichment', *Lithos*, vol. 86, pp. 110–136.
- Baltybaev, S. K, Levchenkov, O. A, Levsky, L. K, Eklund, O, Kilpeläinen, T 2006, 'Two Metamorphic Stages in the Svecofennian Domain', Evidence from the Isotopic Geochronological Study of the Ladoga and Sulkava Metamorphic Complexes, *Petrology*, vol. 14, no. 3, pp. 247–261.
- Bell, F. 2007 '*Engineering geology*'. Amsterdam, Elsevier, 581 p.
- Beunk, F. F, & Page, L. M 2001, 'The structural evolution of a deeply eroded, accretional continental margin in the Palaeoproterozoic Svecofennian orogen in southern Sweden', *Tectonophysics*, vol. 339, pp. 67–92.
- During, I 2006, 'Rock mass classification', *Key Engineering Materials*, vol. 321-323, pp. 1–23.
- Gaal, G, & Gorbatshev, R 1987, ' An outline of the Precambrian Evolution of the Baltic Shield', *Precambrian Research*, vol. 35, pp. 15–52.
- Ghosh, S.K 1993, '*Structural geology, fundamentals and modern developments*', Oxford, Pergamon press, 598 p.
- Gorbatshev, R, & Bogdanova, S 1993, 'Frontiers in the Baltic Shield', *Precambrian Research*, vol 64, pp. 3–21.
- Hermansson, T, Stephens, M. B, Corfu, F, Page, L. M, Andersson, J 2008, 'Migratory tectonic switching, western Svecofennian orogen, central Sweden: Constraints from U/Pb zircon and titanite geochronology', *Precambrian Research*, vol. 161, pp. 250–278.
- Hoek, E & Brown, E.T 1980, *Underground excavations in rock*, Spon Press, pp. 536 p.
- Högdahl, K, Sjöström H 2001, 'Evidence for 1.82 Ga transpressive shearing in a 1.85 Ga granitoid in central Sweden: Implications for the regional evolution', *Precambrian research*, vol. 105, pp. 37-56.
- Korja, A & Heikkinen, P. J 1995, 'Proterozoic extensional tectonics of the central Fennoscandian Shield: Results from the Baltic and Bothnian Echoes from the Lithosphere experiment', *Tectonics*, vol. 14, no. 2, pp. 504-517.
- Krumbholz, M, Volbrecht, A, Aschoff M 2014, 'Recent horizontal stress directions in basement rocks of southern Sweden deduced from open microcracks', *Journal of Structural Geology*, vol. 65, pp. 33-43.
- Nironen, M 1997, 'The Svecofennian Orogen: a tectonic model', *Precambrian Research*, vol. 86, pp. 21–44.
- Oen, I. S 1987, 'Rift-related igneous activity and metallogenesis in SW Bergslagen, Sweden' *Precambrian Research*, vol. 35, pp. 367–382.

Persson, K. S & Sjöström, H 2003, 'Late-orogenic progressive shearing in eastern Bergslagen, central Sweden', *GFF*, vol. 125, pp. 23–36, doi:10.1080/11035890301251023

Persson, L & Persson P 1997, 'U - Pb datings of the Hedesunda and Åkersberga granites of south - central Sweden', *GFF*, vol. 119, pp. 91-95.

Persson, L, Sträng, M, Antal, I 2001, '*Berggrundskartan 10l Stockholm, skala 1:100 000*', Sveriges geologiska undersökning, SGU, Serie Ba, No 60.

Saintot, A, Stephens, M.B, Viola, G, Nordgulen, Ø 2011, Brittle tectonic evolution and paleostressfield reconstruction in the southwestern part of the Fennoscandian Shield, Forsmark, Sweden, *Tectonics*, 30, TC4002, doi:10.1029/2010TC002781.

Singhal, B.B.S. & Gupta, R.P, 2010, 'Applied hydrogeology of fractured rocks' (2nd edition), Springer, 400 p.

Svensk Kärnbränslehantering AB (SKB), 2007, *Quantifying in situ stress magnitudes and orientations for Forsmark, Forsmark stage 2.2*', SKB Rapport R-07-26, 95 p.

Stephens, M.B, Ripa, M, Lundström, I, Persson, L, Bergman, T, Ahl, M, Wahlgren, C-H, Persson, P.O & Wickström, L 2009, '*Synthesis of the bedrock geology in the Bergslagen region, Fennoscandian shield, south-central Sweden*', Geological Survey of Sweden (SGU), Serie Ba, vol. 58, 249 p.

Stephens, M. B, Wahlgren, C. H, Weijermars, R, Cruden, A. R 1996, 'Left-lateral transpressive deformation and its tectonic implications, Sveconorwegian orogen, Baltic Shield, southwestern Sweden', *Precambrian Research*, vol. 79, pp. 261–279.

Stålhös, G, 1976, 'Aspects of the regional tectonics of eastern central Sweden', *GFF*, vol. 98, no. 2, pp. 146-154.

Stålhös, G 1981, 'A tectonic model for the Svecokarelian folding in east central Sweden', *GFF*, vol. 193, no 1, pp. 33-46.

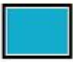
Stålhös, G & Björk, L 1983, 'Interpretation of late Svecokarelian metadiabases associated with eruptive breccias in south central Sweden', *GFF*, vol. 105, no. 4, pp. 321-333.

Internet online resources consulted:

Burg, J.-P, 2014, '*Strike-Slip and Oblique-Slip Tectonics*', Lecture notes in course 'Structural Geology' pp. 157–176. Swiss Federal Institute of Technology in Zurich (ETHZ). Available at: [<http://www.files.ethz.ch/structuralgeology/JPB/files/English/5wrench.pdf>]

Appendix 1

1. Reinforcement properties of shot-concrete

Color	
Liner Type	Standard Beam
Formulation	Timoshenko
Thickness	0.1 m


Elastic Properties

Young's modulus	30000 MPa
Poisson's ratio	0.2

Strength Parameters

Peak compressive strength	35 MPa
Residual compressive strength	5 MPa
Peak tensile strength	5 MPa
Residual tensile strength	0 MPa

2. Reinforcement properties of bolt

Bolt name	Bolt 1
Color	
Bolt Type	Fully bonded bolt
Diameter	25 mm
Young's modulus	200000 MPa
Tensile capacity	0.2 MN
Residual Tensile capacity	0 MN
Pre-tensioning	0 MN
Pre-tensioning force	Constant in install stage
Out-of-plane spacing	0.5 m
Allow Joints to Shear Bolt	Yes

Appendix 2

1. Models with pre-installed support

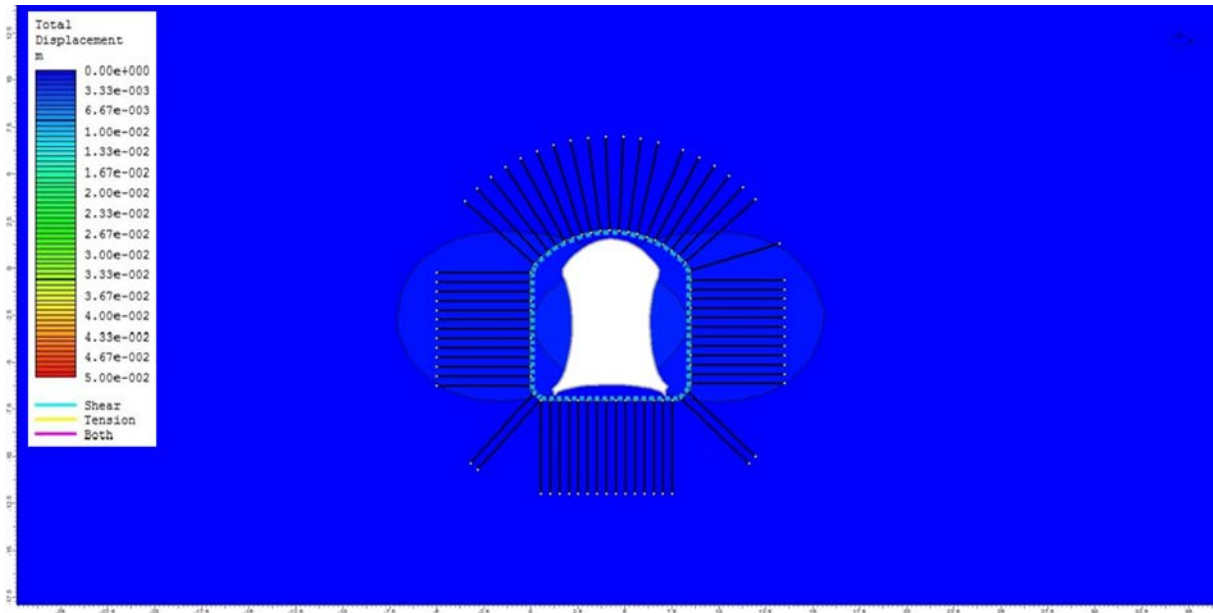


Figure A1. Pre-installed bolts, good quality rock with elastic properties.

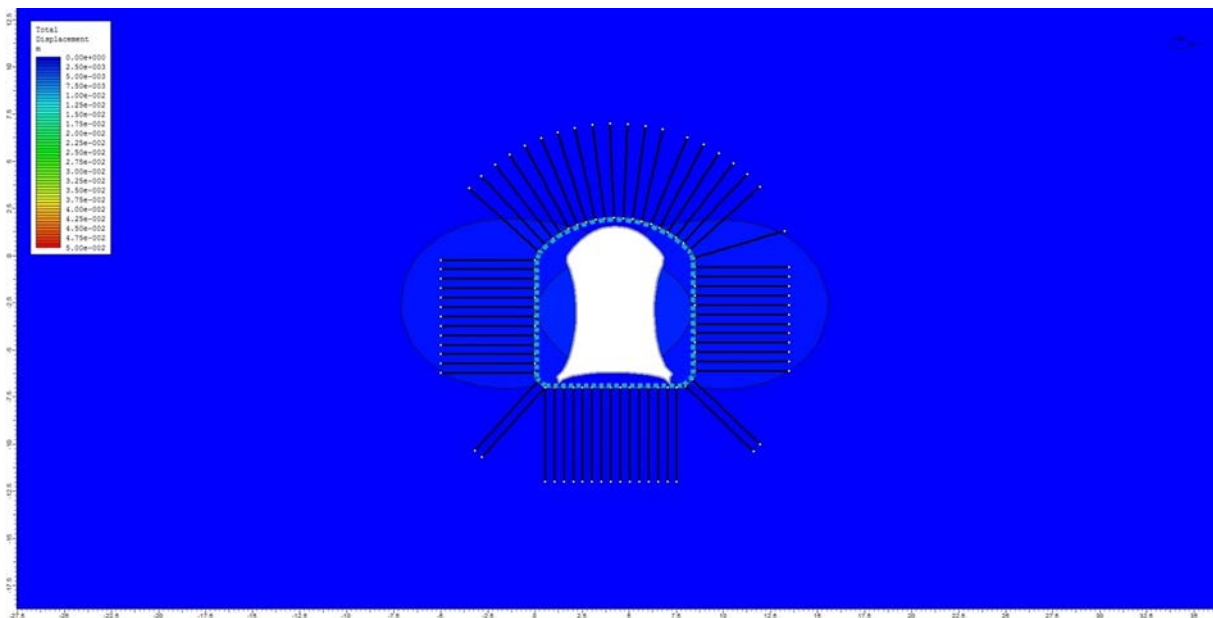


Figure A2. Pre-installed bolts, good quality rock with plastic properties.

2. Models with excavation in two steps

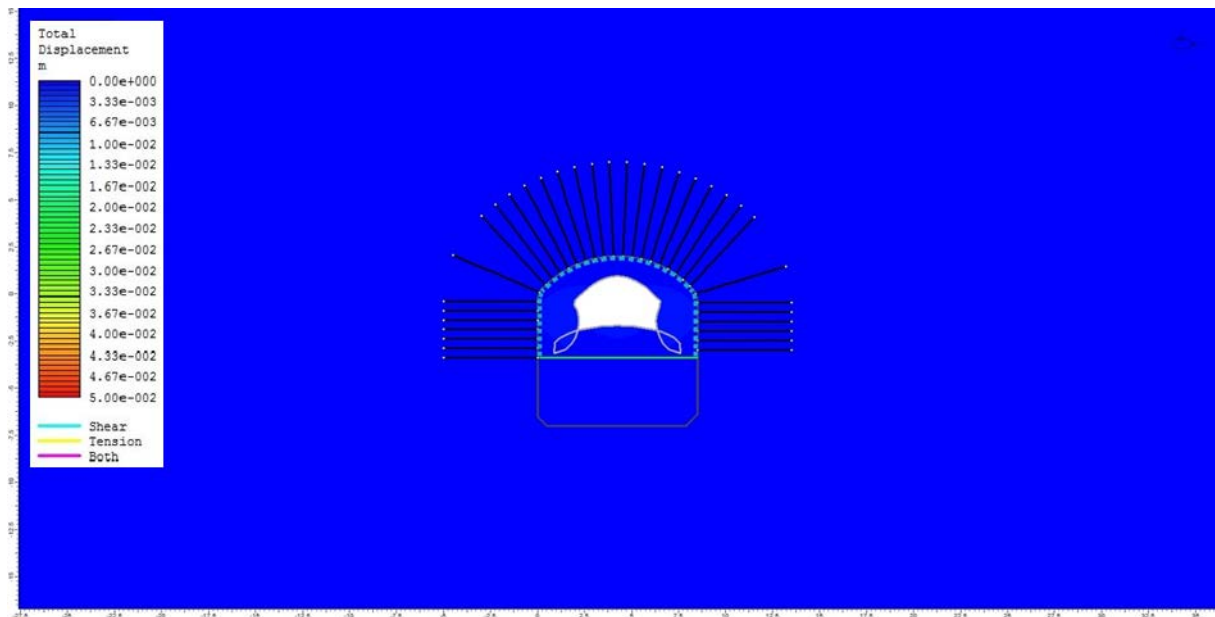


Figure A3. Stage 2 Excavation of the top half of the tunnel for good quality rock with elastic properties.

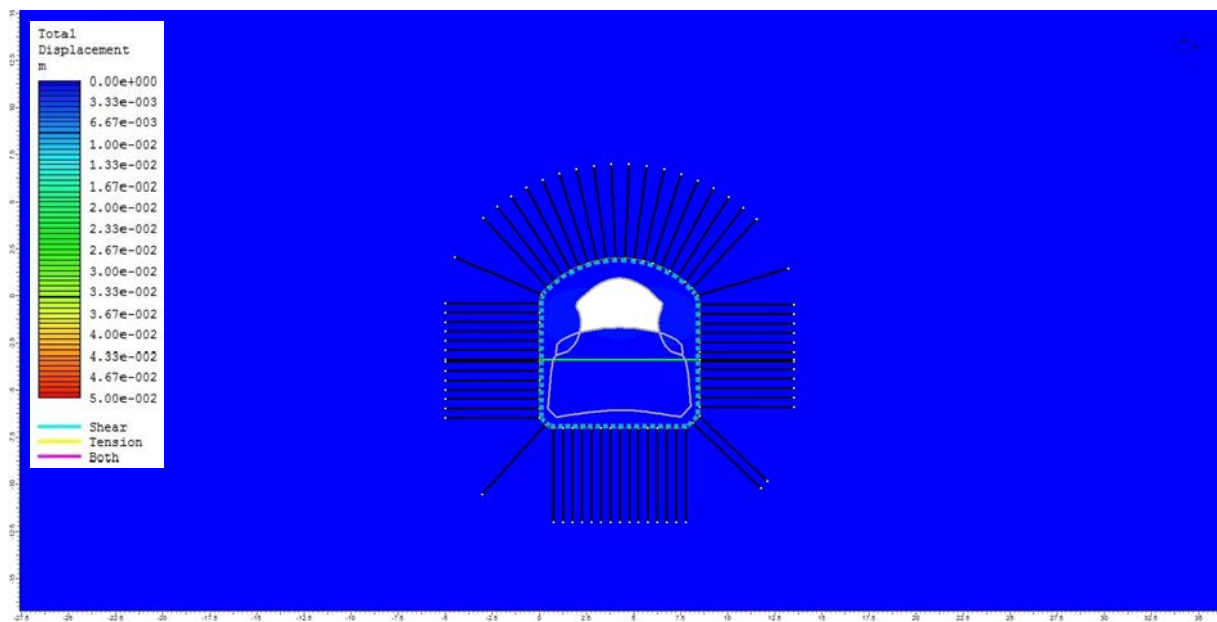


Figure A4. Stage 3, installation of bolts in the floor of the tunnel for good quality rock with elastic properties.

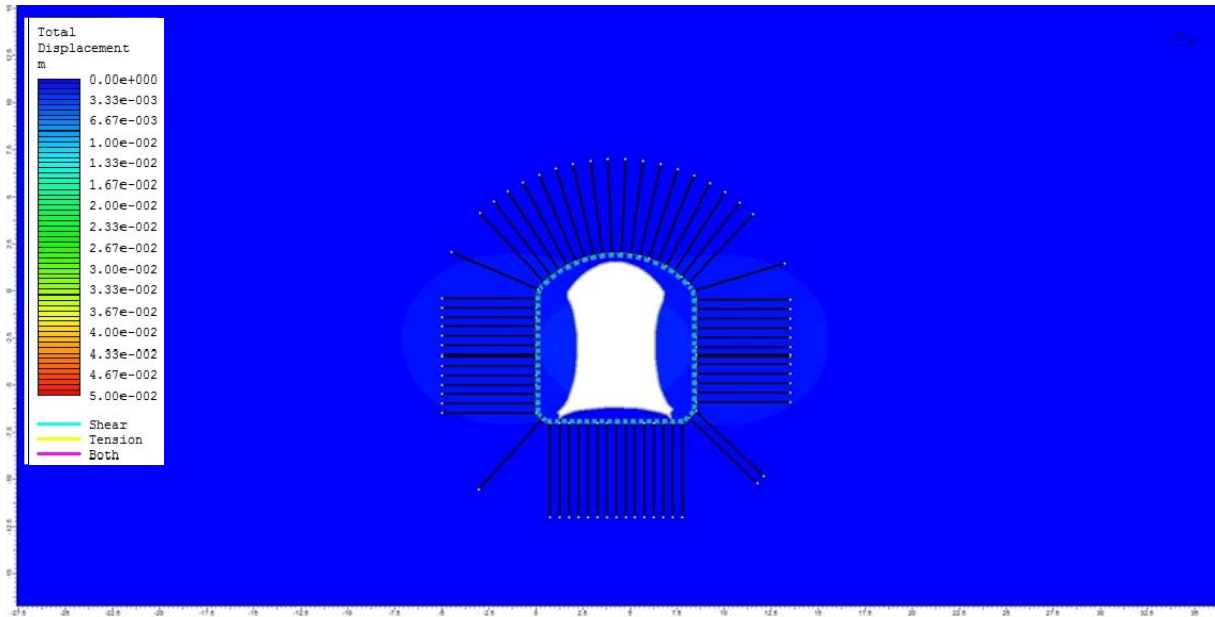


Figure A5. Stage 4, excavation of the floor of the tunnel for good quality rock with elastic properties.

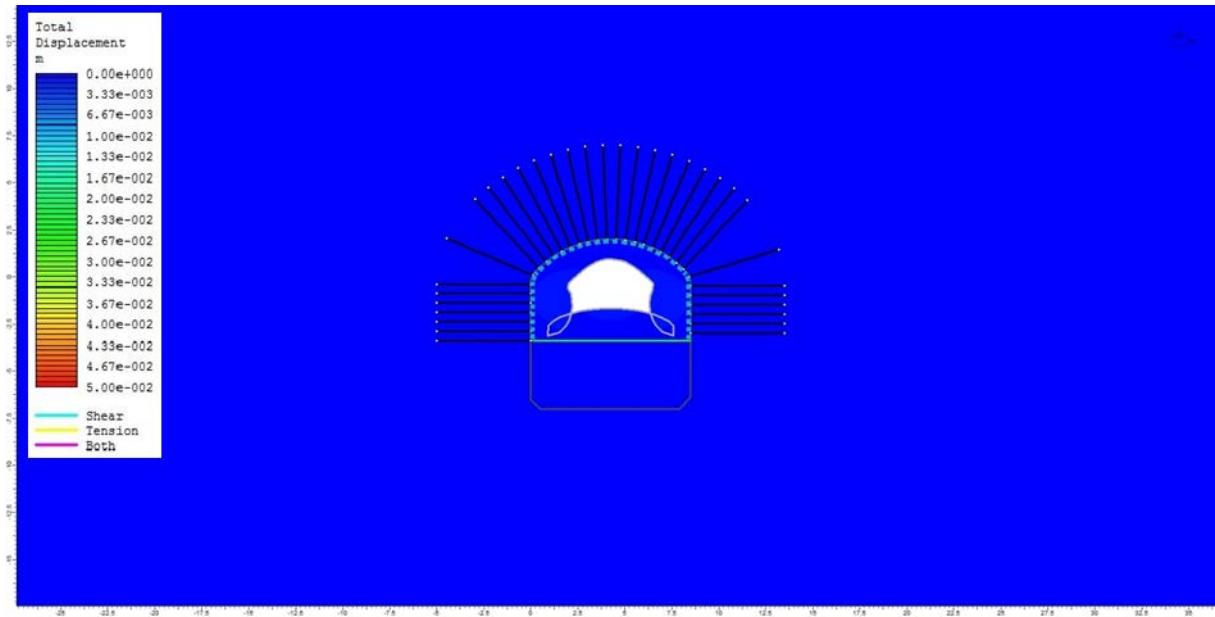


Figure A6. Stage 2, excavation of the top half of the tunnel for good quality rock with plastic properties.

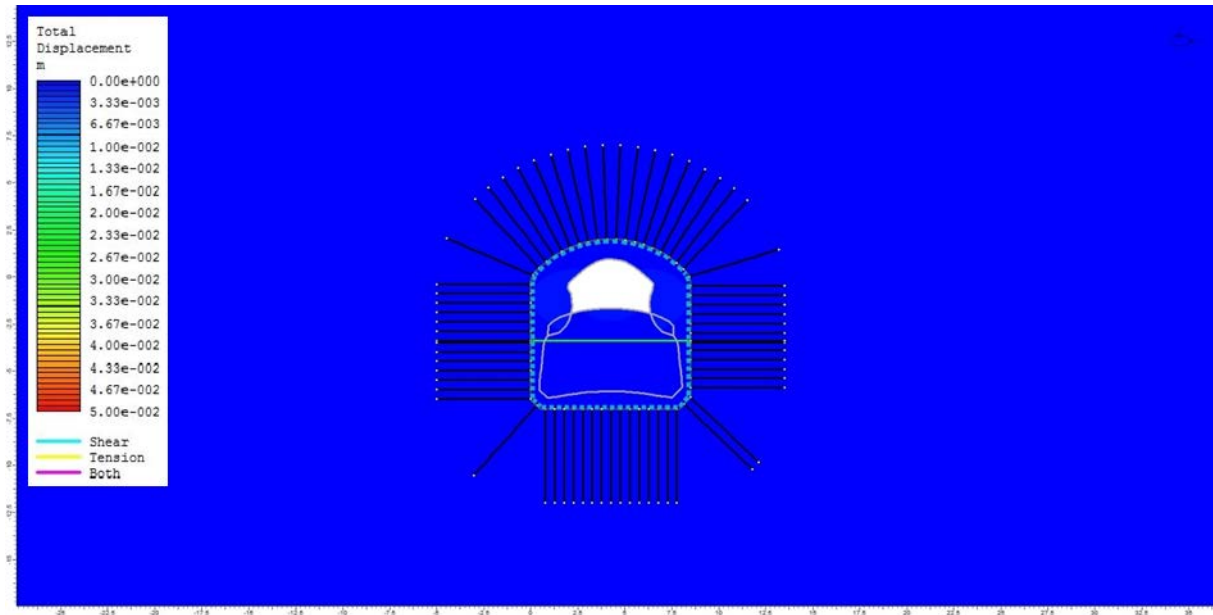


Figure A7. Stage 3, installation of bolts in the floor of the tunnel.

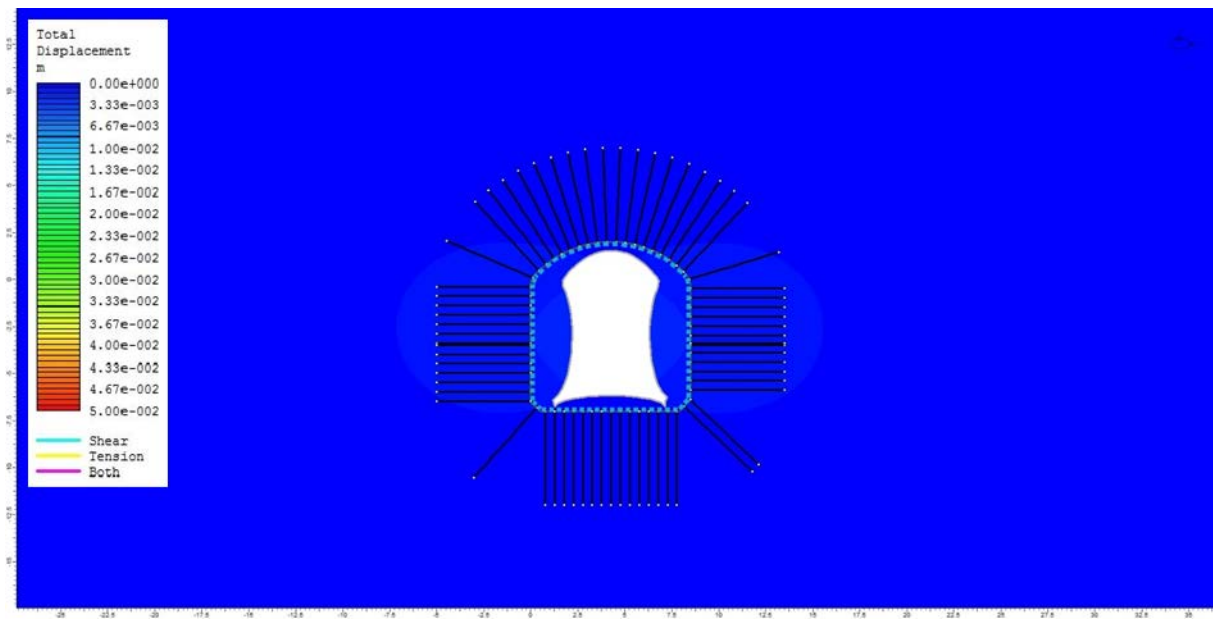


Figure A8. Excavation of the floor of the tunnel for good quality rock with plastic properties.

3. Round models with elastic properties and pre-installed bolt in stage 1

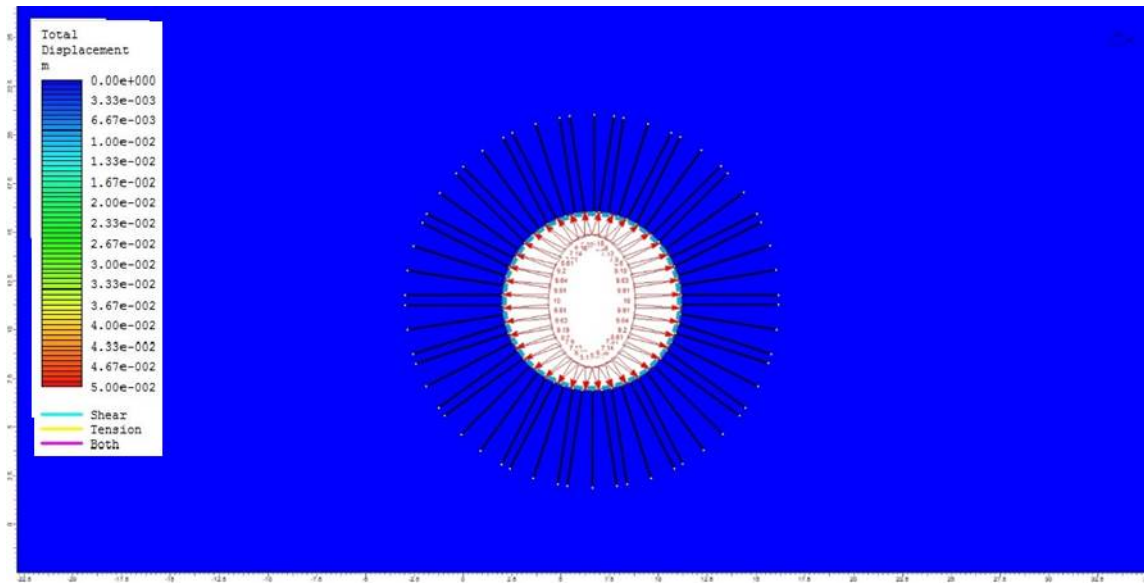
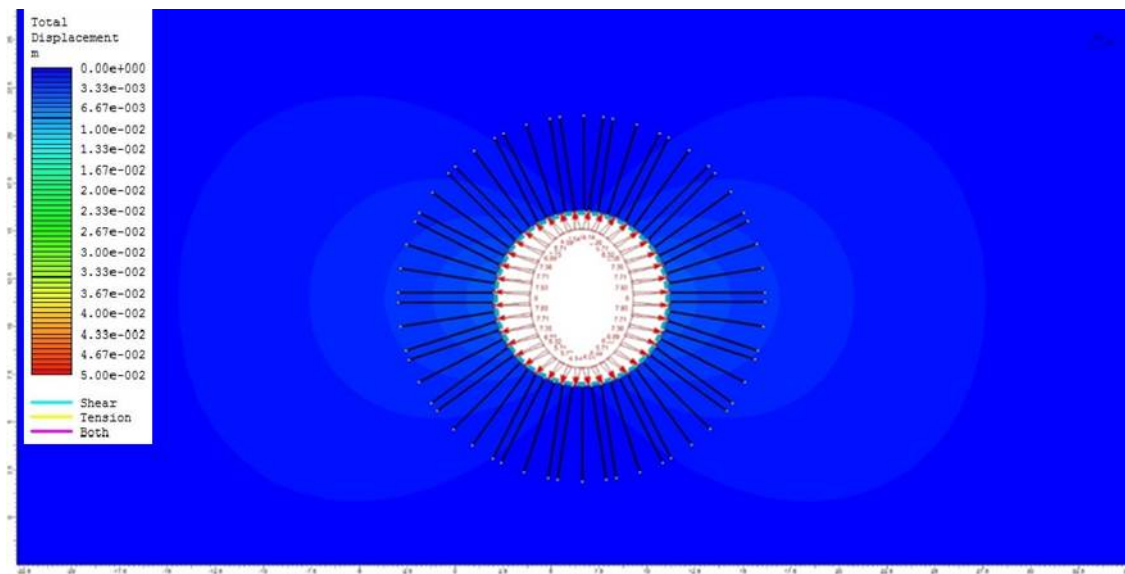


Figure A9. Round model stage 1 internal pressure equal as in-situ pressure



FigureA10. Round model stage 2, decrease of internal pressure.

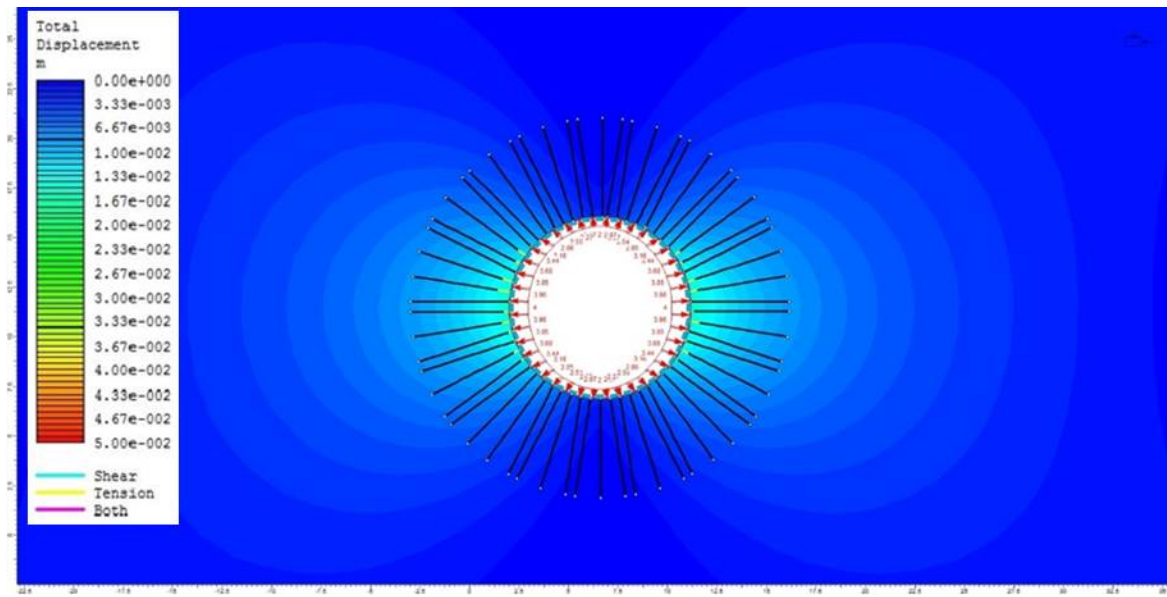


Figure A11. Round model stage 3, bolts are starting to yield, the determined stage to install bolts for maximum support.

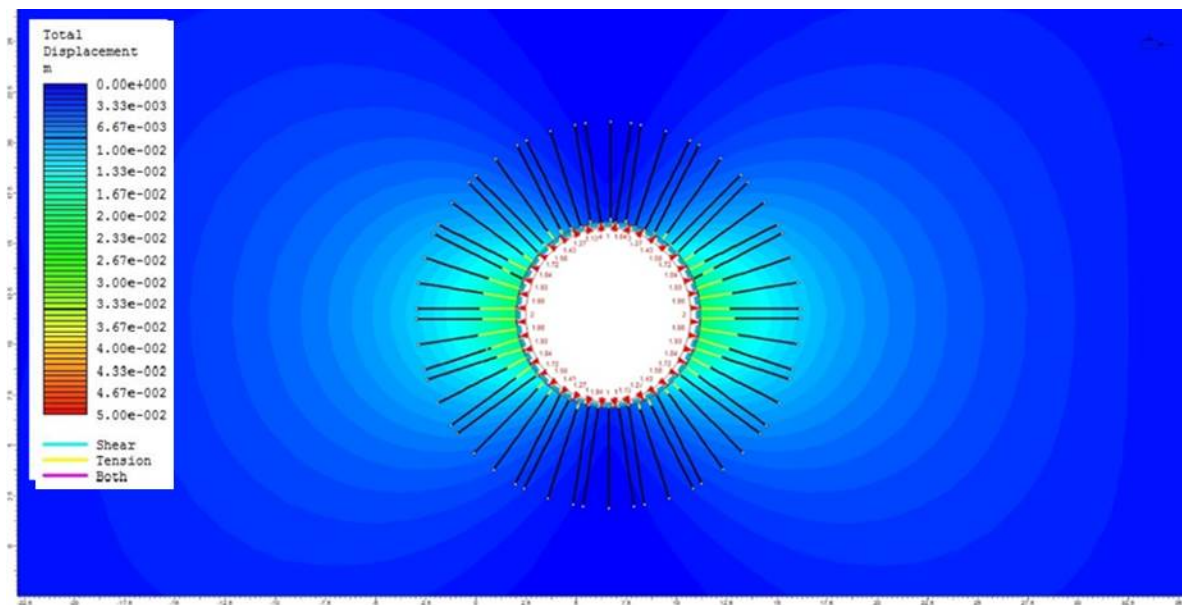


Figure A12. Round model stage 4.

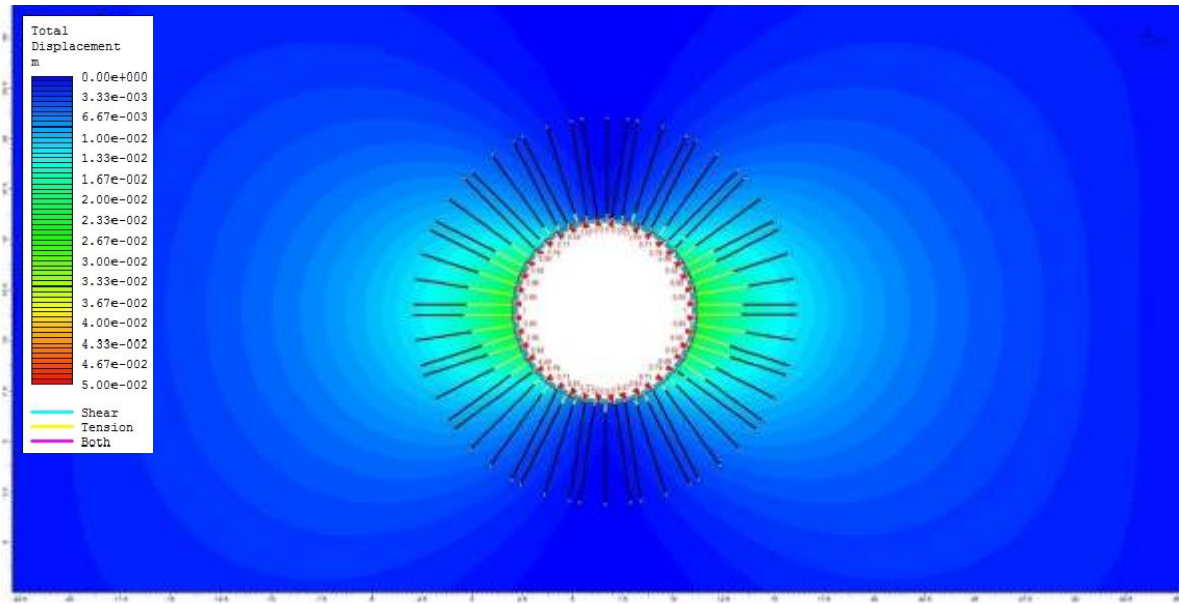


Figure A13. Round model stage 5.

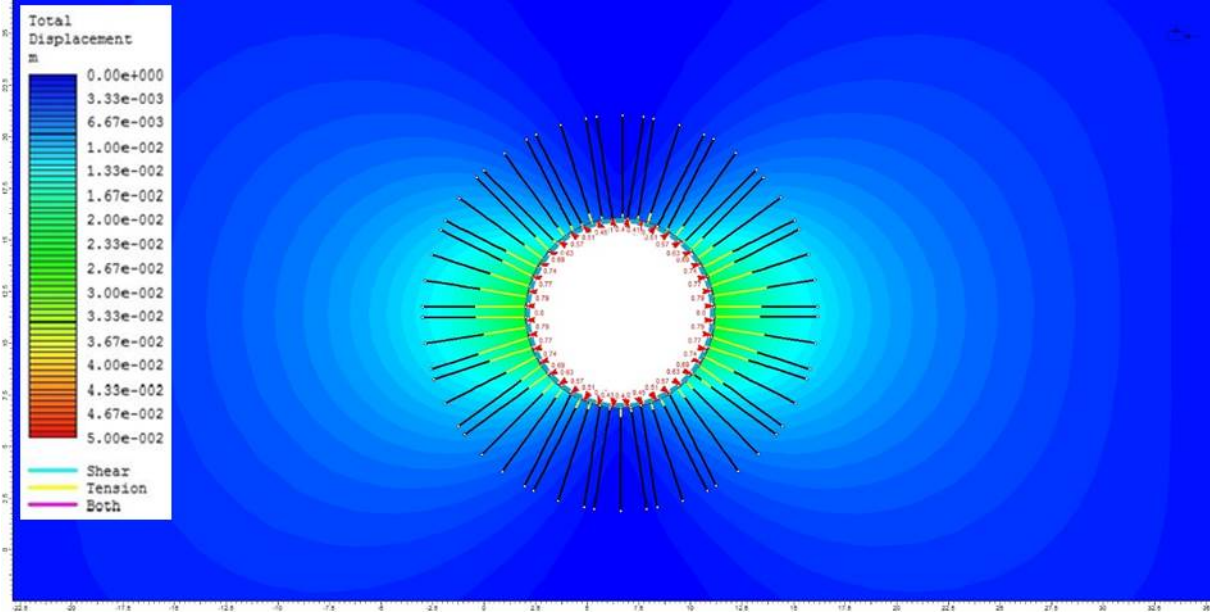


Figure A14. Round model stage 6.

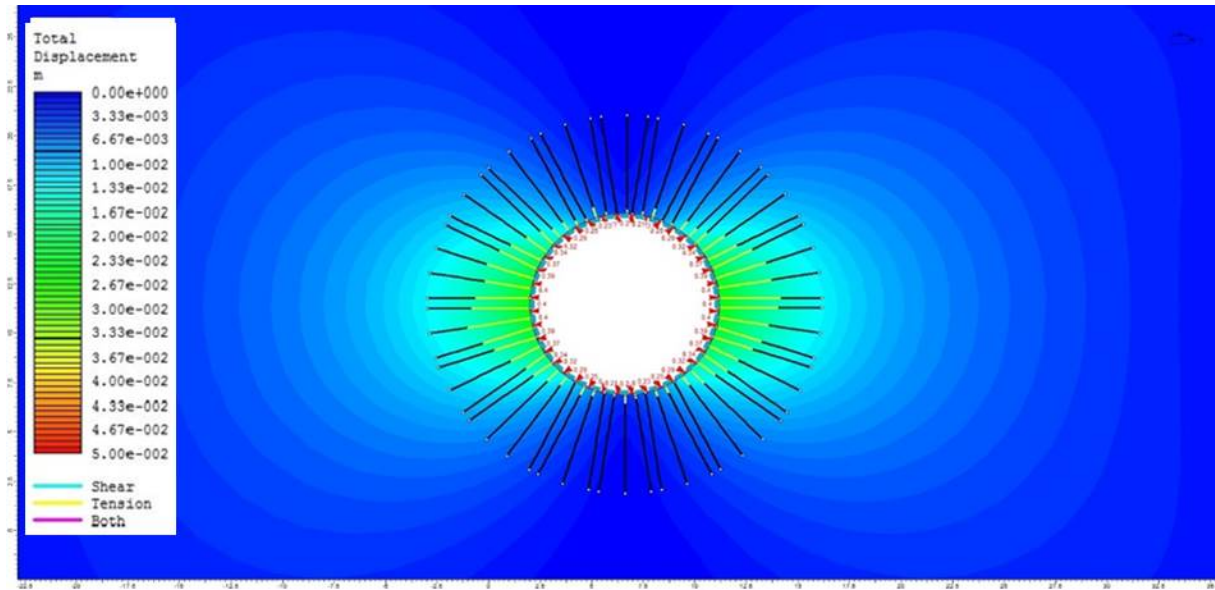


Figure A15. Round model stage 7.

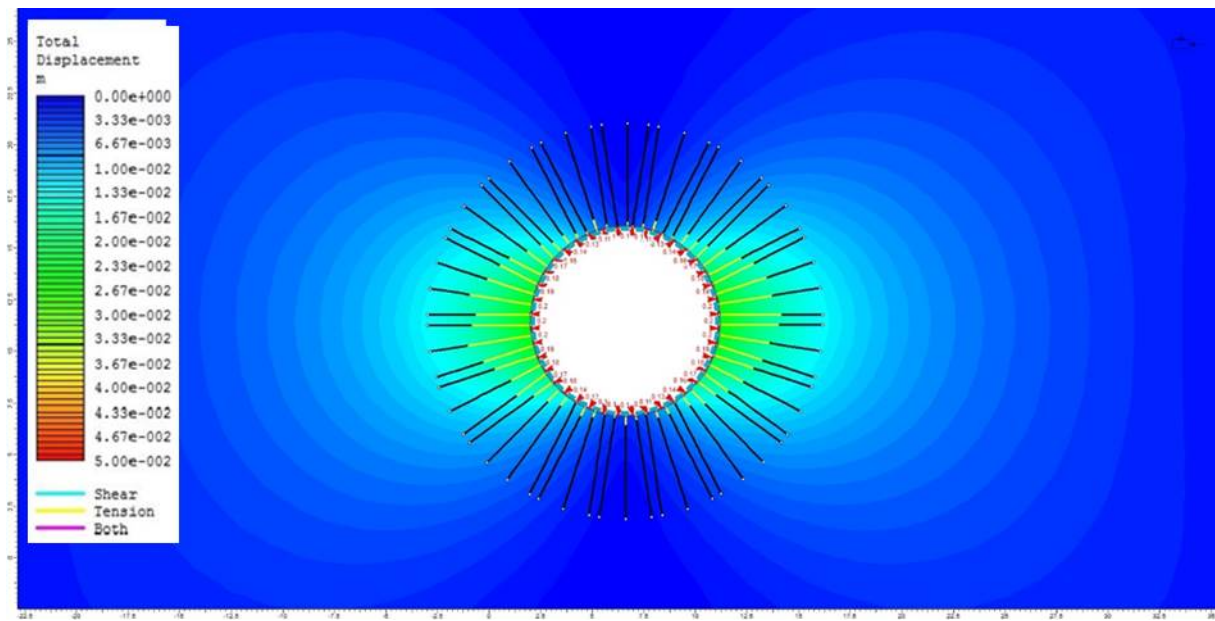


Figure A16. Round model stage 8.

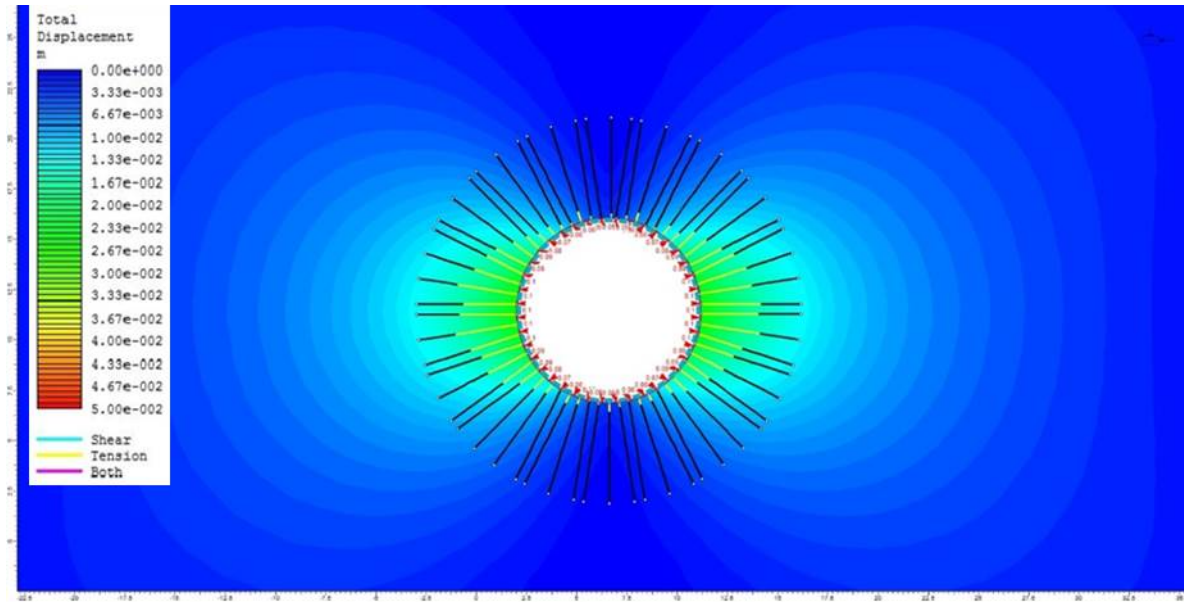


Figure A17. Round model stage 9.

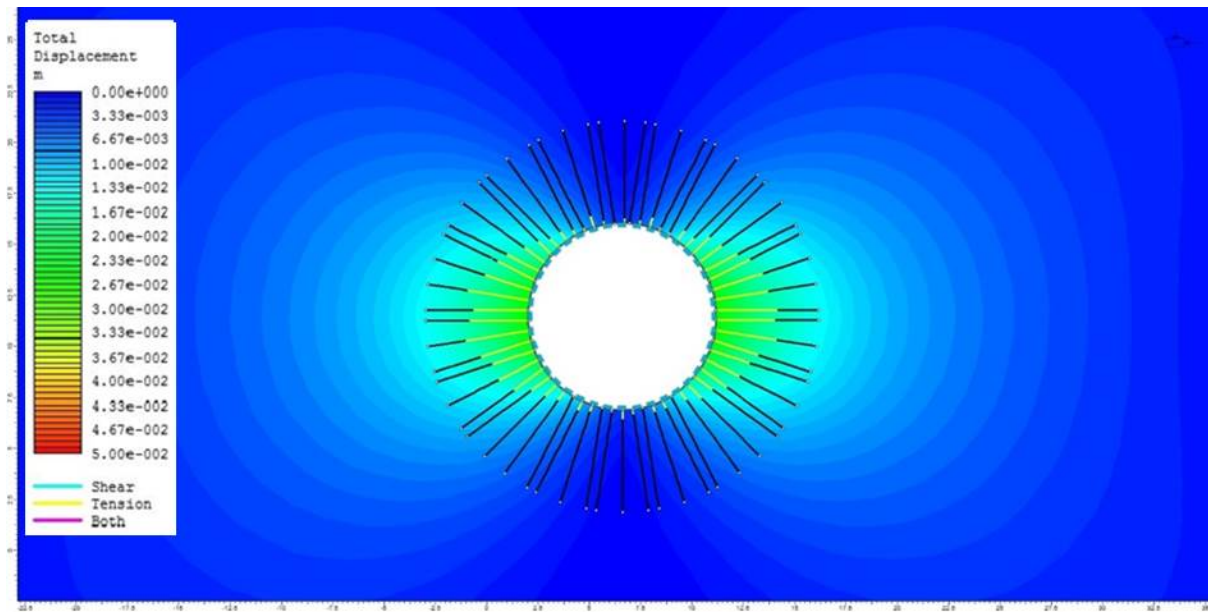


Figure A18. Round model without internal pressure.

4. Round models with plastic properties and pre-installed bolt in stage 1

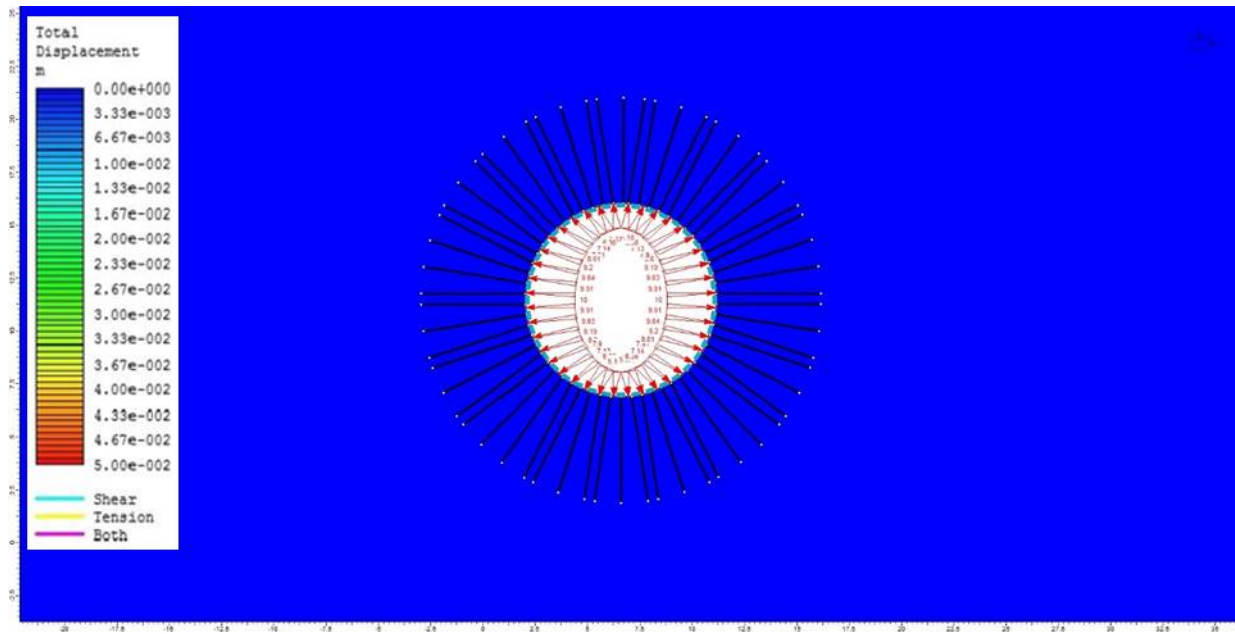


Figure A19. Round model stage 1, internal pressure same as in-situ stress.

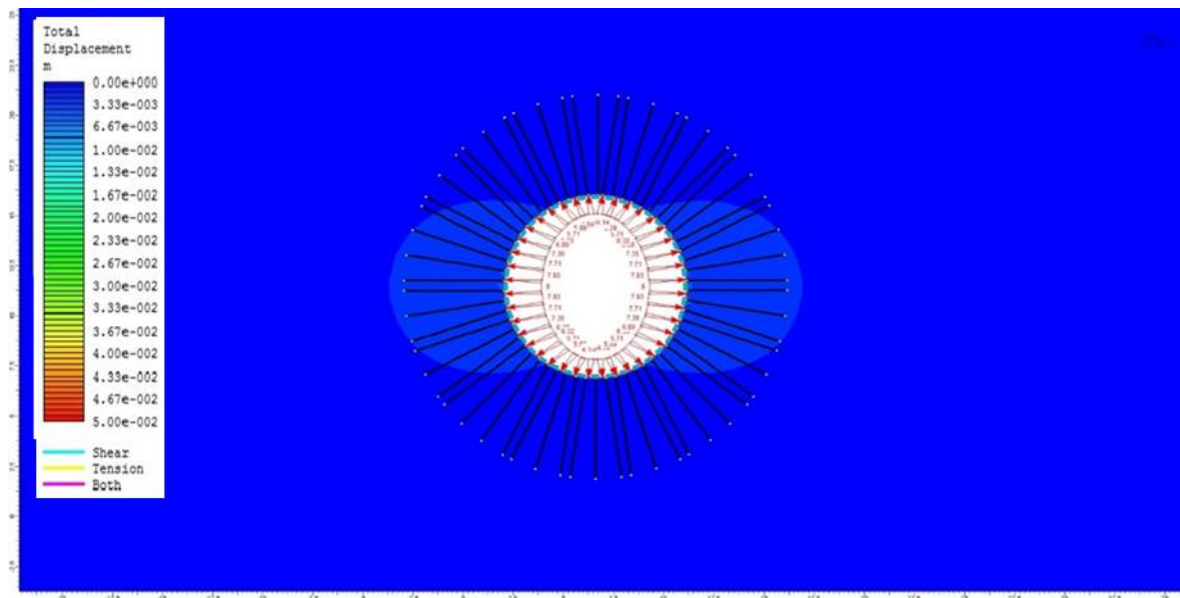


Figure A20. Round model stage 2.

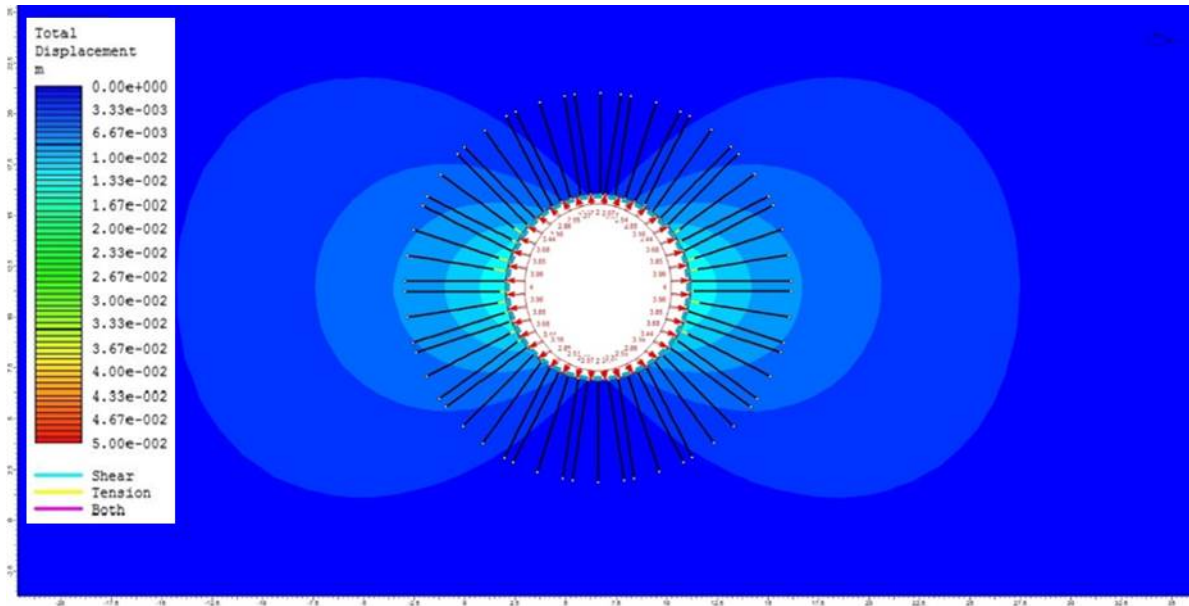


Figure A21. Round model stage 3, bolts starts to yield, determined to install bolt in this stage.

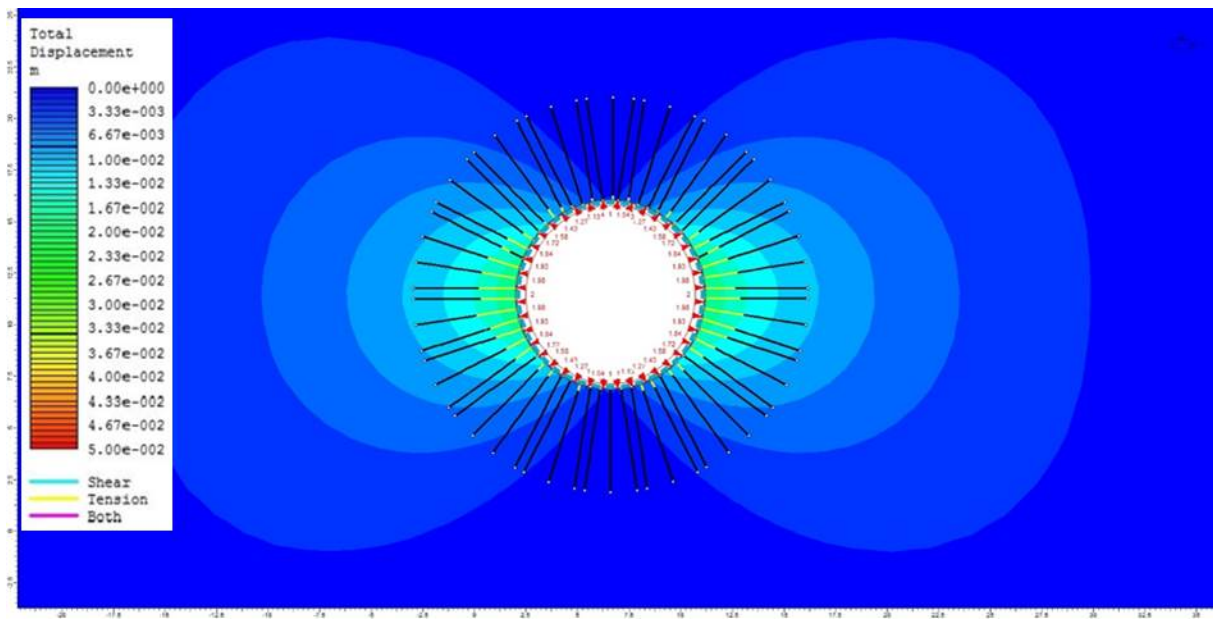


Figure A22. Round model stage 4.

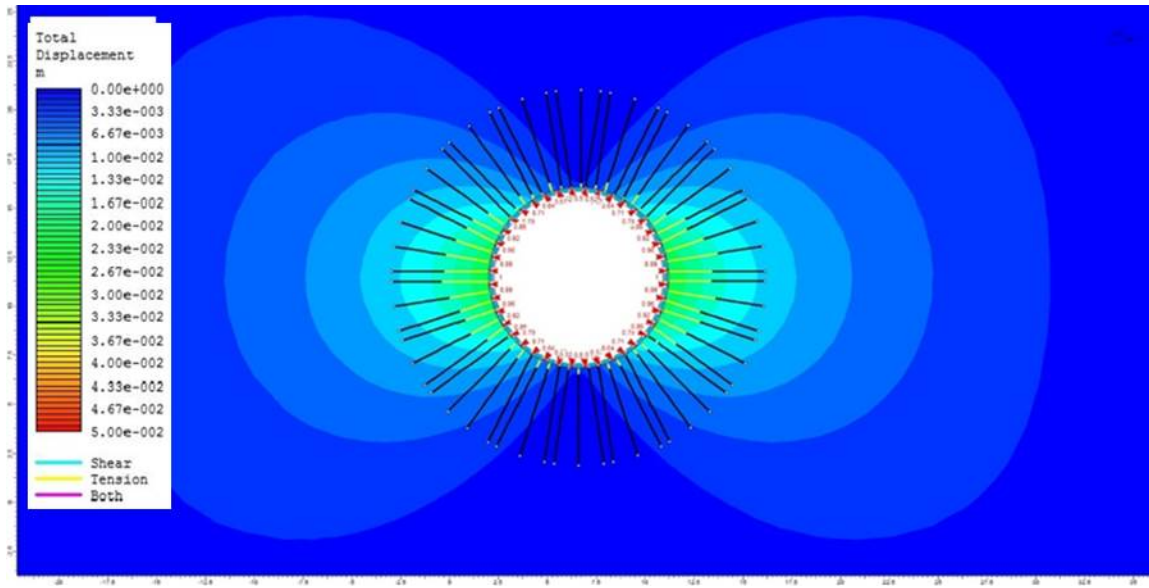


Figure A23..Round model stage 5.

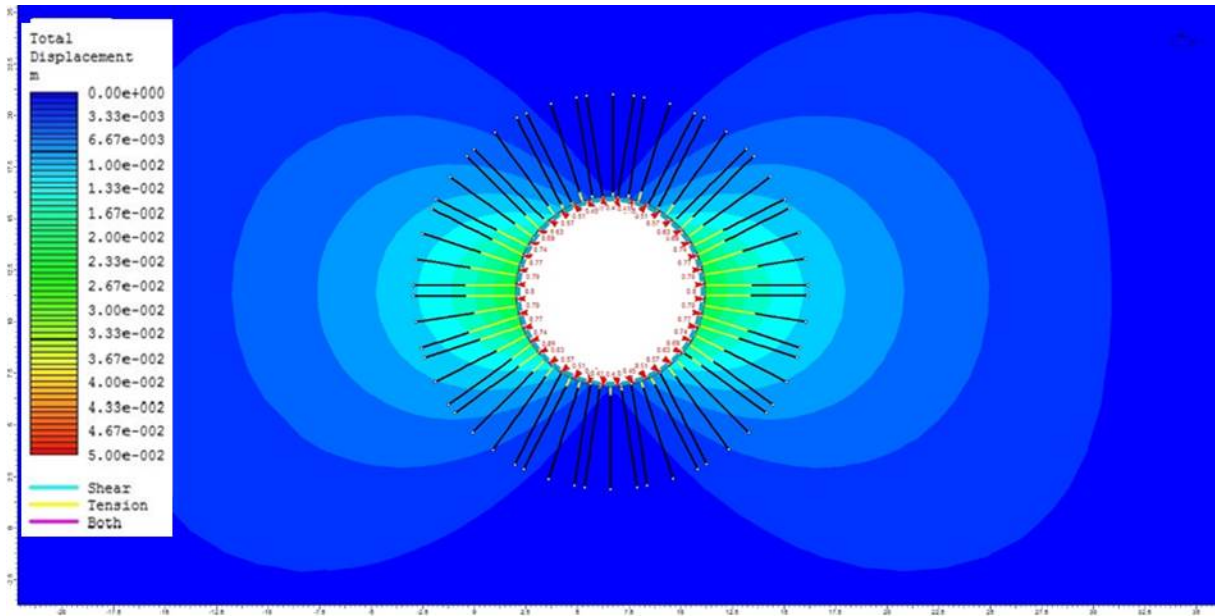


Figure A24. Round model stage 6.

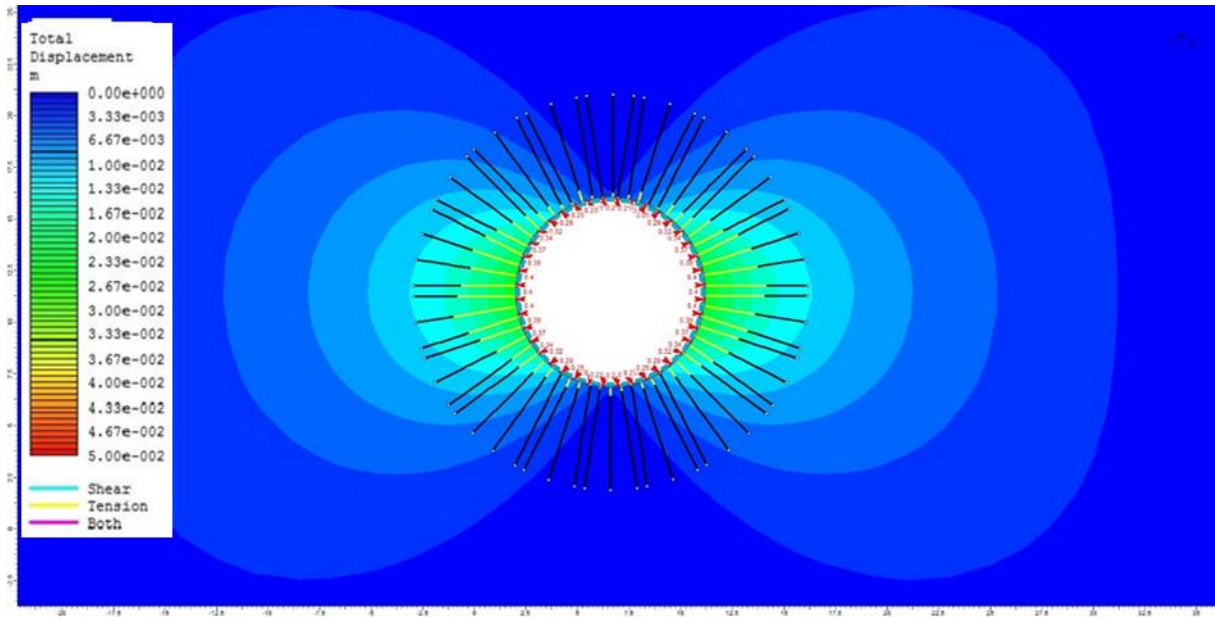


Figure A25. Round model stage 7.

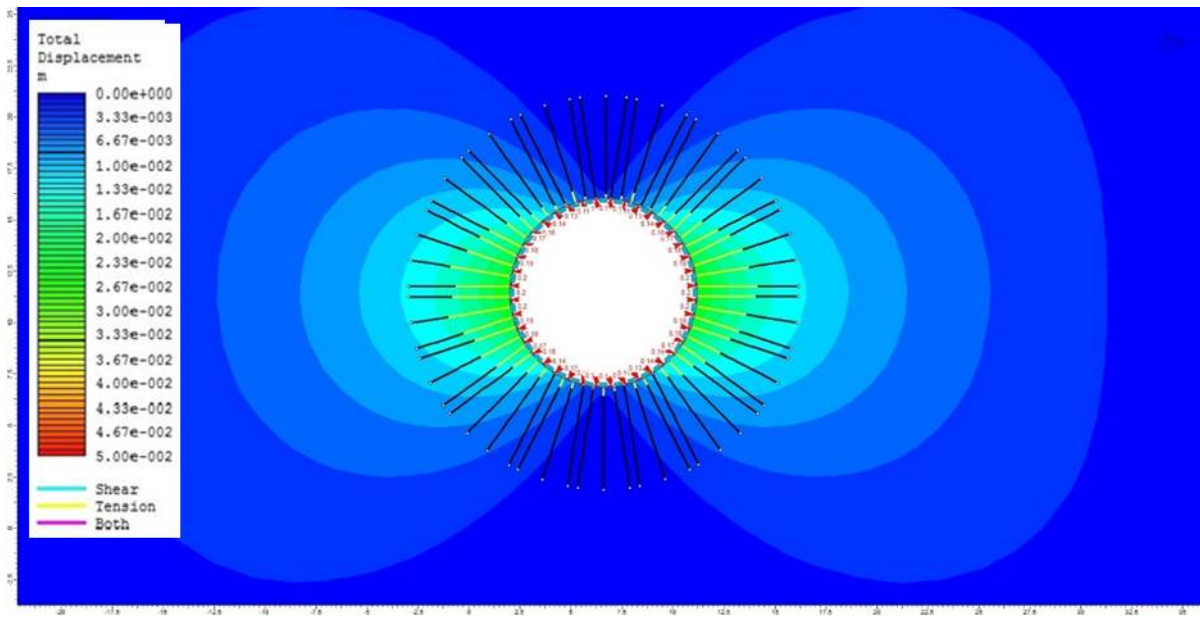


Figure A25. Round model stage 8.

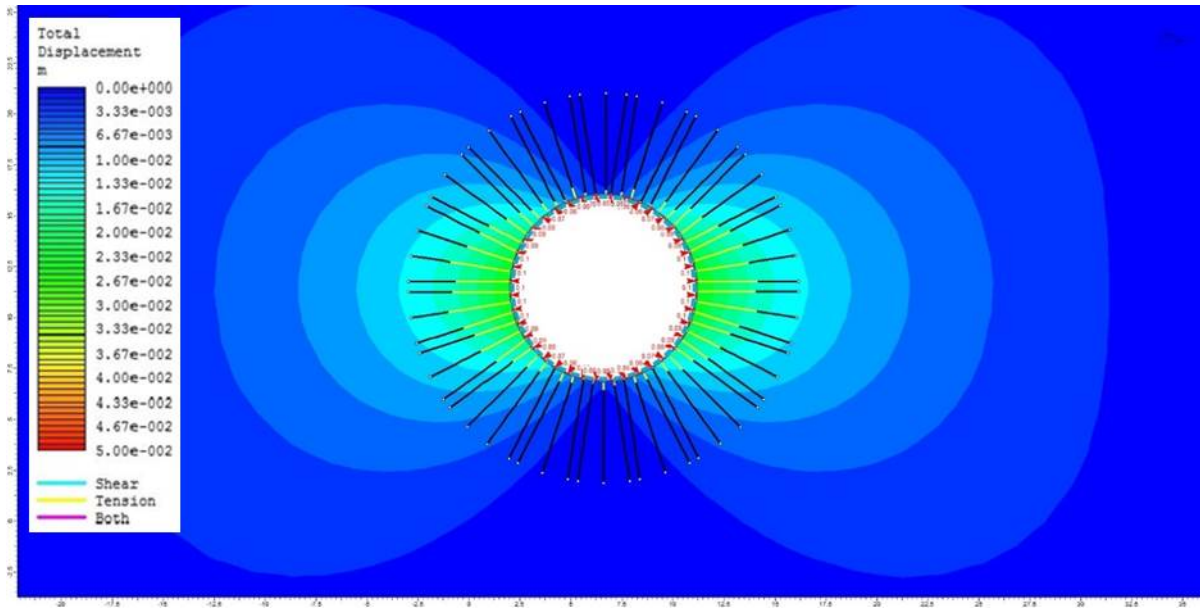


Figure A27. Round model stage 9.

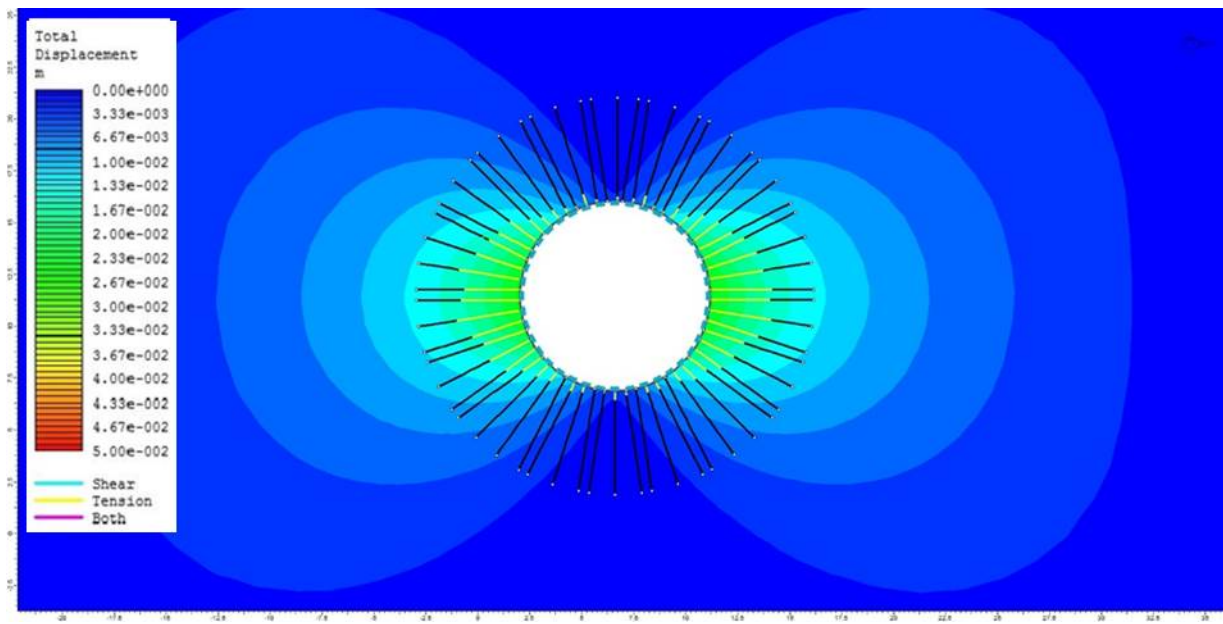


Figure A28. Round model stage 10, without internal pressure.

5. Round model with elastic properties and bolts installed in stage 3

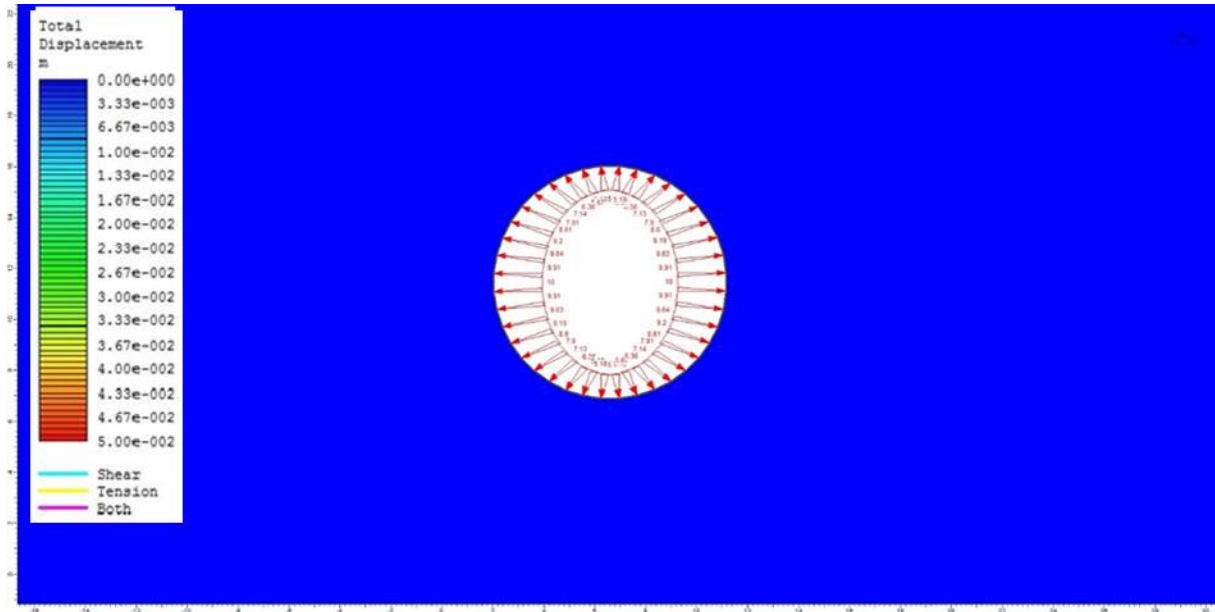


Figure A29. Round model stage 1, with same internal pressure as the in-situ stress.

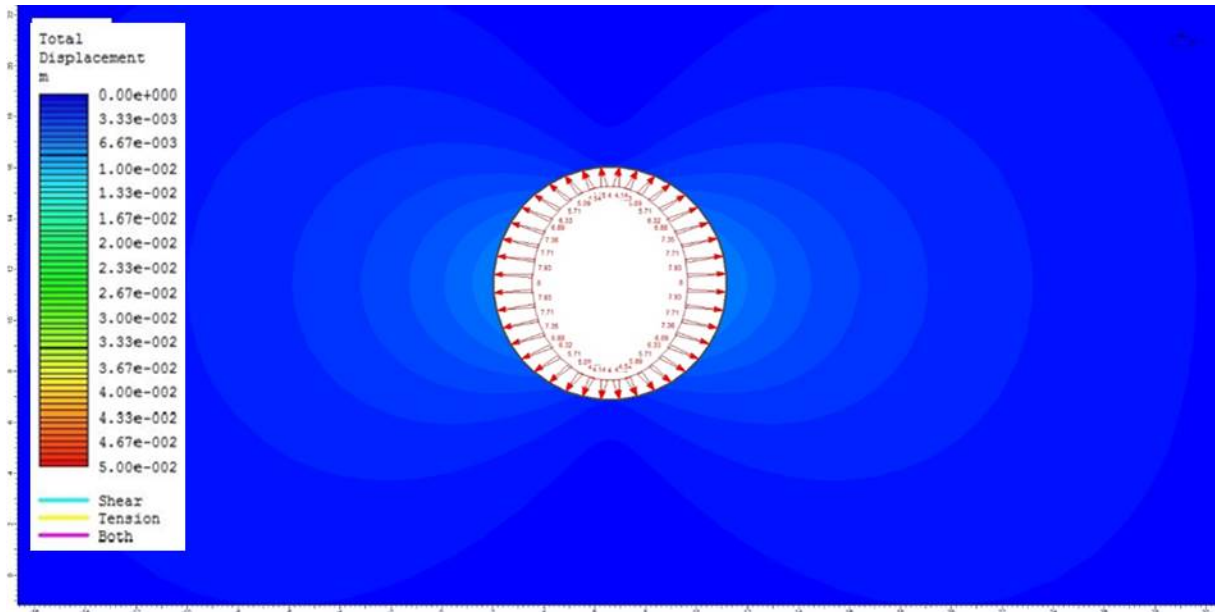


Figure A29. Round model stage 2.

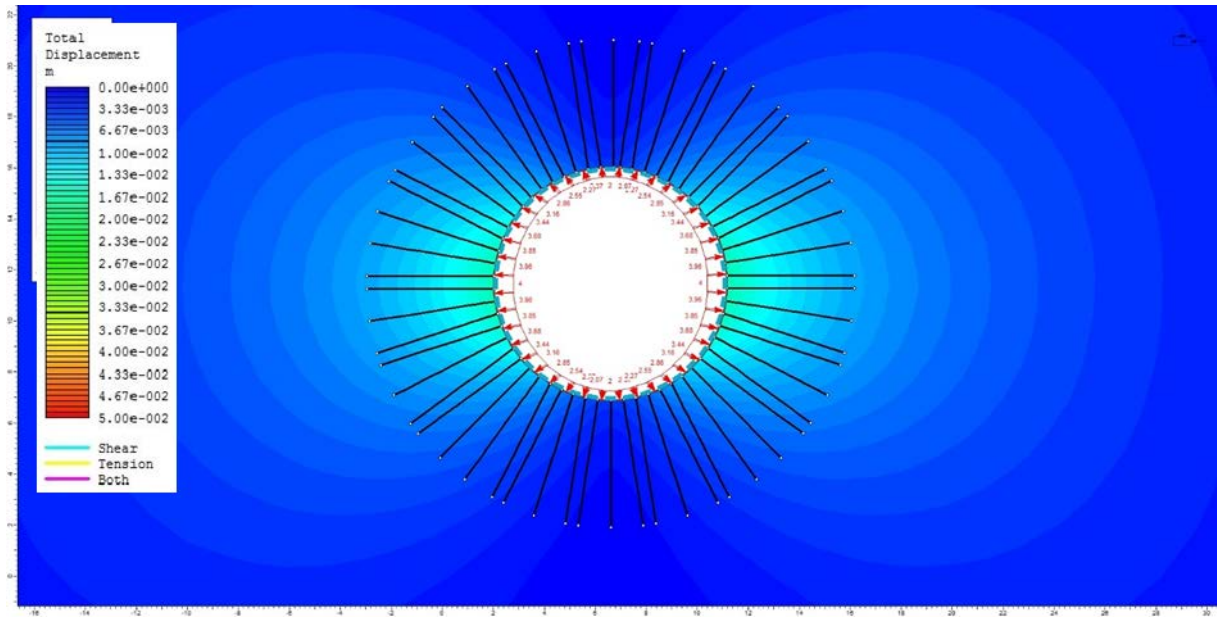


Figure A30. Round model, stage 3 bolts are installed.

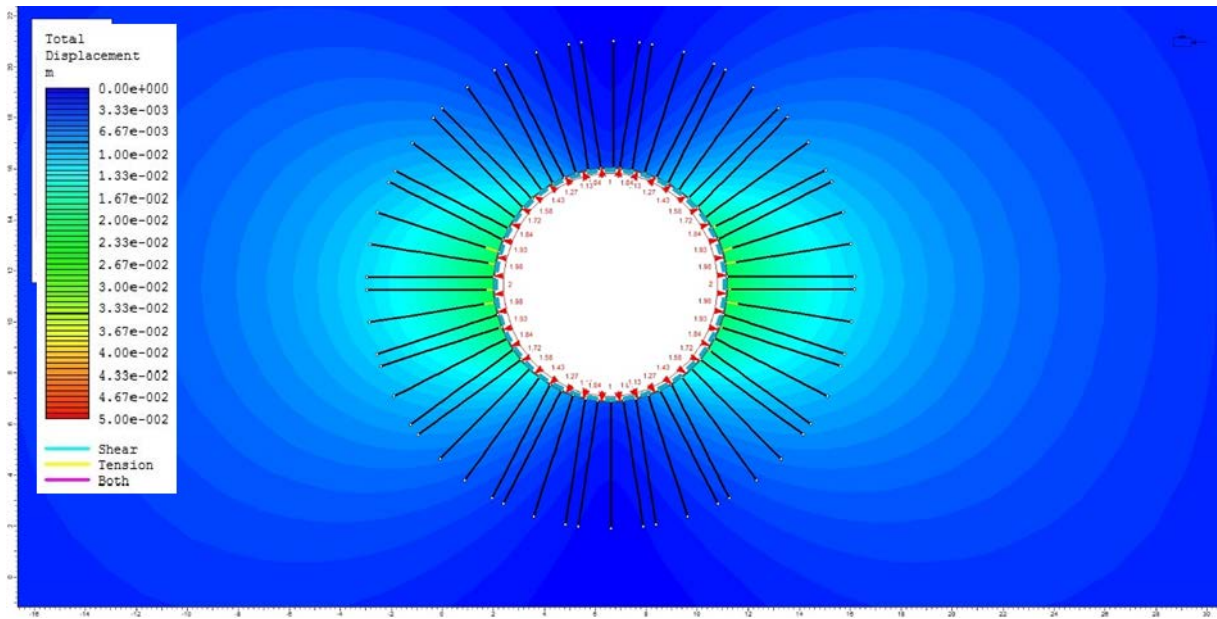


Figure A31. Round model, stage 4.

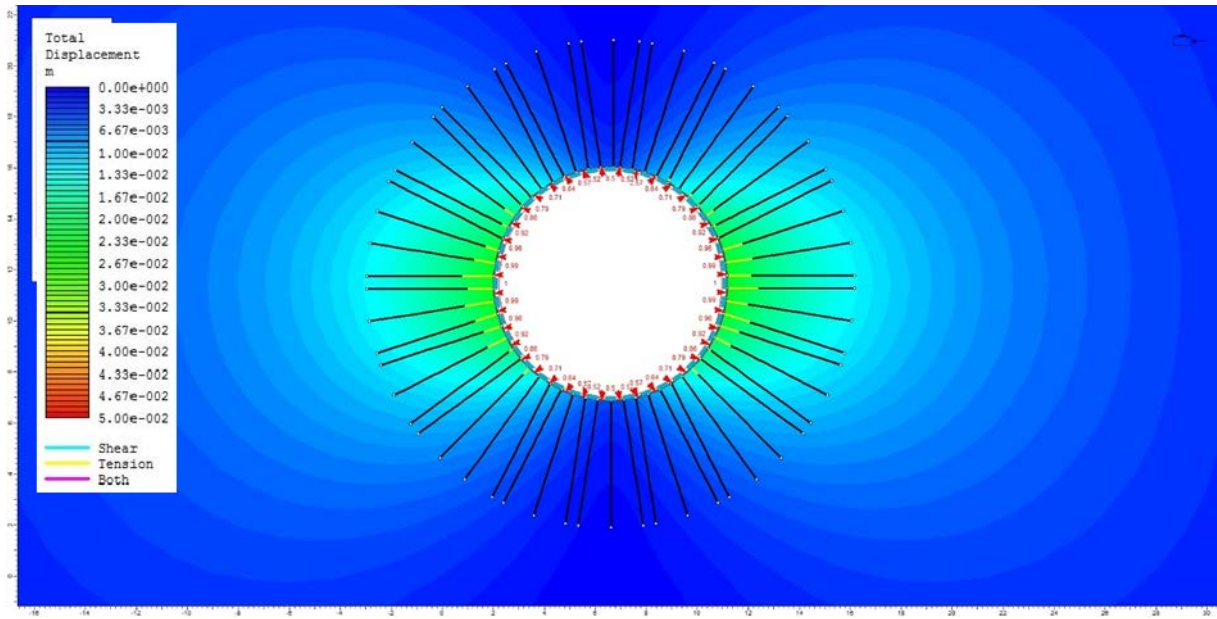


Figure A32. Round model, stage 5.

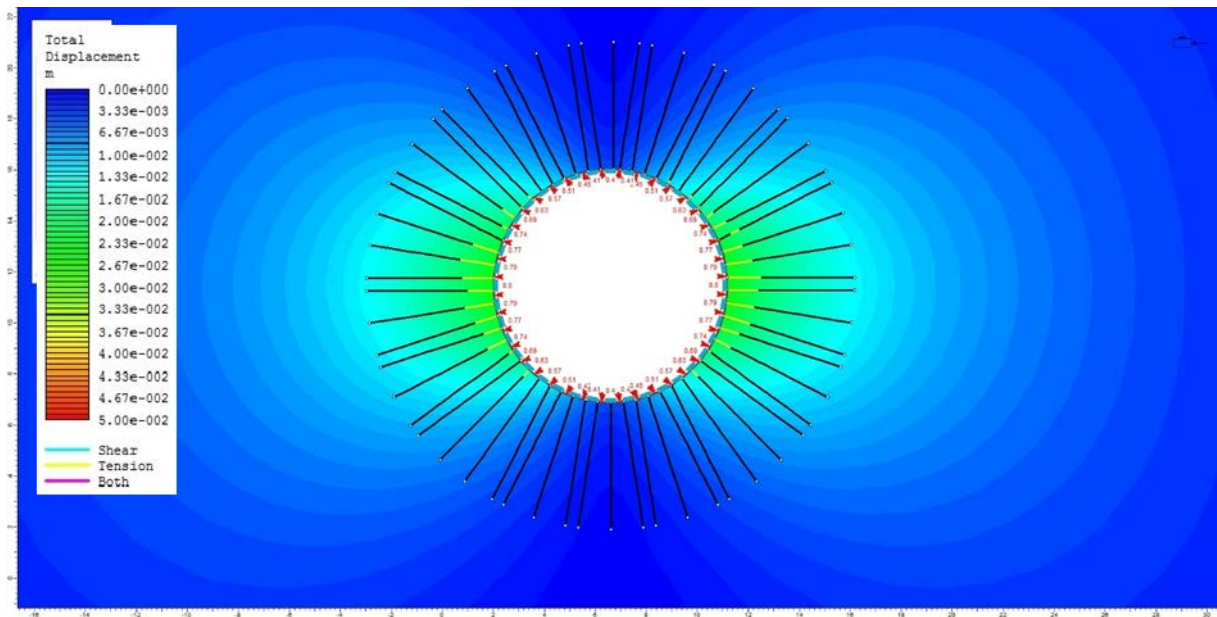


Figure A33. Round model, stage 6.

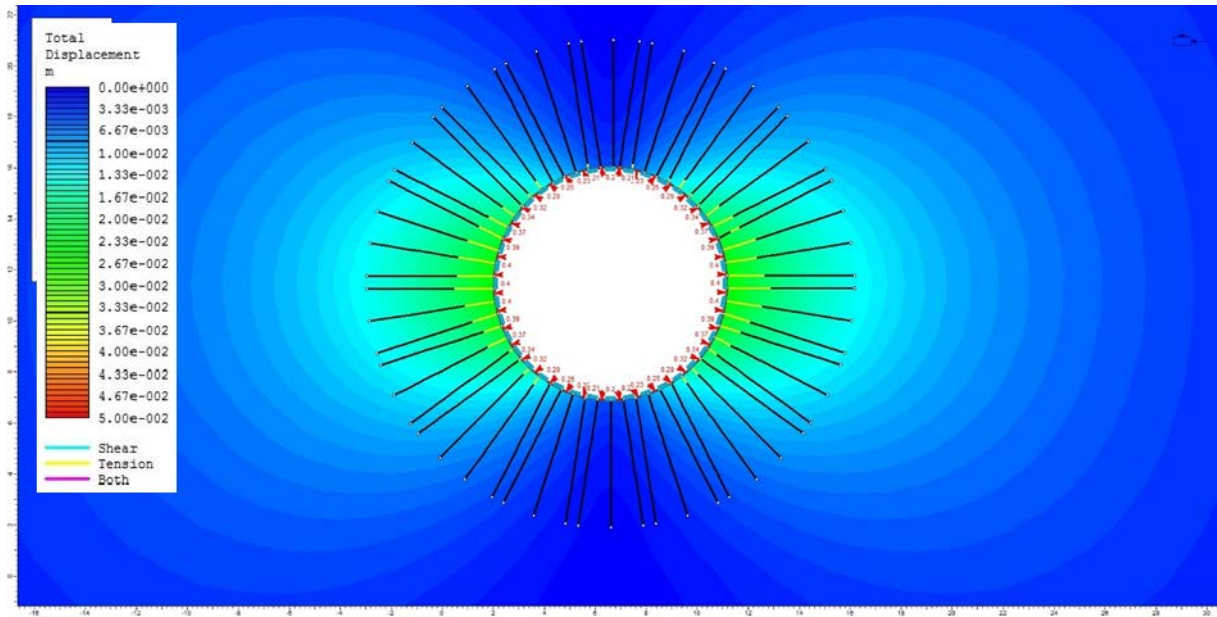


Figure A34. Round model, stage 7.

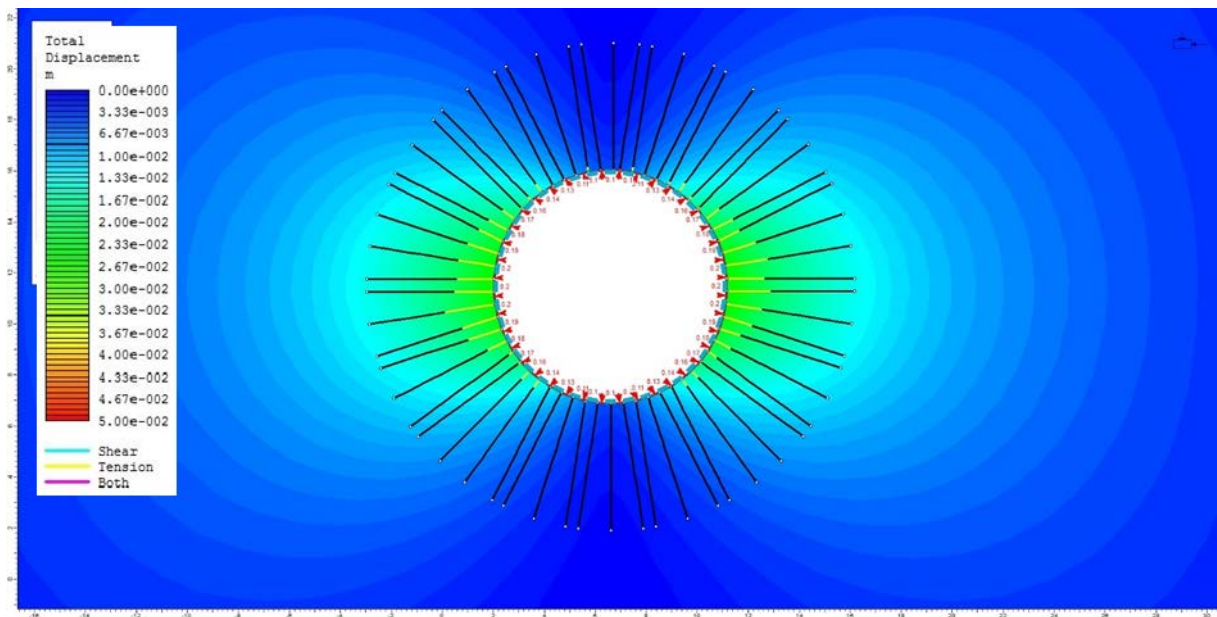


Figure A35. Round model, stage 8.

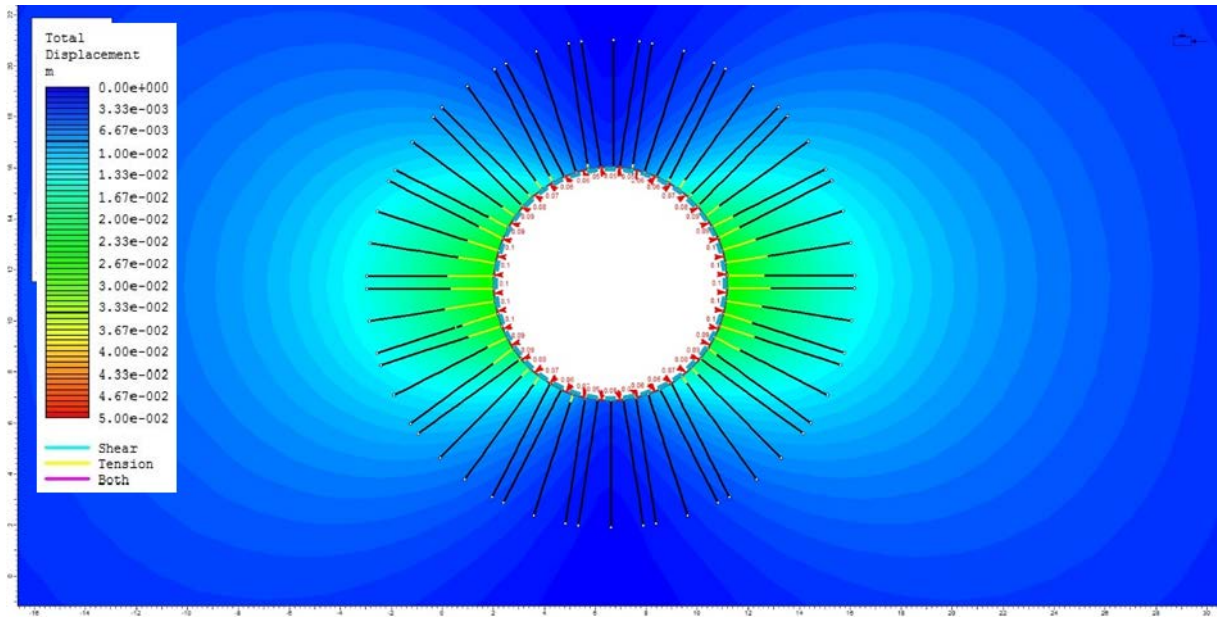


Figure A36. Round model, stage 9.

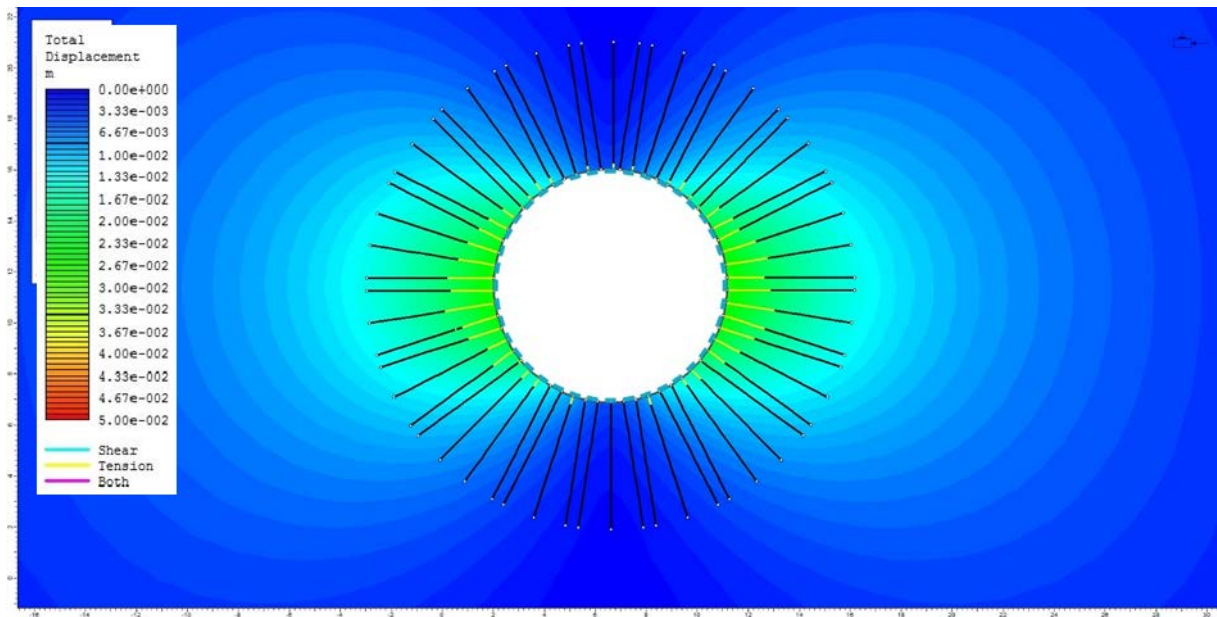


Figure A37. Round model, stage 10 without internal pressure.

6. Round model with plastic material and bolts installed in stage 3

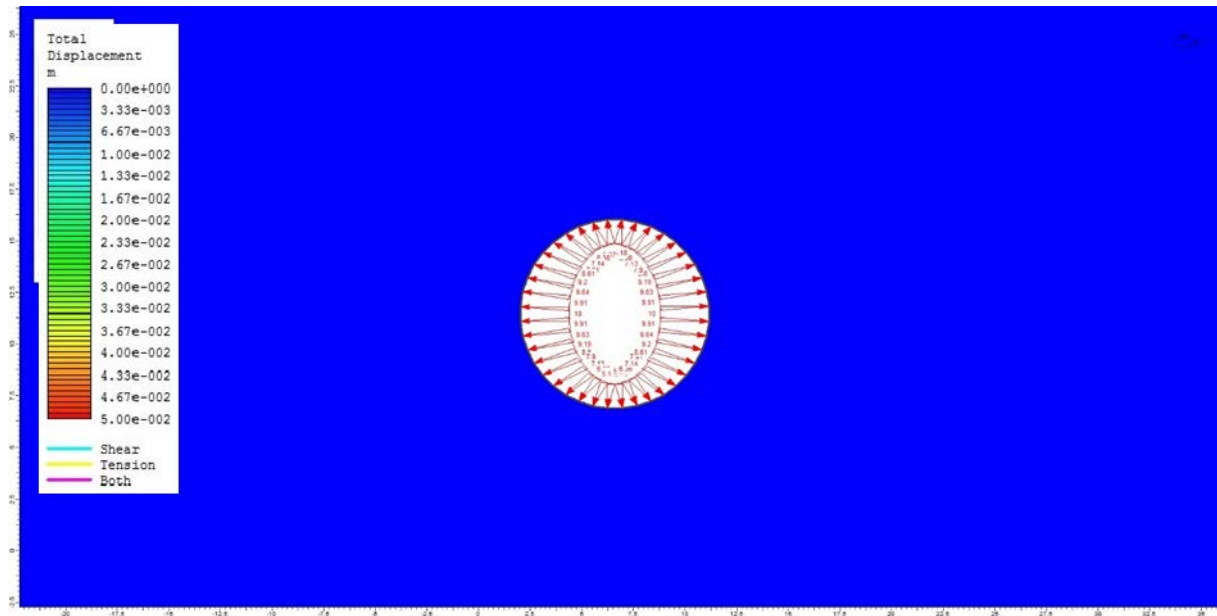


Figure A38. Round model, stage 1 internal pressure same as in-situ stress.

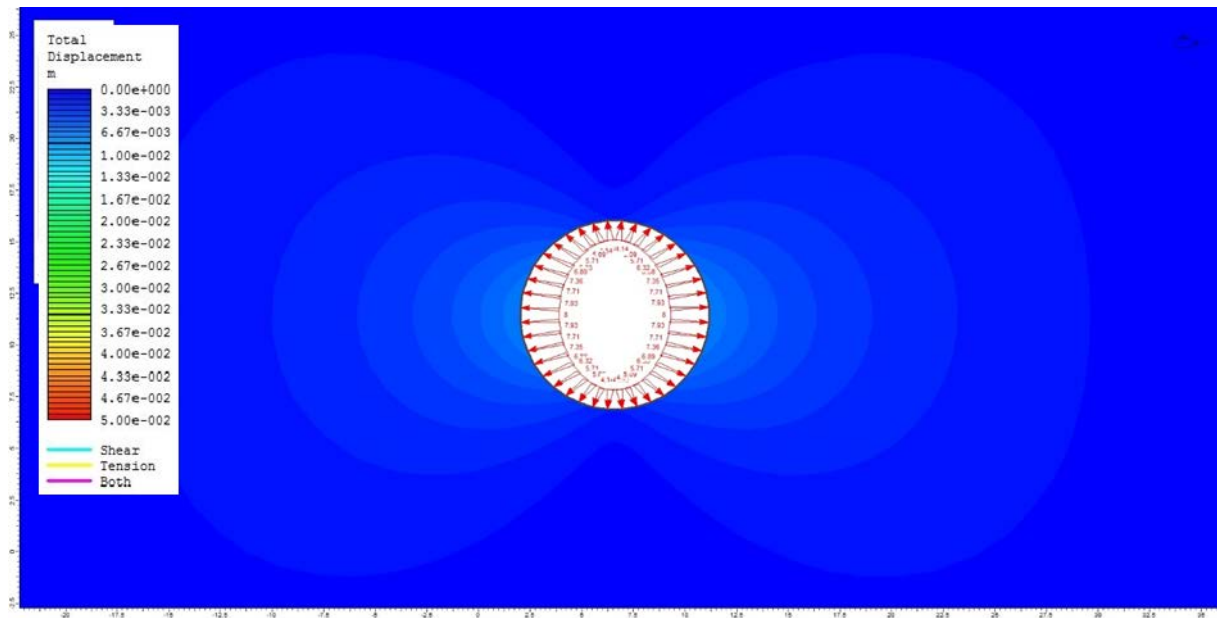


Figure A39. Round model, stage 2.

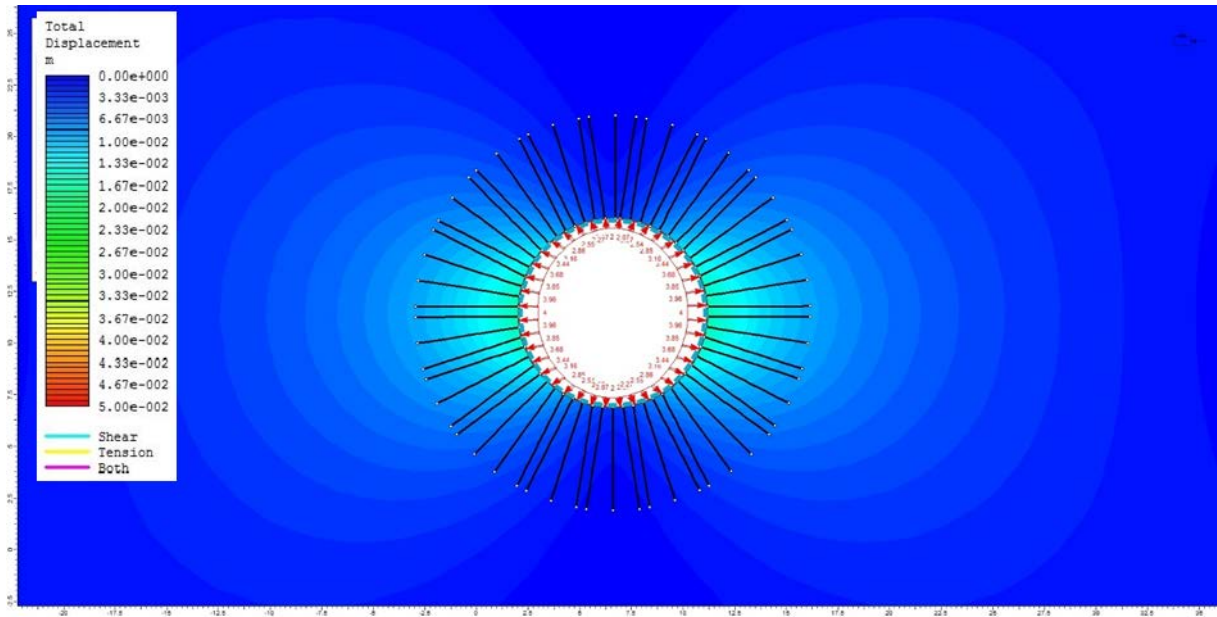


Figure A40. Round model, stage 3 bolt are installed.

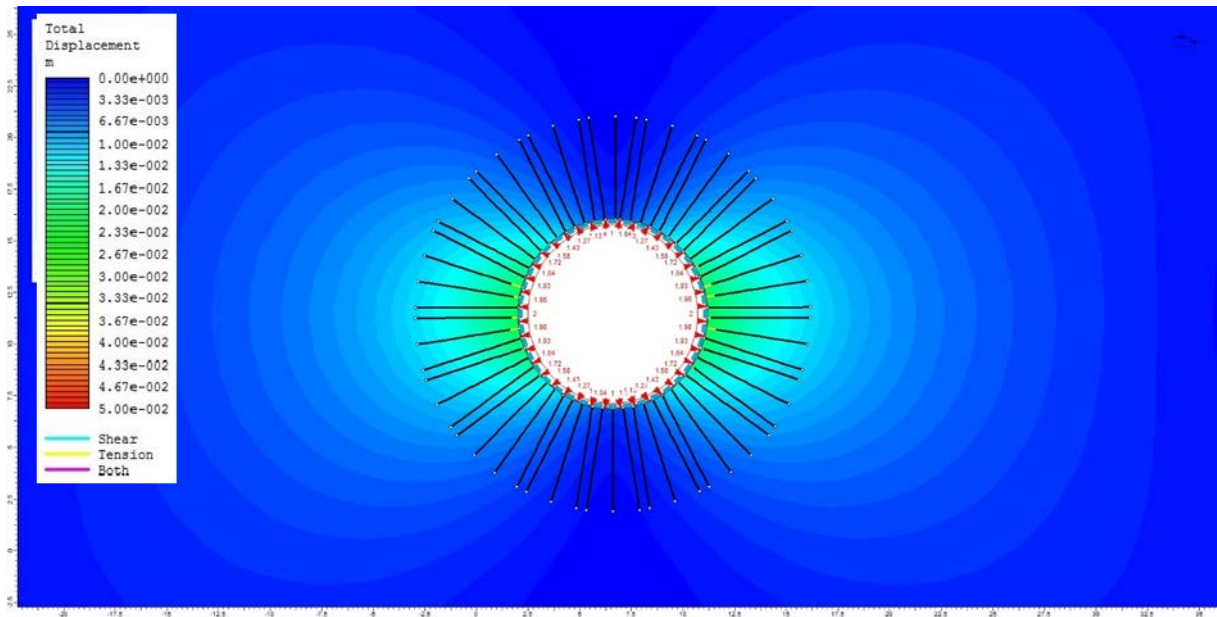


Figure A41. Round mmodel, stage 4.

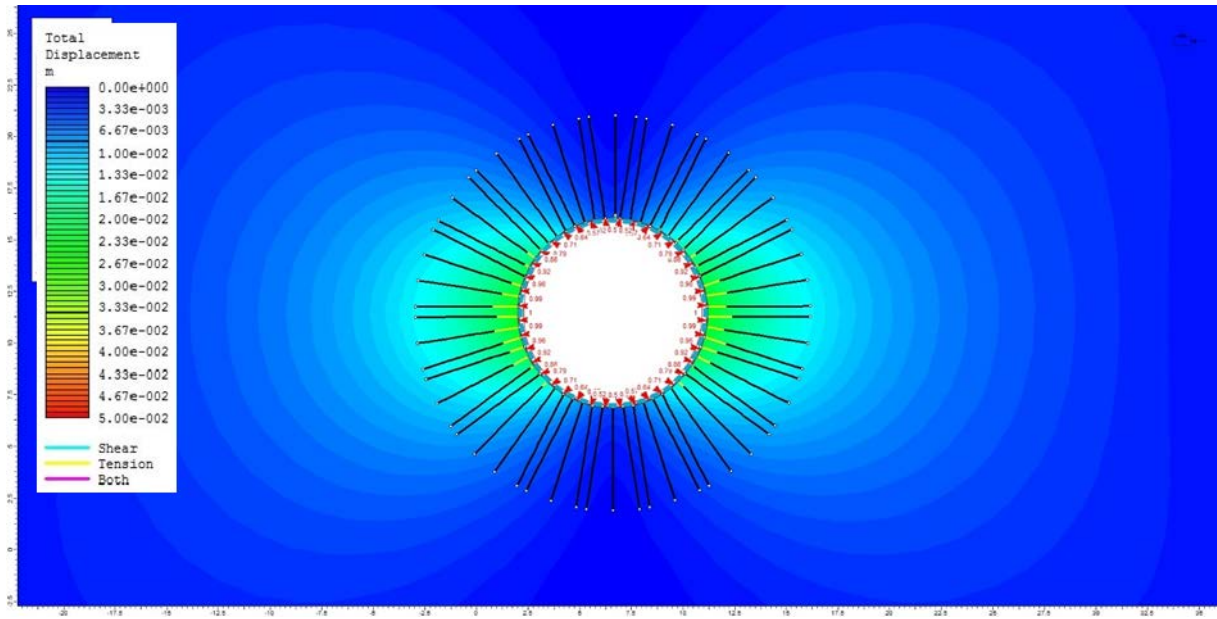


Figure A42. Round model, stage 5.

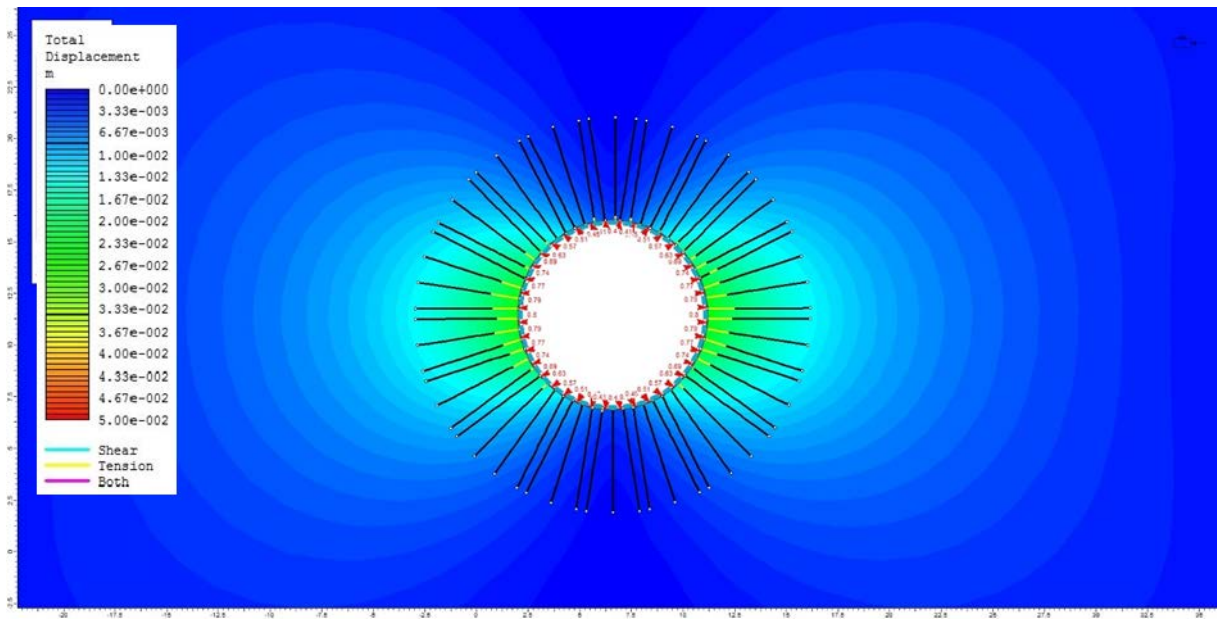


Figure A43. Round model, stage 6.

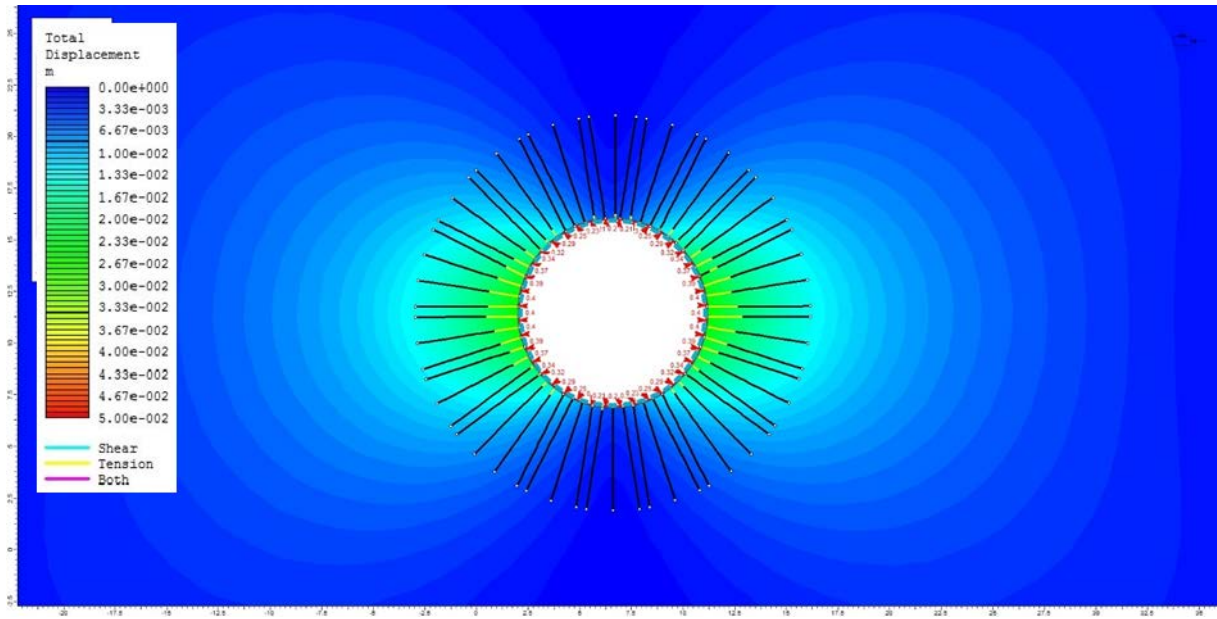


Figure A45. Round model, stage 7.

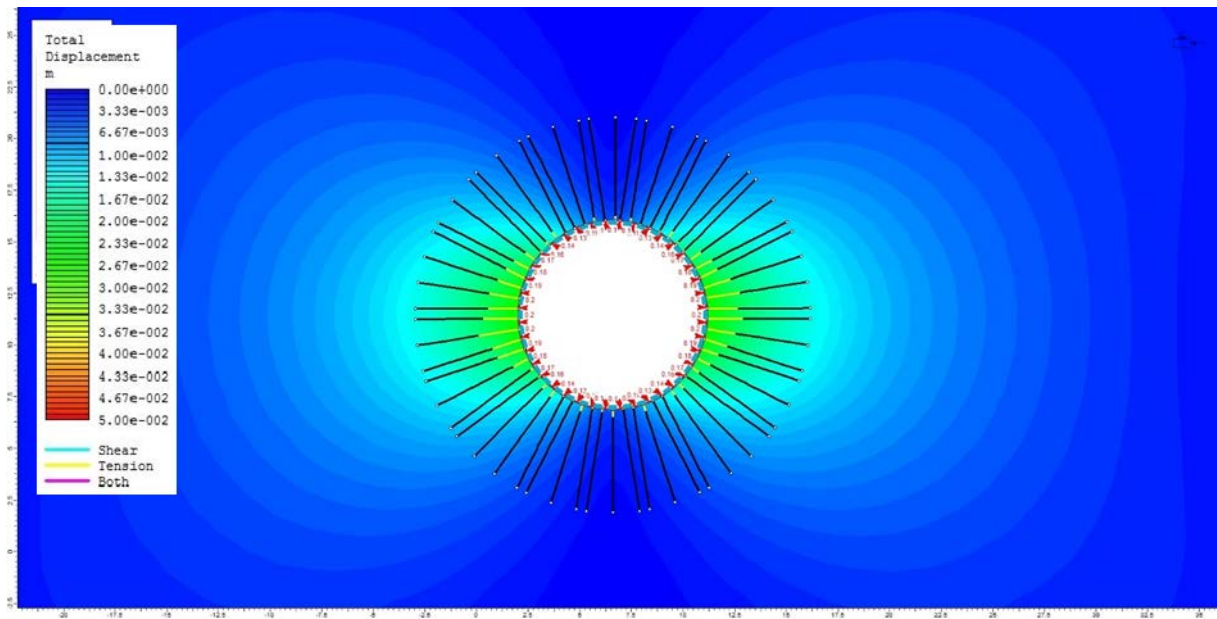


Figure A46. Round model, stage 8.

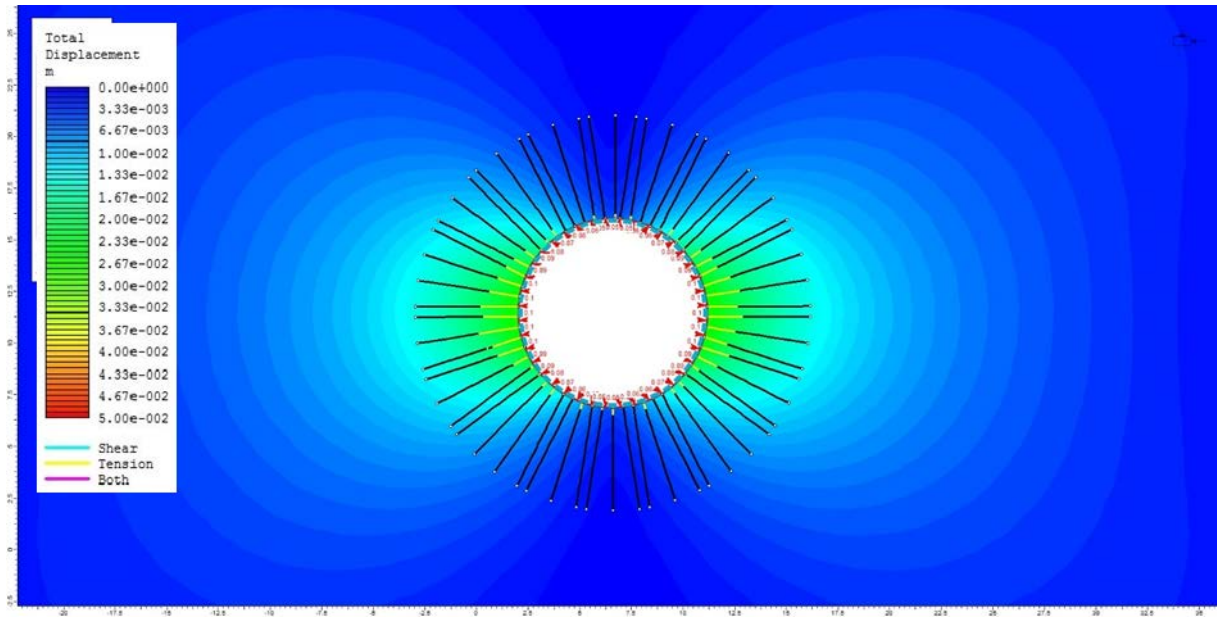


Figure A47. Round model, stage 9.

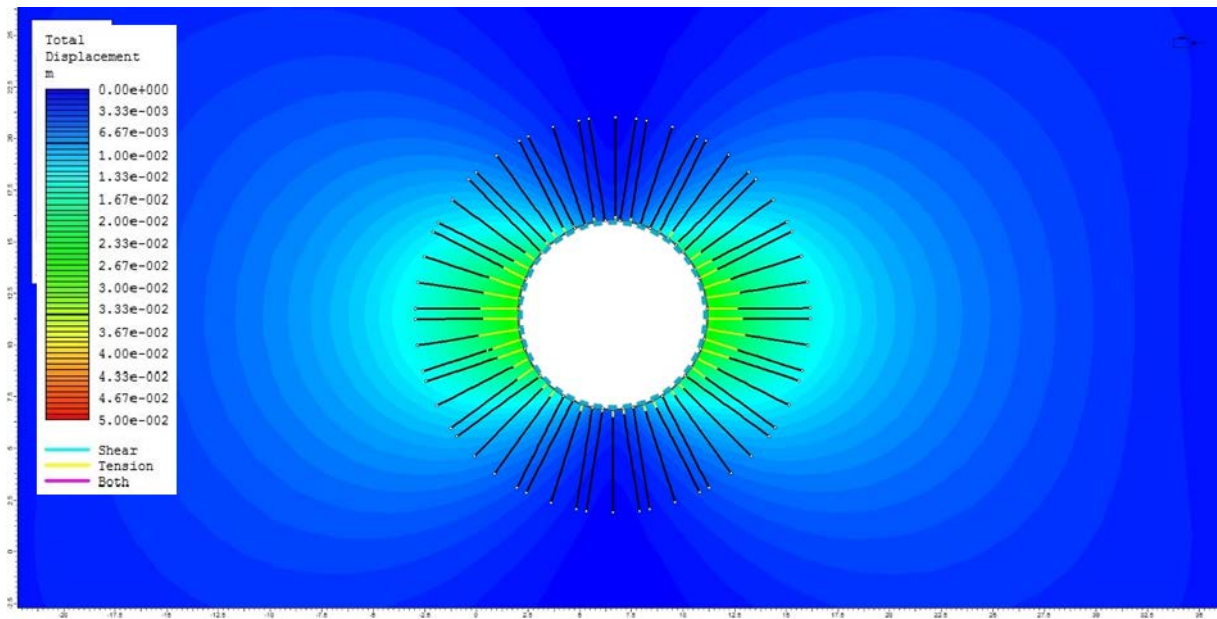


Figure A48. Round model, stage 10 without internal pressure.

